Vibration-based Bayesian FE-Model Updating for High-rise Buildings

Application of a Bayesian model updating technique for estimating the structural properties of high-rise buildings.





TNO

Vibration-based Bayesian FE-Model Updating for High-rise Buildings

Application of a Bayesian model updating technique for estimating the structural properties of high-rise buildings.

by

Rajat Shakya

Student Name: Rajat Shakya Student Number: 5691796

Supervisors of TU Delft: Dr. E. Lourens, Dr. A.A. Núñez Vicencio Supervisors of TNO: Ir. A.J. Bronkhorst, Ir. A.I. Martínez Colán

Project Duration: February, 2025 - October, 2025

Faculty: Faculty of Civil Engineering and Geosciences, Delft

Cover: The New Orleans Tower by Rotterdam Architectuurprijs, 2012

(Modified by Rajat Shakya)

Style: TU Delft Report Style, with modifications by Rajat Shakya



Preface

This research has been conducted in partial fulfillment of the requirements for the Master's degree in Structural Engineering at Delft University of Technology. The work was carried out between February 14, 2025 and October 31, 2025, in collaboration with TNO, the Netherlands Organization for Applied Scientific Research. The study focuses on the analysis of the high-rise building New Orleans Tower, located in Rotterdam.

This research holds special meaning for me. When I began my MSc journey at TU Delft, my goal was to better understand how we can evaluate the safety of existing structures, particularly within the context of structural health monitoring. At that time, I had little knowledge of how such an assessment could be achieved. Although this thesis does not directly address the assessment of safety, working on a method that identifies a building's parameters purely through data has deepened my appreciation for the power of clever mathematics combined with physics and engineering insights. Through this process, I gained valuable understanding not only of model updating, but also of how buildings are modelled, how they behave, how their properties interact, and how uncertainty can be quantified and managed.

Looking back, this experience has been both rewarding and transformative. Beyond developing technical and analytical expertise, I have grown in communication, presentation, problem-solving, and perseverance skills that I know will serve me well in my future career.

I would like to express my sincere gratitude to my supervisors, Eliz-Mari Lourens, Alfredo Núñez, Okke Bronkhorst, Andrés Martínez, and Davide Moretti, for their continuous support, insightful feedback, and encouragement throughout this journey. I am also grateful to Isa Ritfeld for her constant encouragement and for sharing in the excitement and passion for this project. My appreciation extends to TNO for providing the workspace and resources necessary to conduct this research. I would also like to thank the Justus & Louise van Effen Foundation for awarding me the Justus & Louise van Effen Excellence Scholarship, which made my studies at TU Delft possible.

Finally, I would like to thank my friends for their unwavering support and interest throughout the process, and my family, whose constant motivation and belief in me made this journey possible.

I hope the reader finds this research as engaging and inspiring as it was for me to undertake.

Rajat Shakya Delft, October 2025

Summary

This research addresses a persistent challenge in structural engineering: the frequent mismatch between the measured dynamic properties of high-rise buildings and those predicted by their design models. Previous deterministic model updating studies on structures such as the New Orleans Tower, including those by Moretti et al. [23] and Ritfeld [27], were constrained by two major limitations. First, they did not utilize all available modal information, particularly torsional modes, which can provide valuable insight into the structural behaviour. Second, they lacked a means to quantify uncertainty in the estimated parameters, leading to results with unknown reliability.

The primary objective of this thesis was to overcome these limitations and enhance both the accuracy and reliability of structural parameter estimation. To this end, a vibration-based Bayesian finite element (FE) model updating approach was implemented. A simplified three-dimensional FE model, formulated as a lumped-mass stick model, was developed for the New Orleans Tower. The model was specifically designed to capture both torsional and shear deformations while maintaining the computational efficiency required for Bayesian inference.

Within this framework, the Bayesian methodology employs Bayes' theorem together with Markov Chain Monte Carlo (MCMC) sampling to treat uncertain structural parameters, such as foundation stiffnesses and the concrete modulus of elasticity, as random variables. This produces a posterior probability distribution that formally quantifies the uncertainties associated with the updated parameters. The prior distributions were defined based on literature and engineering judgement, while the likelihood function was defined through a data-generating process. Furthermore, a novel mode-matching method based on the modal participation mass ratio was developed to robustly pair measured and modelled modes.

Model updating was performed for the New Orleans Tower through four different cases, each incorporating additional modal information. Overall, the Bayesian updating successfully produced models that closely matched the measured data. Across these cases, several advantages of the Bayesian approach were demonstrated, including the ability to detect parameter redundancy and overfitting, identify uninformative parameters, improve the solution through uncertainty reduction, and reveal the existence of multiple possible solutions.

The proposed modelling approach also exhibited improved performance compared to simplified analytical beam models. It successfully captured the third bending mode without compromising the accuracy of the lower modes. The first torsional mode was also well represented; however, the inclusion of the second torsional mode proved unsuccessful. This limitation is likely due to missing parameters or model features within the updating scheme rather than to deficiencies in the modelling approach itself.

The case study further revealed significant model inadequacies for higher modes. These inadequacies were primarily attributed to the exclusion of the effect of the adjoining low-rise structure and the assumption of rigid connections between structural elements. For studies where models with accurate higher modes are required, these effects may not be neglected.

Contents

Pr	eface	i
Su	mmary	ii
No	omenclature	ix
1	Introduction 1.1 Research Context 1.2 Research Problem 1.3 Research Objective 1.4 Research Scope 1.5 Research Questions 1.6 Organisation of the Text	1 1 2 2 2 2 3
2	Conceptual Background 2.1 Structural Modelling Approaches 2.2 Parameters 2.3 Modal Properties 2.4 Model Updating 2.5 Deterministic Model Updating 2.6 Bayes' Theorem 2.7 Bayesian Model Updating	4 4 6 6 6 7 7 8
3	Literature Review 3.1 Uncertainty in Dynamic properties of High-Rise Buildings	9 10 13
4	Bayesian Model Updating4.1Introduction4.2Prior Distribution4.3Likelihood Function4.4Mode Matching4.5Posterior Distribution4.6Posterior Predictive Distribution4.7Error Metrics4.8Example Problem : Verification of Bayesian Updating Routine4.8.1Problem Formulation4.8.2Model Truths4.8.3Pendulum Example 1: Updating m_1 and m_2 4.8.4Pendulum Example 2: Updating m_2 and l	16 16 17 19 20 22 22 23 24 24 25 26
5	Model Development: New Orleans Tower 5.1 Model Requirements	28 28 28

Contents

	5.4	Comparison of Measured and Calculated Modal Properties
6	Mod 6.1 6.2 6.3	el Updating Configuration and Uncertainty Quantification Candidate Parameters
		6.3.1 Methodology 40 6.3.2 Results 40
	6.4 6.5	Likelihood Function Selection
		6.5.1 Introduction 43 6.5.2 Model Truth 44 6.5.3 Data Generation 44
		6.5.4 Bayesian Updating Settings
	6.6	Conclusion
7	7.1 7.2	Introduction
	7.3 7.4	Results497.3.1 Comparison of Updated Parameters547.3.2 Computational speed56Conclusion57
8		ussions 58
o	8.1 8.2 8.3 8.4 8.5	Uncertainty Quantification
9	Con 9.1 9.2	Simplified FE Modelling Approach 63 Bayesian Model Updating 64
	9.3	Limitations and Recommendations
Re	feren	ces 67
A	Mas	s moment of inertia 70
В	B.1	ional Foundational Stiffness Determination73Approach73Values for the New Orleans Tower75
C	Mod	e Matching 76
D	Mar	kov Chain Monte Carlo (MCMC) 79
E	Fitti	ng Probability Distribution 82
F	Add F.1 F.2	itional Figures and Results Trace Plots
	F.3	Corner Plot for Frequencies

Contents	V

F.4	Standard Deviation of Parameters	91
F.5	Mode Visualization in 3D	92

List of Figures

2.1	(a) Elevation view and (b) analytical beam model of the Millikan Library, as presented by Taciroglu et al. [33]	4
2.2	(a) Elevation view and (b) Shear Building Model of a 20-storey office building, as presented by Lam et al. [18]	5
2.3	(a) Elevation view and (b) Simplified 3D FE Model of the Shanghai Tower, as presented by Pan et al. [24].	5
2.4	(a) Al-Sinyar Tower and (b) Detailed 3D FE Model of the same, as presented by Avci et al. [2]	6
3.1 3.2	Elevation and Side-View of the New Orleans tower depicting the accelerometer positions. (a) Elevation of New Orleans Tower showing different segments, (b) Model of New Orleans Tower by Moretti et al. [23] (c) Model of New Orleans Tower by Ritfeld [27] .	13 14
4.1 4.2 4.3	An example of converged MCMC Chain with burn-in period	22 25 26
5.15.2	(a) New Orleans Tower, (b) Detailed SCIA Model provided by Besix, (c) Opensees Model constructed for the current study	31
5.35.45.5	calculation. Sign Convention for foundational stiffnesses	32 33 33 36
6.1 6.2 6.3	Priors for the candidate parameters	40 42 46
7.1 7.2	Corner plots of the updated parameters for Case 1 through Case 3 Frequency Distribution Comparison for Case 3 (* denotes modes used in the updating	50
7.3 7.4 7.5 7.6	mac Matrix for updated results Measured and Predicted modes for Case 3 Posterior distribution of parameters for Case 4 Log-Likelihood and Log-Posterior around the predicted value of Case 3	52 52 53 54 56
8.1 8.2	New Orleans Tower with the Low-rise building	60 61
Δ 1	A prism of arhitrary area 4	71

List of Figures vii

B.1	Pile Plan for New Orleans Tower		
D.1	Proposal Distribution (Red Curve); Posterior Distribution (Black Curve); Current State θ_i ; Proposed State θ^* . (Figure from Lye et al. [21])	80	
E.1	Marginal posterior distribution of parameters	82	
F.1	Trace Plot for Case 1	83	
F.2	Trace Plot for Case 2	84	
F.3	Trace Plot for Case 3	85	
F.4	Trace Plot for Case 4	86	
F.5	Corner Plot for Parameters for Case 4	87	
F.6	Corner Plot for Frequencies for Case 1	88	
F.7	Corner Plot for Frequencies for Case 2	89	
F.8	Corner Plot for Frequencies for Case 3	90	
F.9	Corner Plot for Frequencies for Case 4	91	
F.10	Mode shapes 1-6 for the converged model of Case 3	92	
F.11	Mode shapes 7-8 for the converged model of Case 3	93	
F.12	Normalized Modal Mass Participation Ratio. Here M refers to Mass, RM refers to		
	Rotational Mass and the X, Y, Z refers to direction. For each mode (row), the entries		
	have been normalised with the highest value for that mode (row)	93	

List of Tables

2.1	Components of Bayesian Formula	8
3.1 3.2 3.3	Summary of literature categorized by modelling approach	11 14 15
4.1 4.2 4.3	Prior Selection based on Maximum Entropy Principle	16 25 27
5.1 5.2 5.3 5.4	Load Details	31 33 34 34
6.1 6.2 6.3	Probabilistic Models for Structural Parameters	38 41
6.4 6.5	frequency f_{nom}	43 44 46
7.1 7.2 7.3 7.4 7.5 7.6 7.7 7.8	Results for Case 1: Frequencies and mode shapes Comparison of stiffness parameters across Moretti et al., Ritfeld, and Case 1. Results for Case 2: Frequencies and mode shapes Comparison of Errors in Frequencies Results for Case 3: Frequencies and mode shapes Results for Case 4: Frequencies and mode shapes Nominal and MAP values for different cases Credible intervals (95%) for prior and posterior distributions across different cases.	49 49 51 51 51 54 55
7.9	Convergence Time for Different Cases	56
E.1 F.1	Parameter Statistics	82 91
	1	

Nomenclature

Abbreviations

Abbreviation	Definition
CV	Coefficient of Variation
CRPS	Continuous Ranked Probability Score
EB	Euler-Bernoulli
DOF	Degree of Freedom
FE	Finite Element
FEM	Finite Element Model
OMA	Operational Modal Analysis
MAC	Modal Assurance Criterion
MAP	Maximum A-Posteriori
MCMC	Markov Chain Monte Carlo
MPM	Modal Participation Mass Ratio
SBM	Shear Building Model
PDF	Probability Distribution Function
PMF	Probability Mass Function

Symbols

Symbol	Definition	Unit
A	Cross-Sectional Area of a member	$[m^2]$
a_r	Scaling factor for r^{th} modeshape	_
A_{sx}, A_{sy}	Shear area of a cross-section in \boldsymbol{x} and \boldsymbol{y} directions respectively	$[m^2]$
α_x, α_y	Shear shape factor in x and y directions respectively	_
bx1, bx2, bx3	First, second and third bending modes in \boldsymbol{x} direction respectively	_
by1, by2	First and second bending modes in y direction respectively	_

List of Tables x

Symbol	Definition	Unit
c	Normalizing constant (in Bayesian inference)	_
D	Dataset (modal properties)	_
D_E	Measured modal properties (experimental data)	_
$D_M(\theta)$	Model-predicted modal properties	_
$ ilde{D}$	Predicted modal properties (based on posterior predictive distribution)	-
δ_r^2	Variance term for modeshape likelihood	_
E_{conc}	Modulus of elasticity of concrete	$[N/m^2]$ or $[GPa]$
f	Frequency	[Hz]
Γ	Selection matrix (for degrees of freedom)	_
g_m	Generalised mass matrix	_
G	Shear modulus	$[N/m^2]$
H	Storey height / height of a member	[m]
I_{xx},I_{yy}	Equivalent moments of inertia about centroid	$[m^4]$
J	Torsional constant	$[m^4]$
$J(\theta)$	Error function (deterministic updating)	_
K_{tx}, K_{ty}	Translational foundation stiffness (x, y)	[N/m]
K_{rx}, K_{ry}	Rotational foundation stiffness (about x -, y -axis)	[Nm/rad]
K_{rz}	Rotational foundation stiffness (torsional)	[Nm/rad]
k_x, k_y	Lateral stiffness of a member in x and y directions respectively	[N/m]
$k_{ heta}$	Torsional stiffness of a member	[Nm/rad]
\mathcal{N}_m	m^{th} -order multivariate normal distribution	_
M	Mass matrix	[kg]
K	Stiffness matrix	[N/m]
X	Displacement vector	[m]
μ	Mean	varies
Σ	Covariance matrix	varies
$\Sigma_{f,E}$	Covariance matrix for frequency measurement error	_
Σ_{ϕ_r}	Covariance matrix for r^{th} modeshape error	_
σ	Standard deviation	varies
q_p	Permanent load	$[kN/m^2]$

List of Tables xi

Symbol	Definition	Unit
q_v	Variable load	[kN/m ²]
q_f	Façade load	$[kN/m^2]$
$ ho_{conc}$	Density of concrete	$[kg/m^3]$
ρ	Building density (deterministic updating)	$[kg/m^3]$
T	Directional matrix (in MPM context)	_
t1, t2	First and second torsional modes respectively	_
w_f, w_ϕ	Weights for frequency and modeshapes	_
x_c, y_c	x and y coordinates of centroid	[m]
x_s, y_s	x and y coordinates of centre of stiffness	[m]
x_m, y_m	x and y coordinates of centre of mass	[m]
X	Set of known/constant parameters in FE model	_
θ	Set of unknown structural parameters	_
η_M	Model bias term	_
η_E	Random measurement error term	_
$\eta_{f,M}$	Model bias term for frequency	_
$\eta_{f,E}$	Measurement error term for frequency	_
$\eta_{\phi_r,E}$	Measurement error term for the r^{th} modeshape	_
ϕ	Modeshape	_
$\phi_{E,r}$	r^{th} measured (experimental) modeshape	_
$\phi_r(\theta)$	r^{th} model-predicted modeshape	_
φ_x, φ_y	Shear deformation factor of a cross-section in x and y direction respectively	-

 \int

Introduction

1.1. Research Context

For any structural system, the structural parameters, such as mass density, stiffness, and foundational stiffnesses influence its natural frequencies and mode shapes. The dynamic properties derived via field measurements can be used to provide insight on the aforementioned structural parameters. Ideally, these measured dynamical properties should be close to the ones estimated during the design phase from a FE model. However, different studies such as ones by Avci et al. [2], Bronkhorst et al. [4], Moretti et al. [23], Pan et al. [24], have shown that the measured dynamical properties of high-rise buildings generally do not match with the ones predicted by the design models. This mismatch in the properties suggests that there are certain design choices taken during the modelling phase which leads to a model that does not accurately represent the building in question [4, 23].

1.2. Research Problem

To improve the predictive capability of the FE model, a technique called model updating can be used, wherein the model's dynamic properties are matched with measured dynamic properties by altering the mass, stiffness, and foundational stiffness of the building. Moretti et al. [23] and Ritfeld [27, 28] developed a deterministic model updating approach based on analytical beam models, which allows for the estimation of global structural properties (i.e., bending stiffness and foundation spring stiffness) of high-rise buildings. While this method successfully matched the modal properties and provided estimates for the global bending and foundation stiffnesses, the developed approach exhibited two major limitations:

- Unused Modal Data: The analytical model which was used to represent the building did not account for torsional displacements. Therefore, the model could only represent bending or sway modes. The identified torsional modes and mixed modes were either not taken into account for model updating or were averaged and converted to bending/lateral modes (which introduces bias in the solution).
- Uncertainty Quantification: The developed deterministic model updating approach aims to find a single "true" set of model parameters by minimizing a cost function between measured and predicted modal properties (natural frequencies and mode shapes). Such a deterministic approach ignores inherent uncertainties associated with measured and modelled dynamical properties, may require bias-inducing regularization for ill-posed problems, and fails to incorporate prior knowledge about parameter ranges. As a result, there is often no indication of the reliability or the uncertainty quantification of the updated model parameters.

The first limitation can be addressed by adopting a 3D model. Increasing the model dimensionality from 1D or 2D to 3D allows the inclusion of previously unused modal data and facilitates the use of higher mode information through a more detailed representation of the structure. The second limitation can be mitigated by incorporating uncertainty within the model updating process, for instance, through Bayesian model updating. In this framework, the higher-fidelity FE model provides richer structural information, while the Bayesian approach quantifies the associated uncertainty, offering a clearer understanding of discrepancies in the dynamic properties. By combining these two improvements into a Bayesian FEM-based approach, more reliable estimates of the global structural properties can be achieved.

1.3. Research Objective

The objective of this research is to improve the accuracy and reliability of structural parameter estimation by incorporating torsional modes and by quantifying the uncertainty in the estimated parameters using vibration-based Bayesian FE model updating.

1.4. Research Scope

The research will focus on the application of Bayesian Model Updating on a high-rise building using vibrational data. Therefore, the outcome and recommendations from the research will be valid only for high-rise buildings. The study will also be focusing on performing model updating on a simplified FE model. Non-linear effects in modal properties due to effects of vibrational amplitude, damping, and building lifespan will not be considered. The frequency dependence of the stiffnesses will not be considered. Additionally, as the data for the study will be obtained from previous studies, Operational Modal Analysis (OMA) will not be conducted and will not be the focus of the study.

1.5. Research Questions

The thesis has two main aspects with which it improves upon the previous works: i) increasing modelling complexity to account for unused modal data, ii) using Bayesian inference to account for the uncertainties in parameters, model, and measurements. As such, the main research question also revolves around these two key areas. The main research question for this thesis is:

"How can Bayesian model updating, combined with a simplified FE model, be effectively utilized to enhance the accuracy and reliability of structural parameter estimation in high-rise buildings?"

To address the above research question, a set of sub-questions have been derived below, which cover the two main aspects of the thesis.

Research sub-questions related to modelling in Bayesian model updating:

- How should the updating parameters be determined?
- What effect does increasing model complexity have on the model updating results?
- What effect does including torsional modes have on the model updating results?

Research sub-questions related to uncertainty quantification and Bayesian inference:

- How should the prior probabilities be defined to best reflect the initial knowledge about the structural properties, including correlation?
- To what extent does the definition of the priors affect the posterior distribution?
- What likelihood function/model should be used?
- What insights can be derived from the updating results?

1.6. Organisation of the Text

This document is organized into nine chapters. Chapter 1 introduces the research context and objectives. Chapter 2 provides background information on high-rise building modelling and model updating. Chapter 3 reviews existing literature on model updating and prior studies on the New Orleans Tower. Chapter 4 presents the theoretical formulation of Bayesian model updating, while Chapter 5 details the simplified finite element model and the modelling of the New Orleans Tower. Chapter 6 outlines the practical choices made for uncertainty quantification and model updating. Chapter 7 presents the corresponding case study. The report concludes with a discussion and final conclusions.

Conceptual Background

This chapter presents an overview of structural modelling approaches for high-rise buildings, ranging from simplified analytical beam models to detailed finite element (FE) representations. It also introduces the fundamental concepts of modal properties and model updating, along with a brief explanation of the key concepts underlying deterministic and Bayesian model updating.

2.1. Structural Modelling Approaches

In structural engineering, the modelling approach strongly influences both the accuracy of results and the computational effort required. Depending on the purpose of the study, models can range from highly simplified analytical representations to detailed three-dimensional finite element (FE) models.

1. Analytical Beam Model

The simplest representation approximates a high-rise building as an Euler–Bernoulli (EB) or Timoshenko beam. Such models are computationally very efficient, making them particularly suitable for tasks like model updating where eigenanalysis must be repeated thousands of times. However, their simplicity often leads to a loss of local information [23, 27].

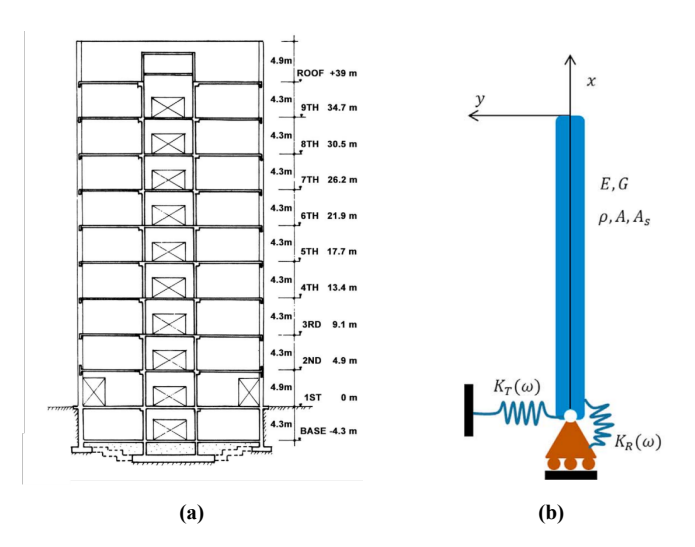


Figure 2.1: (a) Elevation view and (b) analytical beam model of the Millikan Library, as presented by Taciroglu et al. [33].

2. Shear Building Model

This approach idealises the building as a stack of lumped masses connected by lateral stiffness, with rigid-diaphragm floor slabs. Only translational motion in x and y is considered, while rotational effects are neglected. This makes the model suitable for low- to mid-rise buildings dominated by shear behaviour, but less accurate for high-rise buildings where bending effects play a major role.

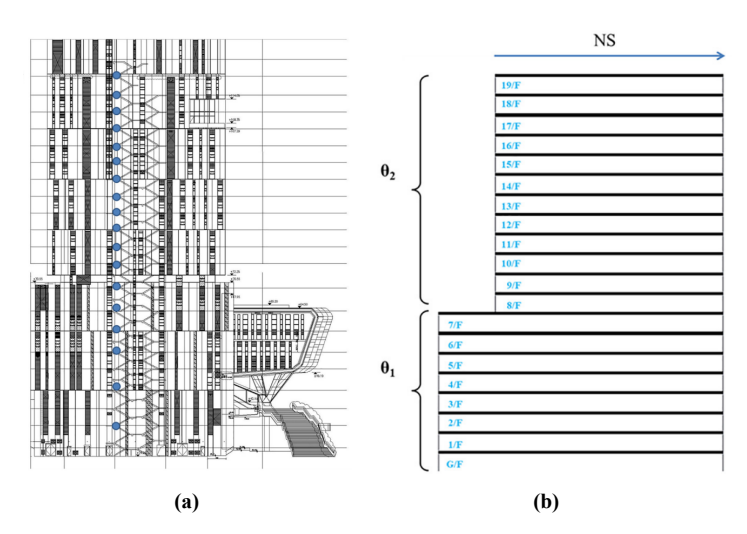


Figure 2.2: (a) Elevation view and (b) Shear Building Model of a 20-storey office building, as presented by Lam et al. [18].

3. Simplified FE Model

Extending the shear model, simplified FE models release the assumption of no rotational displacement. Floors are modelled with both translational and rotational degrees of freedom, and torsional effects may also be included. These models strike a balance between computational efficiency and physical realism.

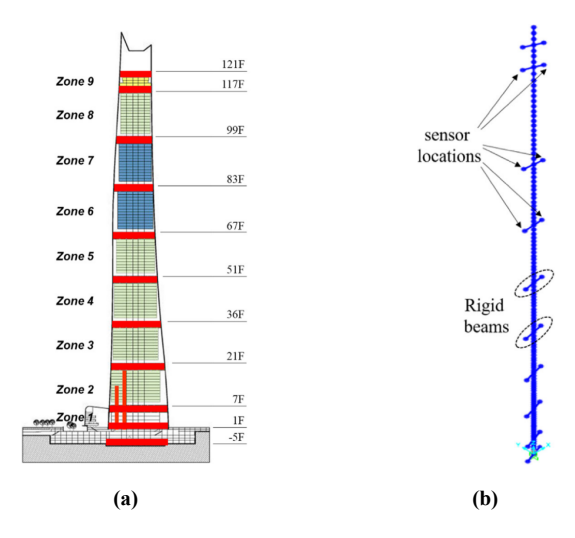


Figure 2.3: (a) Elevation view and (b) Simplified 3D FE Model of the Shanghai Tower, as presented by Pan et al. [24].

4. Detailed FE Model

At the most refined level, detailed 3D FE models represent the geometry and material behaviour with tens or even hundreds of thousands of elements. Such models minimise modelling bias and capture local effects with high fidelity, but they are computationally very demanding, often requiring hours for a single eigenvalue analysis. This makes them impractical for repetitive tasks such as model updating.

2.2. Parameters 6



Figure 2.4: (a) Al-Sinyar Tower and (b) Detailed 3D FE Model of the same, as presented by Avci et al. [2].

2.2. Parameters

The behaviour of a structural model is primarily governed by its geometry, boundary conditions, and material properties. Geometry refers to the spatial configuration of the system, including the location of nodes and the size and shape of elements (e.g., cross-sections and lengths). These are typically derived from design drawings, either directly or through simplifications based on specific assumptions. Boundary conditions define how the system interacts with its supports and external restraints, both at the level of individual elements and the structure as a whole. Material properties, on the other hand, dictate how each element responds to loading, encompassing characteristics such as density, elasticity, and constitutive behaviour.

Collectively, these features are called the model parameters, which are the primary inputs of a system that influence its response or output. They can represent intrinsic physical properties (such as material and geometric characteristics, or boundary conditions) or be embedded within the mass and stiffness matrices, which define the relationship between these physical properties and the model's response. In model updating research, the physical properties are often used as the model parameters due to their clear physical meaning making them directly interpretable to the analyst, and enabling a intuitive link between the model predictions and the real structure. [9]

2.3. Modal Properties

For any structure, its dynamic characteristics and behaviour are described by its modal properties. These include natural frequencies, mode-shapes and damping ratios. Of these, the natural frequencies represent the frequencies at which the structural system would respond to in the absence of any external loading, and the corresponding mode shapes describe how the structural system would respond. The damping ratio describes how quickly the amplitude of the response decrease with time. In this thesis, the natural frequencies and mode shapes of the structure are adopted as the primary modal properties for analysis and model updating.

2.4. Model Updating

The modal properties of a structure can be obtained either through experimental observations or by numerical predictions using finite element (FE) models. In an ideal scenario, the modal properties measured from experiments would match those predicted by the FE model. In practice, however, the two rarely align. This mismatch can arise for various reasons, such as measurement noise, simplifications in the model, or discrepancies between the actual structural properties and those assumed in the model.

To address this issue, model updating is employed. Model updating refers to the process of calibrating uncertain system parameters by using measurement data as the reference for the "true" system. In structural dynamics, vibration-based model updating specifically uses modal properties derived from vibrational data as the basis for this calibration.

The modal properties of a structure are governed by its physical characteristics, such as the stiffness and mass of its elements. Conversely, if the modal properties are known, they can in principle be used to estimate the structural properties. Determining modal properties from given structural properties is relatively straightforward, and most FE software can compute them through eigenanalysis. The reverse task, i.e. inferring structural properties from measured modal properties, often called the 'inverse problem', is much more challenging. This is particularly due to the absence of a closed form solution for this transformation. In addition to this, the presence of non-unique solutions also make this challenging to say with certainty if the obtained solution is the true solution.

Model updating provides a practical way forward. It formulates the inverse problem as an optimization task, where the goal is to minimize the discrepancy between the measured modal properties and those predicted by the FE model. By systematically adjusting selected model parameters, the predicted modal properties are brought into closer agreement with the experimental data, thereby improving the accuracy of the underlying structural model.

2.5. Deterministic Model Updating

Deterministic model updating is a framework of model updating where the calibration of the model is performed via an optimization problem. In this framework, the model parameters are defined as deterministic parameters, without explicitly defining their uncertainties. For the optimization, the objective function is defined as the error between the measured and predicted modal properties, often defined as Eq. 2.1. As the objective function represents the error, the goal of the optimization becomes to minimize this function.

$$J(\boldsymbol{\theta}) = w_f \sum_{i=1}^{N} \frac{|f_i - \hat{f}_i|}{\hat{f}_i} + w_\phi \sum_{i=1}^{N} (1 - MAC(\phi_i, \hat{\phi}_i))$$
 (2.1)

where,

 $J(\theta)$: Error function

 w_f, w_ϕ : weights assigned for frequency and mode shapes respectively

 f_i, ϕ_i : estimated i^{th} frequency and mode shapes respectively that depends on the parameters θ

 $\hat{f}_i, \hat{\phi}_i$: measured i^{th} frequency and mode shapes respectively

N: Number of modes considered

Different algorithms, such as gradient-based algorithm and particle swarm algorithm, have been used in the literature to carry out the deterministic model updating. The main feature of deterministic model updating is that for the given initial definitions of the parameters and error function, the result of the updating will always be exactly the same. The accuracy of deterministic updating depends strongly on the quality of the measurement data, the choice of parameters to be updated, and the conditioning of the inverse problem. While this method can provide a unique, best-fit model, it does not capture the variability or uncertainty in the system.

2.6. Bayes' Theorem

Bayes' theorem is a fundamental concept in probability theory, which describes how the probability of certain outcome changes when new information about the event, called evidence, is obtained. The

expression for Bayes' theorem is given as follows:

$$P(A|B) = \frac{P(B|A) \cdot P(A)}{P(B)}$$
(2.2)

The different terms of this formula are explained in Table 2.1

Table 2.1: Components of Bayesian Formula

Term	Terminology	Meaning
\overline{A}	Hypothesis	Quantity of interest
B	Evidence	Measurable or Observable Quantity
P(A)	Prior of A	Initial probability of hypothesis A being true
P(B)	-	Total probability of observing the evidence B
P(A B)	Posterior of A	Probability of hypothesis A being correct given that evidence B is observed
P(B A)	Likelihood of ${\cal B}$	Probability of observing evidence B given that hypothesis A is true

2.7. Bayesian Model Updating

The concept and philosophy of Bayes' theorem can be applied to system identification problems in structural engineering via *Bayesian model updating*, which allows for the incorporation of both model and measurement uncertainties. In Bayesian model updating, uncertain parameters are treated as random variables with associated probability distributions, allowing Bayesian theory to formally account for uncertainty.

For a set of unknown structural parameters, θ , we can infer its posterior distribution based on a dataset **D** by using equation 2.2 in the following manner:

$$p(\boldsymbol{\theta}|\mathbf{D}) = \frac{p(\mathbf{D}|\boldsymbol{\theta}) \cdot p(\boldsymbol{\theta})}{P(\mathbf{D})}$$
(2.3)

In this formulation:

- The operator $P(\cdot)$ refers to the Probability Mass Function (PMF) for discrete random variables, while the operator $p(\cdot)$ refers to the Probability Density Function (PDF) for continuous random variables.
- The prior distribution, $p(\theta)$, reflects existing knowledge or assumptions about the uncertain structural parameters, θ .
- The likelihood function, $p(\mathbf{D}|\boldsymbol{\theta})$, quantifies the probability of observing the measured data given the model parameters. In practice, this term incorporates some measure of the discrepancy between model-predicted and experimentally observed modal properties.
- The denominator, $P(\mathbf{D})$, is the evidence term. It requires integrating the likelihood over the entire parameter space, which is computationally intractable in most real-world applications.

In practise, sampling-based methods are commonly used to explore the posterior distribution by generating samples proportional to the unnormalised posterior $(p(\mathbf{D}|\boldsymbol{\theta}) \cdot p(\boldsymbol{\theta}))$. The evidence term is then treated as an unknown normalisation constant. Consequently, the posterior probability is then given by:

$$p(\boldsymbol{\theta}|\mathbf{D}) = c \cdot p(\mathbf{D}|\boldsymbol{\theta}) \cdot p(\boldsymbol{\theta})$$
(2.4)

where c is the normalizing constant. [8]

Literature Review

This chapter reviews the existing literature on the uncertainty in the dynamic and structural properties of high-rise buildings and the application of model updating to address such uncertainties. Section 3.1 discusses the sources and nature of uncertainties observed in high-rise structures. Section 3.2 examines previous studies on model updating, with particular emphasis on applications to high-rise buildings. Section 3.3 focuses on research specifically related to the New Orleans Tower.

3.1. Uncertainty in Dynamic properties of High-Rise Buildings

For any building, it is expected that the designed dynamic properties closely match the actual in-situ dynamic properties. Although some deviation is expected due to modelling assumptions and measurement noise, numerous measurement campaigns have revealed significant and repeated discrepancies. For instance, Bronkhorst et al. [4] found that the natural frequencies for the high-rise buildings in the Netherlands were underestimated by design codes by a factor of 1.4 to 2.2. More recent research on structures like the New Orleans Tower and the New Erasmus Medical Center found mismatches in natural frequencies reaching up to 30% and 50%, respectively [3].

Crucially, the mismatch in natural frequencies are often higher for complex and higher modes. Pan et al. [24] found that for the Shanghai Tower, frequency errors reached up to 45% for torsional modes compared to 34% for translational modes, suggesting that torsional behaviour is particularly susceptible to modelling errors or inaccurate initial assumptions.

These mismatch in dynamic properties primarily arises from the inherent idealizations in FE models, which are developed based on engineering judgment. Even the most detailed models rely on simplifying assumptions and may fail to capture important aspects such as connection behaviour, material variability, or foundation—soil interaction [24]. Different authors have proposed various classifications of these modelling errors and uncertainties, which, despite differing terminology, share the same underlying principles. One such classification by Simeon et al. [32] divides the source of modelling uncertainties into three categories:

- a. Model Parameter: This type of uncertainty arises from incorrect assumptions about the structure's parameters or properties. It may include uncertainties in material properties, complex loading conditions, or geometrical imperfections.
- b. **Model Structure:** These errors are introduced during the idealization and simplification of the structural model. For example, assuming a fully fixed connection when it actually exhibits some flexibility introduces structural modelling errors. Such errors may arise from both intentional

simplifications and unintended side effects. Increasing the model fidelity can help mitigate these errors.

c. Model Code: This uncertainty results from numerical or technical limitations in the modelling software or hardware. It includes how numerical algorithms handle calculations. Generally, this type of uncertainty is considered negligible.

To improve the predictive capability of the finite element (FE) model, the Model Parameter uncertainty must be systematically reduced. This can be achieved through model updating. Furthermore, addressing Model Structure uncertainty, particularly the inability to model complex modes like torsion, requires selecting an appropriate structural modelling approach. The following section reviews the literature on Model Updating techniques to establish a foundation for choosing the most suitable method to address these challenges.

Apart from model-based uncertainties, experimental data also contribute to the uncertainty in parameter identification. These arise from random measurement noise, instrument imperfections, and bias introduced by unaccounted loading sources. Moreover, the dynamic properties used in vibration-based model updating are not directly measured, but derived from time-domain vibration data. This extraction process introduces additional uncertainty due to the assumptions involved, the finite length of the data, data filtering, and the choice of a Linear Time-Invariant (LTI) system model. Together, these factors contribute to both bias and variance in the identified dynamic properties [32].

3.2. Model Updating

Model updating is the process of calibrating uncertain system parameters using experimental data as a reference to minimize the discrepancy between measured and predicted modal properties. The choice of model and the updating methodology are critical factors influencing the feasibility and interpretability of the results.

In the past, different authors have used different approaches to perform model updating, with varying degrees of success. Table 3.1. outlines some of the studies done in the past concerning buildings, grouped on the basis of the type of model used.

The analytical beam model has been widely used for deterministic model updating in previous studies by Taciroglu et al. [33], Moretti et al. [23], and Ritfeld [27]. Taciroglu employed a Timoshenko beam model with frequency-dependent foundation stiffnesses to represent the Millikan Library, while Moretti and Ritfeld both modelled the New Orleans Tower using Euler–Bernoulli and discrete Timoshenko beam models, respectively. All three studies reported that fitting the third bending mode degraded the overall results, as the effort to match this mode introduced significant errors in the lower modes. Moretti attributed this to model inadequacy, arguing that the analytical beam models do not have sufficient features to explain these higher modes. Moreover, such models cannot represent torsional behaviour or coupling between the x and y directions, which restricts the range of modal data that can be utilized during the updating process.

The shear building model (SBM) is a simple yet widely used modelling approach. When extended to three dimensions, it can capture torsional and coupling effects between the x and y directions. Aloisio et al. [1] performed deterministic model updating using an SBM to fit three modes, including one torsional mode. The torsional mode was fitted more accurately than the translational modes, although all modes were within reasonable error limits.

Lam et al. [18] and Hu et al. [13] applied Bayesian model updating with SBMs using two translational modes per direction. Both studies reported relatively high errors in one of the first translational modes and were unable to represent torsional behaviour. These errors were attributed to model structure uncertainty arising from oversimplification. In Lam's study, the complex lower floors introduced

 Table 3.1: Summary of literature categorized by modelling approach

Author(s)	Structure	Updating Method	Remarks		
Analytical Beam Models					
Taciroglu et al. [33]	Millikan Library	Deterministic	Timoshenko beam model unable to fit the 3rd bending mode.		
Moretti et al. [23]	New Orleans Tower	Deterministic	Euler–Bernoulli beam model unable to fit the 3rd bending mode.		
Ritfeld [27, 28]	New Orleans Tower	Deterministic	Discrete Timoshenko beam model unable to fit the 3rd bending mode.		
Shear Building Models					
Aloisio et al. [1]	8-storey CLT building (23.21 m)	Deterministic	About 5% frequency error in the 2nd translational mode; good fit for the 1st torsional mode.		
Lam et al. [18]	20-storey office building	Bayesian	Using one mode led to high parameter uncertainty. Using two modes reduced errors, with maximum frequency error of 8%.		
Hu et al. [13]	9-storey coupled building	Bayesian	Large parameter uncertainty and relatively larger errors in the first translational mode, attributed to model uncertainty.		
Simplified FE Models	S				
Wu et al. [36]	Nanjing TV Tower (310 m)	Deterministic	Good results updating with upto 4th bending mode; also matched the 5th and 7th bending modes.		
Pan et al. [24]	Shanghai Tower (632 m)	Deterministic	Using 9 modes, maximum frequency error was 8.6%. Higher validation modes improved, with errors reduced from 17% to 3%.		
Detailed FE Models					
Avci et al. [2]	53-storey tower in Doha (230 m)	Deterministic	Despite using 10 modes (including 3 torsional), torsional frequency errors remained high $(> 10\%)$.		
Kaynardag et al. [17]	26-storey core-wall building (131.2 m incl. basement)	Deterministic	With 4 bending modes in the <i>y</i> -direction, the 2nd mode was not fitted. Mode shapes beyond the 1st mode did not match well, attributed to basement fixed-type behavior. The 1st mode matched well (weighted 80% in optimization).		
Dong et al. [8]	250 m tall building	Bayesian	Using 10 modes, maximum frequency error was 8%. Parameter uncertainty was reduced.		
Liu et al. [19]	13-storey twin-tower masonry structure (48.3 m)	Bayesian	Good agreement between predicted and identified modal parameters. The torsional mode showed relatively higher error (7.8%).		

significant uncertainty when idealized as shear layers, reflected in the high CV (>30%) of the updated inter-storey stiffness. In Hu's case, simplified modelling of structure–structure interaction using translational springs led to similarly high uncertainty (CV>30%) in the updated spring stiffnesses.

Overall, while the SBM offers computational efficiency, its simplifying assumptions limit its suitability for complex or high-rise buildings. The absence of rotational degrees of freedom associated with bending deformation makes it inadequate for capturing the full dynamic behaviour of tall structures.

The simplified finite element (FE) model improves structural representation by incorporating both shear and bending behaviour between storeys. In contrast to the shear building model, it also allows rotational displacements of each floor.

Wu et al. [36] applied this approach to the Nanjing TV Tower for deterministic model updating using the first four bending modes. The updating reduced frequency errors to below 2% for all modes, while higher unupdated modes (fifth and seventh) also showed low errors, demonstrating the model's capability to generalize beyond the calibrated range, and the potential to fit higher modes, a limitation of the previous modelling approaches. Similarly, Pan et al. [24] used a 3D simplified FE model for the Shanghai Tower with nine modes (incl. three torsional modes), achieving good agreement with measurements and a maximum error of 8.6% in the torsional and third bending modes. The model also showed strong predictive performance for higher unupdated modes.

A key advantage of the simplified FE model is its ability to compute mode shapes directly at sensor locations, reducing discrepancies caused by sensor eccentricity, a known limitation of analytical beam models [27]. Additionally, the model provides considerable flexibility in selecting updating parameters, with Pan et al. identifying up to 90 updatable parameters. These features make the simplified FE model a practical and effective choice for vibration-based model updating.

The detailed FE model represents the highest level of structural abstraction, capturing geometry, boundary conditions, and material behaviour with high fidelity. These models often have hundreds and thousand times more elements than the previous modelling approaches. However, the large number of elements makes eigenvalue analysis computationally expensive and often impractical for model updating. While the high fidelity minimizes modelling bias, detailed FE models still exhibit limitations, particularly in fitting torsional and higher bending modes.

Avci et al. [2] performed deterministic model updating on a 230 m tower using ten modes, including three torsional modes. The updated model showed errors up to 16.4% in torsional modes and 7.4% in bending modes, with notable mismatches in mode shapes, particularly on the lower floors. These discrepancies were likely caused by the simplification of the non-standard joints in the structure. Similarly, Kaynardag et al. [17] updated a 26-storey building using four bending modes in one direction. Although the first mode was fitted perfectly, the second bending mode showed an error of 10.22%. The high weighting (80%) assigned to the first mode contributed to this imbalance, while additional inaccuracies likely arose from modelling shear walls as frame elements instead of more accurate shell elements. The idealised simplification of the effect of the surrounding structures using two lateral springs further introduced model structure uncertainty, contributing to the observed mismatch in mode shapes.

Dong et al. [8] applied Bayesian model updating to a 250 m tower using ten modes, achieving frequency errors below 9%. The largest errors occurred in the x-direction bending modes, likely due to the greater structural complexity and associated modelling uncertainties. Likewise, Liu et al. [19] performed Bayesian updating on a complex twin-tower structure using four modes, including one torsional mode. The torsional mode exhibited a relatively higher error of 7.8%, which was considered acceptable by the authors. A plausible reason for this high error could be due to a higher effect of modelling error on torsional mode compared to bending mode, given the complex geometry of the structure. Nevertheless, the parameter uncertainty was significantly reduced, with a maximum coefficient of variation

(CV) of 6.9%.

Based on the reviewed studies, modelling approaches for high-rise buildings reflect a trade-off between simplicity, accuracy, and computational cost. Analytical beam and shear building models offer efficiency but are limited in capturing higher bending modes, torsional behaviour, and coupling effects. Simplified FE models effectively balance accuracy and efficiency, allowing rotational degrees of freedom, higher-mode fitting, and flexible parameter updating. Detailed FE models provide the highest fidelity but remain computationally intensive and still face challenges with torsional and higher bending modes. Overall, simplified FE models emerge as the most practical choice for vibration-based model updating of complex tall structures. Additionally, an error of 8-9% appears to be inevitable particularly for torsional and higher bending modes.

3.3. New Orleans Tower

The New Orleans is a residential tower in Rotterdam. It is the second highest tower in the Netherlands standing at $158\mathrm{m}$, consisting of 45 floors. The tower is fitted with a permanent monitoring system that includes 4 accelerometers (Sundstrand, type QA-700) located in the 34^{th} floor. In addition to this permanent system, four more accelerometers of the same type were temporarily added to the tower with two accelerometers in 15^{th} floor and two in 44^{th} floor. Using the data of the eight sensors, a study was performed by Bronkhorst et al. [4] wherein the natural frequencies of the New Orleans Tower was monitored for four years, from 2012 to 2015. The primary finding of the study was the first natural frequency, which represents the first bending mode in y direction, showed a significant discrepancy between the design and measured values. The measured frequency (0.28Hz) was about 50% higher than the frequency estimated as per NEN 6702 (0.19Hz). The estimates from NEN-EN 1991-1-4, on the other hand, was about 5% higher (0.30Hz) for the same frequency. These results agreed with what had already been observed in other Dutch high-rise buildings prior to the study. Additionally, a difficulty in estimating the frequencies from the FE model was reported, citing possible causes as inaccurate insitu material property estimation, inadequate modelling of connections, and the influence of foundation and soil. [4]

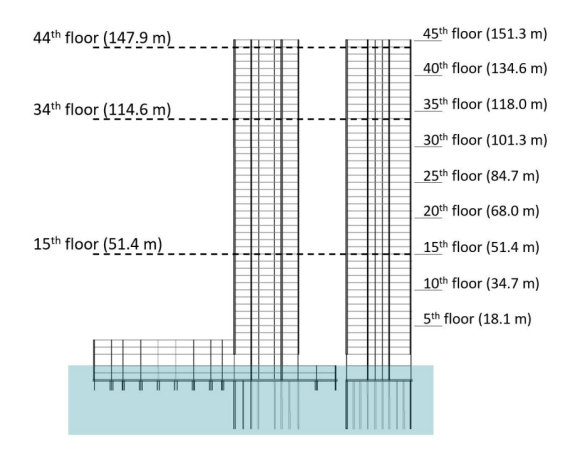


Figure 3.1: Elevation and Side-View of the New Orleans tower depicting the accelerometer positions.

In the subsequent study, 11 modes were identified using the frequency domain decomposition (Table 3.2). Of the 11 modes, modes 1, 2, 4, 5, 7 and 8 were deemed sufficiently identified based on the criteria put forward by Heylen et al. [12] The remaining modes, namely mode 3, 6, 9, 10, and 11 violate this condition, making these modes difficult to distinguish from other lower modes. [5]

Moretti et al. [23] used the results of the above study to estimate the structural properties of the New Orleans tower by using deterministic model updating. The setup of the study involved modelling the tower as a Euler Bernoulli beam in x and y direction, with translational and rotational stiffnesses at the

3.3. New Orleans Tower

Mode	Dominant Direction	Natural Frequency [Hz]
1	y	0.282
2	x	0.291
3	$ heta_z$	0.638
4	x	1.332
5	y	1.527
6	$ heta_z$	2.054
7	x	2.771
8	-	3.560
9	x	4.155
10	-	5.300
11	-	7.250

Table 3.2: Identified modes of New Orleans Tower [5]

foundation. The model updating was performed on all the parameters of the model, namely EI_x , EI_y , K_{tx} , K_{ty} , K_{rx} , K_{ry} and ρ . The model updating was performed on two different cases:

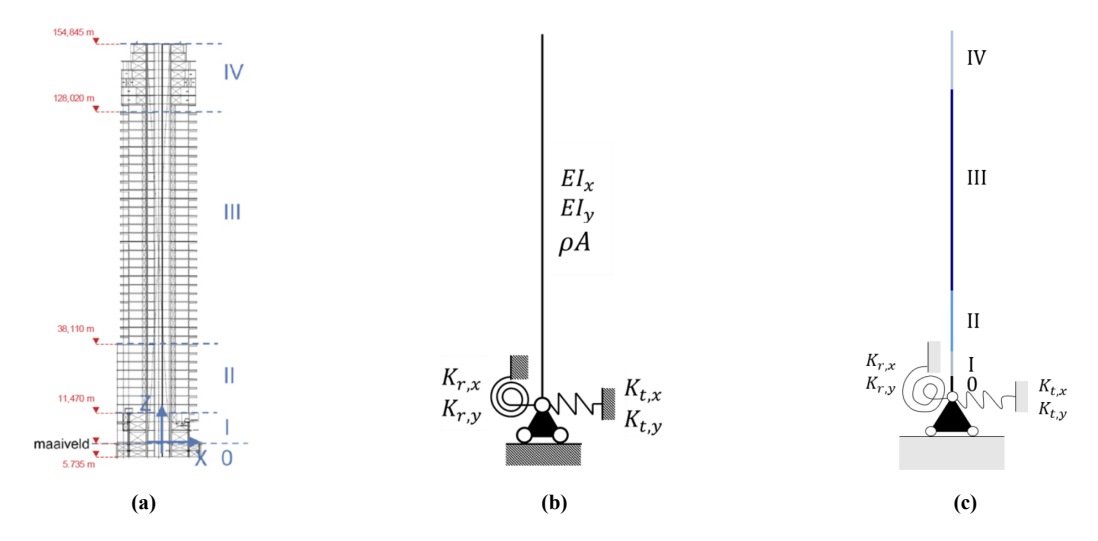


Figure 3.2: (a) Elevation of New Orleans Tower showing different segments, (b) Model of New Orleans Tower by Moretti et al. [23] (c) Model of New Orleans Tower by Ritfeld [27]

- Case 1: Using only two bending modes in x and y direction for model updating,
- Case 2: Using two bending modes in y and three bending modes in x direction for model updating.

Of the two cases, Case 1 resulted in a good fit with the frequencies, while Case 2 showed some error particularly in the first and third bending mode in x direction. The reason for this error was attributed to model simplicity, in that the simplification assumptions applied to construct the model becomes no longer valid to accurately represent these higher modes.

The results of the first case showed that the parameter values obtained from model updating significantly differed from the design values for all parameters except for the equivalent distributed mass ρ . The key result of this study was that the estimates for K_{ry} were quite high compared to the design value, increasing up to a factor of 5.9. The coefficient of variation for this parameter was also quite high at 46.9%. This combined with the result of sensitivity analysis done in the same study suggested that this estimation of K_{ry} may be incorrect. Additionally, the estimates for K_{tx} and K_{ty} suggests that the

previous assumption of fixed conditions in these translational directions at the base may not be valid for higher bending modes.

Ritfeld [27, 28] built upon the works of Moretti et al. [23] by modelling the building now as a discrete Timoshenko beam model in two directions. The model describes the building as a set of Timoshenko beams, called "segments", connected to each other through kinematic and dynamic interface conditions. The key improvement of this approach is it allowed for varying the beam properties across segments caused due to the change in structural configuration between these segments.

The model updating performed in this study was once again deterministic, with the same two cases as the previous study. The parameters selected for updating were EI_x , EI_y , K_{tx} , K_{ty} , K_{rx} , and K_{ry} . As the model has multiple EI values due to multiple segments, the ratio between the different EI values across the segments were kept constant, and all of them were updated simultaneously through a common scaling factor. Despite the added complexity in the model through the inclusion of shear effects and varying stiffnesses across the height, the updating was still not able to fit the third bending mode. Similar to the Euler Bernoulli beam model, accuracy of the first bending mode was compromised when attempting to fit to the third bending mode. When comparing the results from updating using only two bending modes per direction, this study was able to obtain a more reasonable value of rotational stiffness K_{ry} , now having a factor of about 1.2. The coefficient of variation also improved from the previous 49.6% to 6.91%. The results of the two studies have been compiled in Table 3.3.

Parameter	Moretti et al.	Ritfeld
$EI_x \left[\times EI_{x,nom} \right]$	2.68	2.19
$EI_y \left[\times EI_{y,nom} \right]$	3.17	1.98
$K_{tx} [{ m N/m}]$	2.2×10^{9}	1.9×10^{9}
$K_{ty} [{ m N/m}]$	2.85×10^9	2.4×10^9
K_{rx} [Nm/rad]	3.07×10^{12}	2.36×10^{12}
K_{ry} [Nm/rad]	11.1×10^{12}	2.62×10^{12}
$\rho \; [\mathrm{kg/m^3}]$	468.6	-

Table 3.3: Comparison of Deterministic Model Updating by Moretti et al. [23], Ritfeld [27, 28]

While the two studies were successful in estimating the parameters of the New Orleans Tower, they also highlighted three key limitations. The first limitation was that the model updating process did not account for the inherent uncertainties in the models or the measurements, nor did it provide any quantification of uncertainty in the updated parameters themselves. As a result, the calibrated models risk overfitting to the available data, potentially leading to misleading or overly confident conclusions about the structural parameters. The second limitation concerns the interpretability of the parameters themselves. Although the methods provided estimates of the equivalent bending stiffnesses of the beam models, these parameters do not explicitly reveal the source of the discrepancies in the real structure. For example, it remains unclear whether the deviations arise from the modulus of elasticity, the moment of inertia, or other factors such as mass-density of the structure. Finally, the third limitation is the modal data that were not used in the model updating process. The torsional modes and the third bending modes were not used in the updating process, which could have valuable information about the updated parameters.

These shortcomings emphasize the need for more advanced approaches that can incorporate uncertainty in the updating process and provide parameters with clearer physical interpretation. Probabilistic methods, or more refined structural models, may therefore be necessary to obtain results that are not only accurate but also robust and practically meaningful.

Bayesian Model Updating

This chapter outlines the model updating methodology employed in the present study. Section 4.1 provides an overview of Bayesian updating, followed by Section 4.2, which introduces the prior distributions and the guidelines for their selection. Section 4.3 describes the data generation process, while Section 4.4 defines the corresponding likelihood function. Section 4.5 explains the computation of the posterior distribution, and Section 4.6 presents the posterior predictive distribution. Section 4.7 details the error metrics used for comparison, and finally, Section 4.8 illustrates the methodology through a simple example problem.

4.1. Introduction

Bayesian model updating utilizes Bayesian inference together with prior information about the structure and the observed data to make conclusions about the probable properties of the structure. The general equation used for Bayesian model updating is given in Eq 2.4, which is also given below:

$$p(\boldsymbol{\theta}|\mathbf{D}) = c \cdot p(\mathbf{D}|\boldsymbol{\theta}) \cdot p(\boldsymbol{\theta}) \tag{4.1}$$

To calculate the posterior from this equation, it is clear that a choice for the prior and a definition of the likelihood functions is required. These will be explained in the subsequent sections.

4.2. Prior Distribution

The prior distribution, $p(\theta)$, refers to the information already available to the analyst before the data is collected. The choice for prior generally depends on previous experiment results and/or expert opinions. When a specific distribution is not available from a previous uncertainty quantification studies, the principle of Maximum Entropy can be utilized to determine the best choice of prior for the given statistical properties of the parameter [14, 15, 32]. The Maximum Entropy principle dictates the following distributions based on the available information:

 Table 4.1: Prior Selection based on Maximum Entropy Principle

Known information	Assumptions on Prior	
Finite range of values	Uniform Distribution	
Mean and Variance	Normal Distribution	
Log-mean and Variance	Log Normal Distribution	
Positive domain with a known mean	Exponential Distribution	

4.3. Likelihood Function 17

In the cases where the parameter of interest, θ , is more than one, the joint probability distribution $P(\theta)$ needs to be defined. The maximum entropy principle dictates that the parameters be assumed independent unless if correlation is explicitly known. Assuming independence of parameters, the prior distribution for each parameter can be combined into a joint probability distribution as:

$$p(\boldsymbol{\theta}) = \prod_{i=1}^{N_{\theta}} p(\theta_i)$$
 (4.2)

For specific structural parameters, the Joint Research Centre of European Commission has compiled the recommendations on the priors to be used in the absence of project-specific information [26]. These choices will be further discussed in chapter 6.

4.3. Likelihood Function

Before defining the likelihood function, a data generation process must first be established to explain how the observed data may have been produced. This definition serves as a preliminary assumption regarding the relationship between the model output and the experimental data.

To define the data generation process, the finite element (FE) model M is considered a fully deterministic model that takes an input set of parameters (θ, \mathbf{X}) and produces an output of modal properties $\mathbf{D}_M(\theta, \mathbf{X})$. The input set includes a group of unknown parameters θ , which are subject to updating, and another group of parameters \mathbf{X} , which are assumed to be known with certainty and excluded from the updating process.

For simplicity, from here on out, the notation $\mathbf{D}_M(\boldsymbol{\theta}, \mathbf{X})$ will be shortened to $\mathbf{D}_M(\boldsymbol{\theta})$, and it will be implicitly understood that the parameters \mathbf{X} stays constant in the model, and the output of the model only depends on the unknown parameters $\boldsymbol{\theta}$.

Due to the inherent uncertainties in the model, as discussed in section 3.1, any derived quantity will also carry uncertainty. As the FE model is a deterministic model, this uncertainty manifests as a bias term in the output (i.e. modal properties). If $\mathbf{D}_M(\boldsymbol{\theta}_{truth})$ denotes the modal properties obtained from the model, $\boldsymbol{\eta}_M$ the model bias, and \mathbf{D} the true modal properties of the structure, the relationship is expressed as:

$$\mathbf{D} = \mathbf{D}_M(\boldsymbol{\theta_{truth}}) + \boldsymbol{\eta}_M \tag{4.3}$$

Here the subscript, M, denotes model.

Similarly, the measurement of modal properties is considered a random variable \mathbf{D}_E , where the superscript E denotes experimental data. These measurements represent the actual modal properties with an added random error. Let η_E be this error, then the measured data can be written as:

$$\mathbf{D}_E = \mathbf{D} + \boldsymbol{\eta}_E \tag{4.4}$$

By eliminating the true structural behaviour *D* using Eqs. 4.3 and 4.4, the following expression is obtained:

$$\mathbf{D}_E = \mathbf{D}_M(\boldsymbol{\theta_{truth}}) + \boldsymbol{\eta}_M + \boldsymbol{\eta}_E \tag{4.5}$$

It is important to note that η_M is a randomly distributed noise term, while η_M is a bias term, which are, in theory, deterministic in nature.

Equation 4.5 will serve as a starting point for the likelihood definition.

4.3. Likelihood Function 18

The likelihood function relates the observed data with the current model, quantifying how well the current model explains the observed data. Due to this, the likelihood function generally includes some variant of error function that is seen in deterministic model updating.

From Eq. 4.5, the discrepancy between the model predictions and the experimentally derived modal properties represents the combined model and measurement uncertainties.

$$\mathbf{D}_E - \mathbf{D}_M(\boldsymbol{\theta}_{truth}) = \boldsymbol{\eta}_M + \boldsymbol{\eta}_E \tag{4.6}$$

In practice, the value of θ_{truth} is not known a-priori, and only its estimation, θ is known. The goal of the likelihood function is to give a measure of how likely is the available data observed due to the current estimation of θ . This measure is given as a probabilistic value. Simoen et al. (2015) have shown that the likelihood function can be formulated as a probabilistic model of the error terms in absence of information on the individual error observed in the data. [32].

$$p(\mathbf{D}_E|\boldsymbol{\theta}) \equiv p(\mathbf{D}_E - \mathbf{D}_M(\boldsymbol{\theta})|\boldsymbol{\theta}) = p(\boldsymbol{\eta}_M + \boldsymbol{\eta}_E|\boldsymbol{\theta})$$
(4.7)

The data, D_E represents frequencies and mode shapes in this thesis. For frequencies, the above definition stays the same, with **D** being replaced with **f**.

$$\mathbf{f}_E - \mathbf{f}(\boldsymbol{\theta}) = \eta_{\mathbf{f}, \mathbf{M}} + \eta_{\mathbf{f}, \mathbf{E}} \tag{4.8}$$

$$p(\mathbf{f}_E|\boldsymbol{\theta}) \equiv p(\eta_{\mathbf{f},\mathbf{M}} + \eta_{\mathbf{f},\mathbf{E}}|\boldsymbol{\theta}) \tag{4.9}$$

Here, a common choice for the measurement error $\eta_{f,E}$ is to assume that it follows a zero-mean Gaussian error with a diagonal covariance matrix $\Sigma_{f,E}$ with the i^{th} diagonal terms equalling $\sigma_{f_i,E}$. Similarly, the model error, although deterministic in nature, can also be modelled as another zero-mean Gaussian term, with a diagonal covariance matrix $\Sigma_{f,M}$. It is important to note here that the random measurement random noise is generally accepted to follow a Gaussian process [31], the model error is set to follow the Gaussian distribution because its deterministic value is currently unknown. This is different to the measurement error, where the assumption is that the error itself is inherently normally distributed. Further discussion on this point will be done in section 6.4.

For mode shapes, the case studies in this thesis will not consider the effect of the model uncertainty, due to the data showing little deviation from the nominal mode shapes. Due to this, the expression for the r^{th} mode shapes reduces to:

$$\phi_{E,r} - a_r \Gamma \phi_r(\theta) = \eta_{\phi_r, E} \tag{4.10}$$

$$p(\phi_{E,r}|\theta) \equiv p(\eta_{\phi_r,E}|\theta) \tag{4.11}$$

Here, Γ refers to a selection matrix, that picks the degrees of freedom for which the measurement is available. a_r refers to a scaling factor which may be defined as:

$$a_r = \frac{\langle \phi_{E,r}, \Gamma \phi_r(\theta) \rangle}{\| \Gamma \phi_r(\theta) \|}$$
(4.12)

Vanik et al. [34] suggests the use of zero-mean Gaussian distribution for the error in the above formulation, following the justification from the Principle of Maximum Entropy. [34] As each mode shape contains m degrees of freedom, a multivariate Gaussian distribution is proposed, which is represented as follows:

$$\eta_{\phi_n,E} \sim \mathcal{N}_m \left(\mu = \mathbf{0}, \mathbf{\Sigma} = \mathbf{\Sigma}_{\phi_n} \right)$$
(4.13)

4.4. Mode Matching

The suggested definition of covariance matrix, Σ_{ϕ_r} , is a diagonal matrix with all terms equal to $\delta_r^2 \|\phi_{E,r}\|^2$ with δ_r^2 being defined as: [34]

$$\delta_r^2 = \frac{1}{N_s} \sum_{i=1}^{N_s} \frac{\|\phi_{E,r}^{(i)} - \bar{\phi}_{E,r}\|^2}{\|\phi_{E,r}^{(i)}\|^2}$$
(4.14)

where,

 N_s : number of measurements used

 $\phi_{E,r}^{(i)}$: r^{th} mode shape of measurement i

 $ar{\phi}_{E,r}$: mean measured mode shape of mode r

 $\|\cdot\|$: vector norm (typically Euclidean)

The above defined likelihood functions for frequency and mode shapes compute the likelihood for each mode r and one instance of measurement. To use in the Bayesian model updating, the likelihood has to be calculated for all the modes and for all the available measurement data. In order to combine the frequency and mode shape likelihood, an assumption is made that the frequencies are independent of mode shapes and vice versa. To combine the likelihood over all the measurements, an additional assumption that the measurement are independently and identically distributed is made. These assumptions allow us to combine all the likelihood in the following manner:

$$p(\mathbf{D}_E|\boldsymbol{\theta}) = \prod_{k=1}^{N_s} \prod_{r=1}^{N_m} p(f_E^{(r,k)}|\boldsymbol{\theta}) \cdot p(\boldsymbol{\phi_E}^{(r,k)}|\boldsymbol{\theta})$$
(4.15)

where,

 N_s : number of measurements used N_m : number of modeshapes used

4.4. Mode Matching

In Bayesian model updating, computing the likelihood function requires first calculating the observed error between the model and the measured frequencies and mode shapes. It is crucial that this error is calculated for corresponding modes, that is, the first bending mode in the x direction from the measurement must be compared with the first bending mode in x from the model, and so on. While this may seem trivial, in symmetric buildings where modes are closely spaced, mode switching can occur as model parameters change, causing the previously first mode to appear as the second, and so on. To avoid misleading likelihood values and ensure proper convergence, a *mode matching* process is necessary.

The mode matching process pairs measured modes with their most likely counterparts in the model. Various approaches exist, using frequencies, mode shapes, or both [22]. In this thesis, a novel method is developed that primarily uses the *modal participation mass ratio* (MPM) to classify and match modes. The MPM quantifies the fraction of total mass mobilized in each mode, considering contributions in three translational and three rotational directions. Based on which mass components are activated, the algorithm can classify modes as bending in x or y, torsion, axial, or mixed, providing a physically meaningful basis for pairing with measured modes.

The proposed method requires the following assumptions to be valid:

• The measured modes are pure global modes in bending, torsion or axial compression.

- The order of the measured modes are known a-priori.
- There is no missing mode in the measurements. For example, bx_{n-1} must exist in the measurement mode list before b_n for all considered n. Similar condition applies for the other types of modes $(by_n \text{ and } t_n)$

In practice, these conditions are generally met for the lower modes of high-rise buildings, which supports the practical applicability of the method. The algorithm begins by classifying the modes obtained from the model into four categories: bx, by, t, and "unidentified/mixed" modes. For the simpler case, where no unidentified or mixed modes are present, the procedure continues as follows. The classified modes are first arranged in ascending order of their modal frequencies. The measured modes are then read sequentially from their ordered list, starting with the lowest mode. Each measured mode is paired with the first unpaired model mode of the same type from the ordered list. Once a model mode has been paired, it is removed from the list to prevent reassignment. This approach naturally ensures that paired modes of the same type maintain the order of appearance in both the measured and model datasets. In cases where mixed modes are present in the model, the algorithm becomes more involved; the extended procedure is described in Appendix C.

The main advantages of this approach are as follows:

- It establishes a clear one-to-one correspondence between measured and model modes, preventing duplication and reducing mismatches.
- It is less sensitive to errors or ambiguities that arise from sparse sensor distributions, which can
 mislead traditional methods based on modal assurance criterion (MAC) or weighted error functions.
- It does not require arbitrary weighting factors, unlike traditional error-based approaches.

This algorithm does have limitations. Missing modes in the measurements can propagate errors for all modes of the same type. Local modes are less accurately classified since the method relies on global mass participation and mode direction. Mixed modes in the measurement data can also pose challenges, though these can be addressed with relatively minor adjustments in the algorithm.

The full step-by-step procedure, including equations for MPM calculation, is provided in Appendix C. In summary, the proposed method enables robust classification and matching of modes, which is a crucial prerequisite for accurate likelihood computation and reliable model updating.

4.5. Posterior Distribution

With the prior and likelihood distributions defined, the posterior distribution can be obtained based on Eq. 4.1. The calculation of the constant term, c, requires solving the following integral:

$$c^{-1} = \int_{D} p(\mathbf{D}|\boldsymbol{\theta}) \cdot p(\boldsymbol{\theta}) \cdot d\boldsymbol{\theta}$$
 (4.16)

Often, the parameter set θ contains multiple parameters, leading to high-dimensional integrals when evaluating this constant [32]. To address this computational challenge, sampling-based methods are typically employed. One of the most widely used approaches is the Markov Chain Monte Carlo (MCMC) method.

MCMC has the useful property of sampling directly from the posterior distribution. Consequently, with a sufficient number of samples, the statistical properties of the samples will reflect those of the posterior, and their histogram provides a reasonable visualization of its shape [32]. This eliminates the need to explicitly evaluate the constant term c. The theoretical background and working principle of the MCMC process are outlined in Appendix D.

In this research, the MCMC process was implemented using the open-source Python module emcee, which provides an efficient and flexible implementation of MCMC as proposed by Goodman & Weare [10, 11]. The module offers a practical abstraction for implementing MCMC without requiring in-depth knowledge of the underlying algorithmic details, such as the choice of proposal distributions or type of moves.

The class <code>emcee.EnsembleSampler()</code> initializes the MCMC process. It requires the number of walkers, the number of parameters, and the function used to evaluate the log-posterior. After initialization, the MCMC is executed through the <code>run_mcmc()</code> method, which additionally requires the initial state of the walkers and the number of steps to be performed.

Walkers are independent sampling entities that traverse the parameter space following the rules of the MCMC algorithm. They collectively explore the posterior distribution. The recommended minimum number of walkers is twice the number of parameters [25], although in practice, a factor of ten is commonly used to ensure adequate coverage of the parameter space.

The initial state of the walkers must be selected carefully to ensure that each walker starts from distinct locations in the parameter space to avoid internal errors in the sampler. Furthermore, it is recommended for the initial states to span the plausible parameter domain to promote efficient exploration. Sampling the initial states randomly from the prior distribution often suffices these criteria, and hence the same will be done in this thesis.

The number of steps determines how long the walkers explore the parameter space. Typically, this number is large, often on the order of 10,000 or more, to allow the sampler to reach convergence. If convergence is not achieved within the initially chosen number of steps, the sampling process can be extended.

Alternatively, the convergence of the MCMC can itself be used as the stopping criterion. Foreman-Mackey et al. [10] recommend using the integrated autocorrelation time, τ_f , as a convergence metric, defined as:

$$\tau_f = \sum_{\tau = -\infty}^{\infty} \rho_f(\tau) \tag{4.17}$$

Here, $\rho_f(\tau)$ represents the normalized autocorrelation function of the stochastic process that generated the chain f. The integrated autocorrelation time measures the persistence of correlation between successive samples, essentially quantifying how many subsequent states are influenced by the current state. Therefore, for a chain of length N, approximately N/τ_f samples can be considered statistically independent. A chain is generally considered to have converged if its total length exceeds $50 \times \tau_f$ [10]. This criterion was adopted in this research to determine convergence. For more information on this, the reader is encouraged to the sources [10]

After sampling, it is necessary to discard the initial portion of the chains where the sampler is still exploring the parameter space, as these early samples may bias the posterior statistics. This initial region is known as the burn-in period. In this thesis, the first $4 \times \tau_f$ samples of each chain were discarded as burn-in. This ensures that the retained samples are independent of the starting conditions and represent valid draws from the converged posterior distribution. An example of a converged MCMC chain with its burn-in period is shown in Figure 4.1.

The MCMC process typically involves hundreds of thousands of model evaluations before convergence. Even when each model computation takes less than a second, the total runtime may extend to several hours. The emcee module supports parallelization, which can significantly reduce computation time. However, this functionality was not utilized in the present study due to compatibility issues between emcee and the openseespy module used for structural modelling.

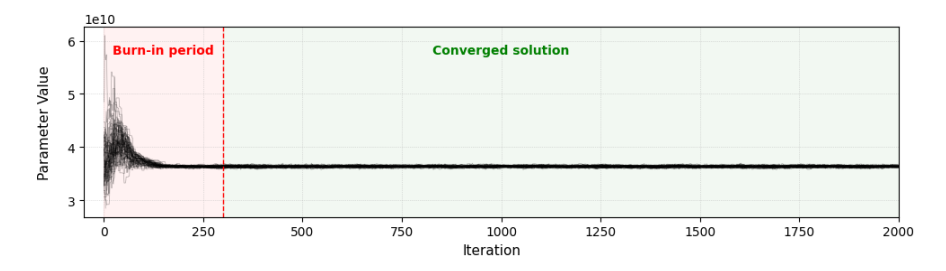


Figure 4.1: An example of converged MCMC Chain with burn-in period

Once the posterior samples are obtained, the most likely value of each parameter can be determined through the Maximum A Posteriori (MAP) estimate, which corresponds to the mode of the joint posterior distribution. It should be noted that the MAP value is derived from the joint posterior, not from individual marginal distributions. Therefore, the MAP estimate may not coincide with the peak of any single parameter's marginal posterior. The MAP value can be computed by constructing a histogram in the multidimensional parameter space and identifying the bin with the highest count.

4.6. Posterior Predictive Distribution

The posterior distribution gives us the distribution of the parameters being investigated after incorporating the information from the priors and the data. This distribution, although very useful for parameters, is not enough to predict the frequencies and mode shapes of the structure. The main reason behind this is that the exact value of θ is still unknown. To obtain the distribution of frequencies and mode shapes, it is then required to integrate over all the possible values of θ based on the posterior distribution. In other words, this requires us to solve for the following integral:

$$p(\tilde{\mathbf{D}}|\mathbf{D}_E) = \int p(\tilde{\mathbf{D}}|\boldsymbol{\theta}) \cdot p(\boldsymbol{\theta}|\mathbf{D}_E) d\boldsymbol{\theta}$$
 (4.18)

Here, $\tilde{\mathbf{D}}$ refers to the predicted modal properties and $p(\tilde{\mathbf{D}}|\mathbf{D}_E)$ is the posterior predictive distribution. Evaluating this integral poses problems, especially with the absence of closed form expression for the posterior. To overcome this, a numerical approximation is obtained with a Monte Carlo approach, through the following expression:

$$p(\tilde{\mathbf{D}}|\mathbf{D}_E) \approx \frac{1}{N} \sum_{i=1}^{N} p(\tilde{\mathbf{D}}|\boldsymbol{\theta}^{(i)})$$
 (4.19)

Here, $\theta^{(i)}$ refers to the samples generated from the posterior distribution. To construct a probability distribution function from the above equation, it will be required to evaluate the expression for all $\tilde{\mathbf{D}}$ values. An alternative to this would be to generate the samples of \mathbf{D}_E from the conditional distribution directly for every $\boldsymbol{\theta}^{(i)}$.

This arises from the fact that, even if the model is calibrated to represent the real structure, the measured frequencies and mode shapes inherently contain measurement errors. Consequently, when predicting the frequencies and mode shapes that may be observed from the structure, these measurement errors must be incorporated into the model predictions. Applying this process to the posterior distribution yields the *posterior predictive distribution*, which, as the name suggests, possesses predictive capabilities.

4.7. Error Metrics

In order to evaluate the results of Bayesian model updating, various metrics are employed to compare their predictions with measured data. Specifically, both frequencies and mode shapes are assessed using

appropriate statistical and error measures.

For comparing model-predicted and measured frequencies, the statistical mode (maximum count) of the frequency samples is used. The mode is computed by constructing a histogram in the n-dimensional sample space, where n is the number of modes. The error metric employed is the absolute relative percentage error.

Nominal Error (%) =
$$\frac{|f_{\text{init}} - f_{\text{meas}}|}{f_{\text{meas}}} \times 100\%$$
 (4.20)

Prediction Error (%) =
$$\frac{|f_{\text{ppd}} - f_{\text{meas}}|}{f_{\text{meas}}} \times 100\%$$
 (4.21)

For comparing updated frequency results from Bayesian and Deterministic model updating, the Continuous Ranked Probability Score (CRPS) is used. This metric accounts for both the spread of the predictions and any bias, penalizing high uncertainty and high deviation. Comparisons are made with the statistical mode of the measured frequencies, with the CRPS defined as in Eq. 4.22 for Bayesian results and Eq. 4.23 for Deterministic results. [16]

$$CRPS(f_{ppd}, f_{meas}) = \frac{1}{N} \sum_{i=1}^{N} |f_{ppd,i} - f_{meas}| - \frac{1}{2N^2} \sum_{i=1}^{N} \sum_{j=1}^{N} |f_{ppd,i} - f_{ppd,j}|$$
(4.22)

$$CRPS(f_{det}, f_{meas}) = |f_{det} - f_{meas}|$$
(4.23)

where

 $f_{\text{ppd},i}, f_{\text{ppd},j} = i^{\text{th}}$ and j^{th} samples of the posterior predictive distribution (PPD) of f,

N = number of PPD samples.

 f_{det} = frequency predicted in deterministic model updating

The CRPS has the same units as frequency [Hz] and can also be expressed as a percentage for easier comparison (Eq. 4.24) [16].

$$CRPS [\%] = \frac{CRPS [Hz]}{f_{meas}} \times 100\%$$
 (4.24)

For mode shape comparison, posterior predictive mode shapes are compared with the measured mode shapes by selecting those that best represent the mean displacement across all degrees of freedom. The comparison is performed using the Modal Assurance Criterion (MAC), with the i^{th} mode shape calculated as per Eq. 4.25.

$$MAC(\phi_{ppd,i}, \phi_{meas,i}) = \frac{\left(\phi_{ppd,i}^{T} \phi_{meas,i}\right)^{2}}{\|\phi_{ppd,i}\|^{2} \|\phi_{meas,i}\|^{2}}$$
(4.25)

4.8. Example Problem: Verification of Bayesian Updating Routine

The Bayesian Updating Routine developed for this thesis is first verified with a simple double pendulum, before applying it to the building model. The double pendulum provides a simplistic model, that can be determined analytically, while still having a level of complexity associated with it.

4.8.1. Problem Formulation

For the double pendulum, a small vibration assumption is considered, which allows us to express the equation of motion in the linear form as follows:

$$\mathbf{M}\ddot{\mathbf{X}} + \mathbf{K}\mathbf{X} = \mathbf{0} \tag{4.26}$$

Here,

$$\mathbf{X} = \begin{bmatrix} x_1 \\ x_2 \end{bmatrix} \tag{4.27}$$

$$\mathbf{M} = \begin{bmatrix} (m_1 + m_2)l^2 & m_2l^2 \\ m_2l^2 & m_2l^2 \end{bmatrix}$$
 (4.28)

$$\mathbf{K} = \begin{bmatrix} g(m_1 + m_2)l & 0\\ 0 & gm_2l \end{bmatrix} \tag{4.29}$$

Solving the eigenvalue problem, the two natural frequencies will be expressed as:

$$f_{1,2} = \frac{1}{2\pi} \sqrt{\frac{g(m_1 + m_2 \mp \sqrt{m_2(m_1 + m_2)})}{lm_1}}$$
(4.30)

Similarly, the two mode shapes are then given by:

$$\phi_{1,2} = \begin{bmatrix} -1 + \frac{4\pi^2}{f_{1,2}^2} \cdot \frac{g}{l} \\ 1 \end{bmatrix}$$
 (4.31)

Some key insights to note from these equations are that Eq. 4.30, the two natural frequencies are dependent on the ratio $\frac{m_2}{m_1}$. Eq. 4.31 suggests that the mode shapes are independent of the length, l.

To study how Bayesian routine works, and to also check the sanity of the method, following two example cases were investigated.

Example 1: The two masses, m_1 and m_2 , are chosen as updating parameters.

Example 2: Mass m_2 and length l are chosen as updating parameters.

It is important to note that the choice of the parameters do not have any physical significance in this study in terms of real-life uncertainty.

To perform the analysis, it is required to have a data-generation process, which mimics the actual measurement data. For this, the error is introduced in the true frequency and measurement as per the Eq. 4.9 and Eq. 4.11. The model uncertainty in frequency was omitted for the sake of simplicity.

4.8.2. Model Truths

The truth values for the pendulum system are listed in Table 4.2. To simulate the measurement data, a zero-mean normally distributed error was introduced with a coefficient of variation, $CV_{\eta}=0.05$. With these errors, 10 different measurement points were generated. The same coefficient of variation was used for both error in frequencies and mode shapes.

Parameter	Value
m_1	4.5
m_2	6.8
L	3.2

Table 4.2: Model Truth for the Double Pendulum System

4.8.3. Pendulum Example 1: Updating m_1 and m_2

For the first case, the two masses were chosen as updating parameters. For the choice of prior, two uncorrelated normal distributions centred around the true value with a coefficient of variation $CV_{\theta}=0.2$ was chosen.

The result of Bayesian model updating on this problem is shown in figure 4.2.

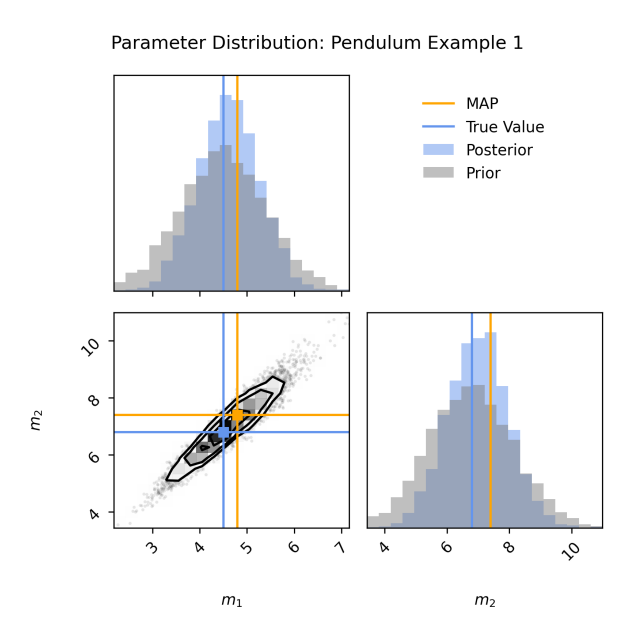


Figure 4.2: Probability Distributions for Pendulum Example 1

From Figure 4.2, a strong correlation between the posterior distributions of m_1 and m_2 is clearly evident, with a correlation coefficient of approximately 95%. This is expected, given that the system's frequencies are primarily governed by the ratio $\frac{m_2}{m_1}$. As a result, precise knowledge of one mass effectively eliminates the uncertainty in the other. This relationship is further supported by the observed ratio of the masses in the region, approximately $\frac{6.8}{4.5}=1.51$. The method's ability to reveal such correlations is particularly valuable when applied to more complex models, where such interdependencies may not be as immediately apparent.

From the figure, it is also clear that the marginal uncertainty (the two histograms) in each parameter did not change significantly. This can once again be attributed to the choice of parameters, particularly because the modal properties depend on the ratio of the selected parameters. Although the marginal uncertainty of each parameter did not appear to decrease, the total uncertainty was reduced from an initially independent distribution to a narrower, correlated one.

4.8.4. Pendulum Example 2: Updating m_2 and l

For the second case, the m_2 and l were chosen as updating parameters. All other input parameters were kept same as previous. The results are shown in figure 4.3a and Table 4.3.

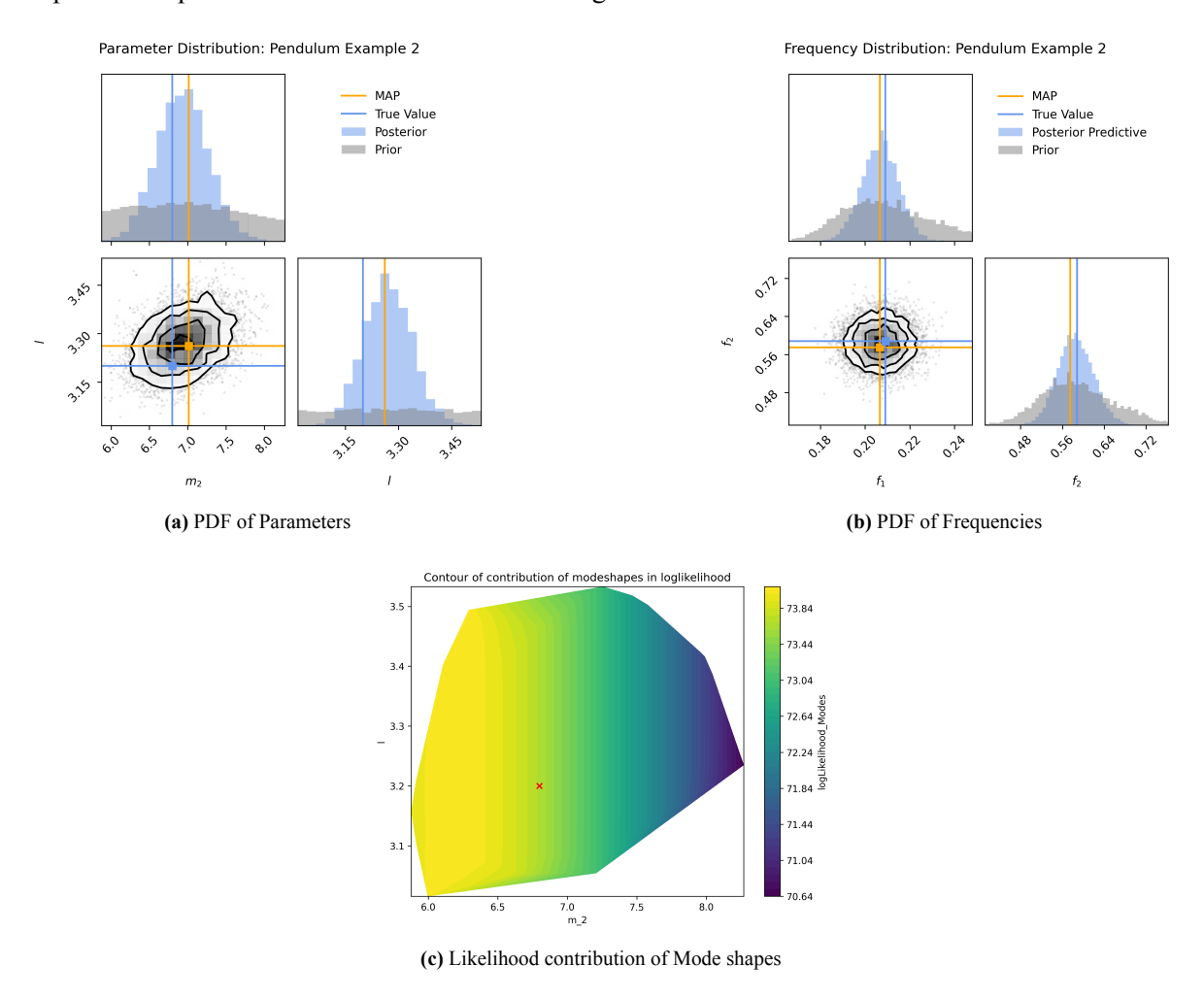


Figure 4.3: Probability Distributions for Pendulum Example 2

Here, the two posterior probabilities do not show any correlation. This is again expected, as neither the frequency nor the mode shapes show any dependence on the ratio of m_2 and l. Figure 4.3c shows the contour of the log-likelihood components of frequency and mode shapes. An interesting observation here is that the log-likelihood contribution of mode shapes are parallel to the y-axis, suggesting that the parameter l does not influence the likelihood of observing a mode shape. From Eq. 4.31, it is evident that the mode shapes are independent of l, validating this observation.

The results in Table 4.3 show that the method was able to reduce the uncertainty in parameter by a factor of $\sim 5-10$. Similarly, the uncertainty in frequency was reduced by a factor of ~ 10 and for mode shapes this reduction was by a factor of $\sim 2-4$. Further reduction in uncertainty is possible if the number of measurement points, i.e. the available data, is increased. The error metric for the posterior of parameters is worse in this case. However, this result is due to the choice of the prior distribution, which is centred around the true solution. In reality, the true solution is not known, and it is unlikely that the initial distribution is centred around the truth. Therefore, in real cases, the error is expected to reduce. For the modal properties, the error metric is already good for the prior, which again is due to the choice of the prior. Due to this, the posterior error does not see significant improvement. The mode shapes show almost perfect match in posterior.

Table 4.3: Prior and Posterior comparison for Pendulum case 2

	Erroi	· metric	(CV .
Parameter/Property	Prior	Posterior	Prior	Posterior
l	0%	3.14%	20%	4.77%
m_2	0%	1.92%	20%	2.08%
f_1	1.7%	1.08%	11.1%	1.12%
f_2	1.28%	0.12%	13.0%	1.63%
$oldsymbol{\phi}_1$	99.07%	99.99%	$\begin{bmatrix} 2.87\% \\ 1.66\% \end{bmatrix}$	$\begin{bmatrix} 0.79\% \\ 0.48\% \end{bmatrix}$
ϕ_2	98.99%	99.99%	$\begin{bmatrix} 2.87\% \\ 1.66\% \end{bmatrix}$	$\begin{bmatrix} 1.57\% \\ 0.95\% \end{bmatrix}$

As the expected results are obtained in the two example problems, the Bayesian updating routine is validated for the simple case.

Model Development: New Orleans Tower

This chapter presents the development of the structural model used for parameter estimation of the New Orleans Tower. Previous studies primarily relied on analytical beam models, which could not account for torsional displacements or higher bending modes without compromising the accuracy of the lower modes. To address these limitations, this thesis uses a simplified 3D FE model. The model is designed as a lumped-mass stick representation, capturing structural behaviors that were previously neglected, such as shear and torsional deformations. This approach strikes a balance between including sufficient complexity to utilize additional modal data (for example, torsional modes) and keeping the computational cost low, which is important for procedures like Bayesian model updating. The following sections describe how the procedure for constructing the model, and the values used for developing the simplified FE model of the New Orleans Tower.

5.1. Model Requirements

To build a simplified 3D FE model, several information about the building is required. These information may be obtained directly from the design documents, or there may be some derivations required from the available data. The required information for constructing the model are as follows:

- 1. Nodal coordinates of centre of stiffness, centre of mass, and location of sensors
- 2. Elemental properties, $(E, G, A, I_{xx}, I_{yy}, J, f_x, f_y)$ for each storey
- 3. Mass and Rotational Mass for each storey
- 4. Boundary conditions, and restraints

5.2. Modelling Theory

The current approach of modelling the high-rise building as a lumped-mass stick model was proposed by Liu et al. [20] as a generalised method for modelling a structure with mixed wall-column components. The method utilizes the concept of a macro beam element to represent each storey [20]. A theoretical formulation of the model parameters is given here.

First, the total area A of the vertical members, as well as the centroid of these members considered together are determined. The area is calculated as the sum of all the cross-section of the vertical stiffness

members.

$$A = \sum A_i \tag{5.1}$$

Using this, the centroid, (x_c, y_c) , of the vertical elements can be determined by the general formula:

$$x_c = \frac{\sum x_i A_i}{A}, \quad y_c = \frac{\sum y_i A_i}{A} \tag{5.2}$$

Next, to estimate the equivalent moment of inertias about the calculated centroid, I_{xx} and I_{yy} , Steiner's rule is used. It is important to note that when using this rule, no assumptions about the individual vertical members are made.

$$I_{xx} = \sum I_{xx,i} + A_i(y_c - y_i)^2, \quad I_{yy} = \sum I_{yy,i} + A_i(x_c - x_i)^2$$
 (5.3)

To determine the nodal coordinates of centre of stiffness, first the storey stiffness contribution of each vertical member, as well as the total storey stiffness need to be determined. To determine this stiffness, first a few assumptions about the structure needs to be made. As the high-rise structure has a concrete slab, the in-plane stiffness of the slab is sufficiently high as compared to the lateral stiffness of the vertical elements, allowing us to apply the rigid diaphragm assumption. This assumption states that the floor experiences a rigid body motion. Additionally, the connection between the vertical members and the floor are also assumed to be rigid as a part of the rigid diaphragm assumption. Under these assumptions, the equivalent storey stiffnesses k_x and k_y are estimated as:

$$k_x = \sum k_{x,i} = \sum \frac{12EI_{yy,i}}{H^3(1 + \varphi_{x,i})}$$
 (5.4)

$$k_y = \sum k_{y,i} = \sum \frac{12EI_{xx,i}}{H^3(1 + \varphi_{y,i})}$$
 (5.5)

Here, H represents the storey height. The factors $\varphi_{x,i}$ and $\varphi_{y,i}$ account for the shear deformation in the x and y directions for the vertical member i. They are calculated as:

$$\varphi_{x,i} = \frac{12EI_{yy,i}}{H^2GA_{sx,i}}, \quad \varphi_{y,i} = \frac{12EI_{xx,i}}{H^2GA_{sy,i}}$$
(5.6)

 $A_{sx,i}, A_{sy,i}$ are the shear areas defined for the i-th element in the x and y directions, respectively.

The determination of stiffnesses allows us to incorporate the effects of torsion. For this, the centre of stiffness for each level needs to be calculated with the following relations:

$$x_s = \frac{\sum k_{x,i} x_i}{k_x}, \quad y_s = \frac{\sum k_{y,i} y_i}{k_y} \tag{5.7}$$

For structures with shear wall, it is recommended to determine the torsional stiffness through the "stiffness centre method" as follows: [20]

$$k_{\theta} = \sum \left[k_{xi} (y_i - y_s)^2 + k_{yi} (x_i - x_s)^2 \right]$$
 (5.8)

From the torsional stiffness, the torsional constant, J, can then be derived with the following relation:

$$J = \frac{k_{\theta}H}{G} \tag{5.9}$$

Next, we require the storey element to also represent shear deformations. The shear deformations are considered through the shear shape factor in an FEM software. The use of shear shape factor is to get the shear area from the cross-sectional area as follows:

$$A_{sx} = \alpha_x A, \quad A_{sy} = \alpha_y A \tag{5.10}$$

To get this factor, k_x and φ_x can be used, which has similar formula as for the individual i^{th} member as Eq 5.6, 5.4. Substituting A_{sx} from Eq 5.10, we can get α as follows:

$$\alpha_x = \frac{12EI_{yy}}{GAH^2} \cdot \left(\frac{12EI_{yy}}{k_x H^3} - 1\right)^{-1} \tag{5.11}$$

Similarly, for α_y

$$\alpha_y = \frac{12EI_{xx}}{GAH^2} \cdot \left(\frac{12EI_{xx}}{k_y H^3} - 1\right)^{-1} \tag{5.12}$$

It is important to note here that all the quantities in Eq 5.11 and 5.12 are equivalent quantities for the storey, and not for any one individual element. Furthermore, in the case of multiple elements with different material properties in a given floor, the equivalent E for the storey property can be chosen as the material of the elements that dominates the stiffness. For the current case, the elastic modulus of concrete is taken as the equivalent E.

In addition to these parameters, it is required to calculate the mass, centre of mass and the rotational masses of each floor. The mass is considered as follows:

$$M = \text{Self Wt.} + \text{Permanent Load} + 0.3 \times \text{Variable Load} + \text{Facade Load}$$
 (5.13)

For the self weight, the mass of the slabs, beams, and 50% of the mass of the vertical elements above and below the slab were considered. The mass deduction due to openings in the slab were also considered.

Similarly, the rotational masses are also considered for torsion, i.e. $I_{\theta,zz}$. To determine this, all the same elements used in the mass calculation were also used. The effect of permanent and variable load on the rotational mass was incorporated in the form of uniformly distributed additional mass on the slab.

Rotational masses in the other two directions, i.e. $I_{\theta,xx}$ and $I_{\theta,yy}$, were not considered.

The calculated masses and rotational masses per floor were applied to the centre of mass of the storey. The centre of mass is determined via the following formula:

$$x_m = \frac{\sum m_i x_i}{M}, \quad y_m = \frac{\sum m_i y_i}{M} \tag{5.14}$$

5.3. Model Description: New Orleans

In this thesis, a case study on the *New Orleans Tower* located in Rotterdam, will be performed. The tower is $158.4~\mathrm{m}$ tall and is used for residential purposes. A picture of the high rise, along with its design FE model and the simplified FE model used in this study is shown in Figure 5.1

The FE model for this thesis is built by determining the equivalent storey properties as outlined in the previous section. The model consists of nodes at centre of stiffnesses, centre of masses and the location of measurements. The open-source module openseespy in Python was used to develop the model. This model is then compared with a design detailed FE Model developed in SCIA by Besix, as well as the measured mode shapes.

Stiffness Calculations

The centre of stiffnesses are used to make the vertical part of the model. The nodes are created at the centre of stiffness due to all the considered vertical stiffness members between the j^{th} and $(j+1)^{th}$. The two vertically adjacent centre of stiffness nodes are then connected via an elastic beam member, whose equivalent properties are determined as described in the previous section. For the stiffness calculations,





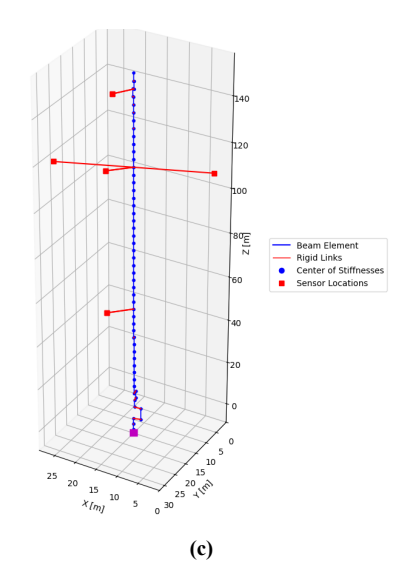


Figure 5.1: (a) New Orleans Tower, (b) Detailed SCIA Model provided by Besix, (c) Opensees Model constructed for the current study

the contribution of the columns and shear walls are considered. Fig 5.2a and 5.2b show the members considered for the stiffness calculation at two typical cross-sections.

In case if the centre of stiffnesses of the two adjacent stories do not share the same (x, y) coordinates, then these centre of stiffnesses, at the same elevation, are connected via a rigid beam element.

Mass Calculations

For the mass calculation, the beams, columns, walls and the floor slabs were considered. The openings in the slabs were deducted to ensure a sense of reality. Figure 5.2c show a typical cross-section with beams being considered, and Figure 5.2d show the openings that have been deducted from the mass calculations.

In addition to the mass, the effect of loads were also considered to have an effect in the form of additional mass. For this, the permanent loads, variable loads and facade loads were considered as per the original design. The details of these loads are given in Table 5.1. The loads were converted from $[kN/m^2]$ to [kg] using appropriate factors to ensure consistent dimensionality.

Load Name	Symbol	Value	Unit	Applied over
Permanent Load	q_p	1	$\mathrm{kN/m^2}$	Slab Area
Variable Load	q_v	1.75	$\mathrm{kN/m^2}$	Slab Area
Facade Load	q_f	1	$\mathrm{kN/m^2}$	Storey Perimeter, distributed 50% between upper and lower storey level

Table 5.1: Load Details

These masses are added to the centre of masses at every level, which are connected with the centre of stiffnesses via a rigid beam element.

Boundary Conditions

Table 5.2 describes the boundary conditions applied to the structure. The sign convention for the foundational stiffnesses are outlined in Figure 5.3. The design values for the translational stiffnesses, K_{tx}

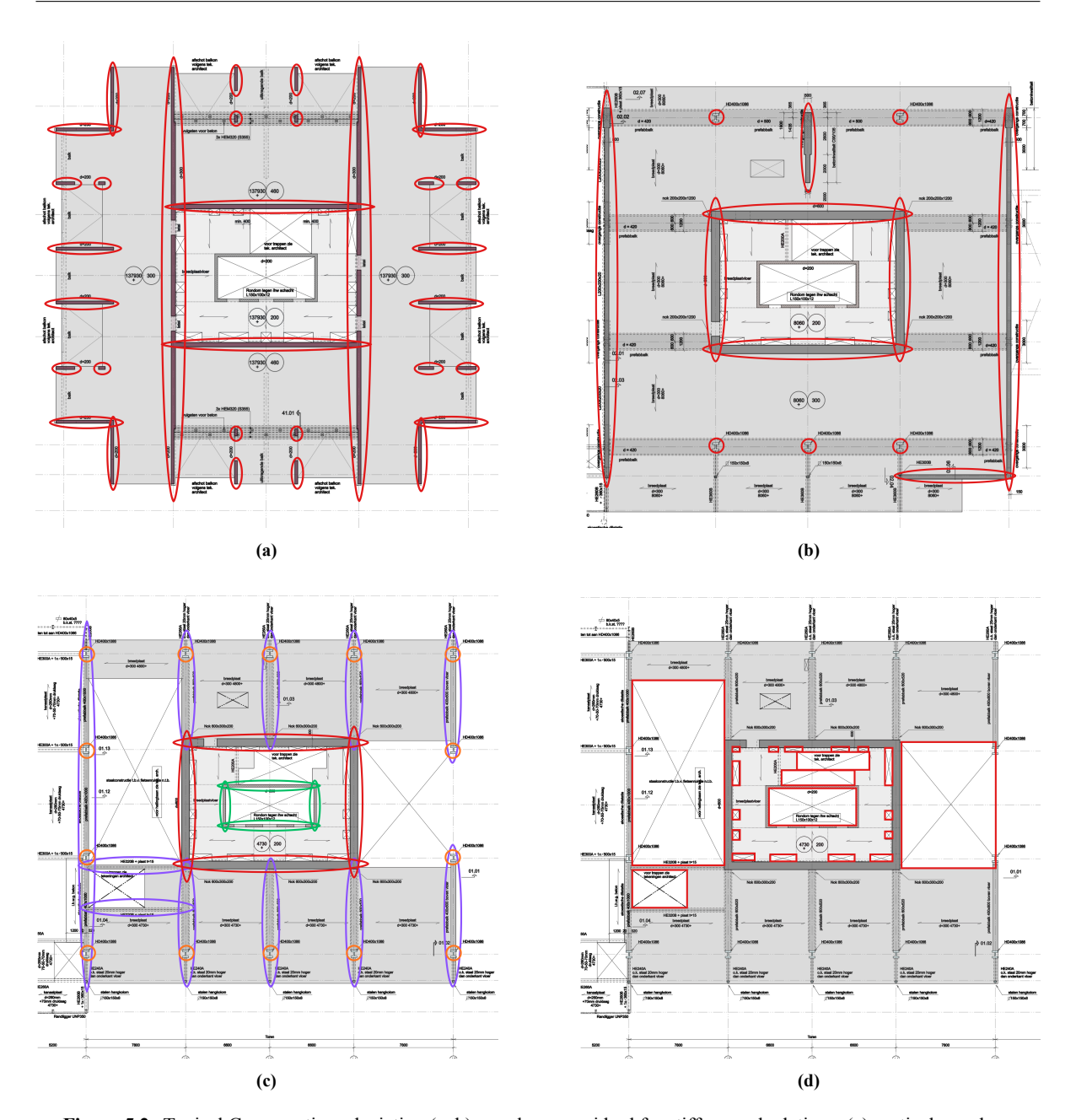


Figure 5.2: Typical Cross sections depicting (a, b) members considerd for stiffness calculations, (c) vertical members considered for mass calculation, (d) openings deducted from mass calculation.

and K_{ty} , and the rotational stiffnesses, K_{rx} and K_{ry} were provided by Besix. The value of K_{rz} was derived from the design drawings, and more details on this is provided in Appendix B.

Sensor Setup

The tower is fitted with a permanent monitoring system that includes 4 accelerometers located in the 34^{th} floor with 2 sensors that measures in the x-direction and two that measures in the y-direction. In addition to the permanent setup, four additional accelerometers were placed on the 15^{th} and the 44^{th} floors, with one sensor per direction in each floor. The location of these sensors, along with their direction of measurements are outlined in Table 5.3 and their location in cross section is shown in Figure 5.4

As the mode shapes obtained from the measurement represent the modal displacement observed at the

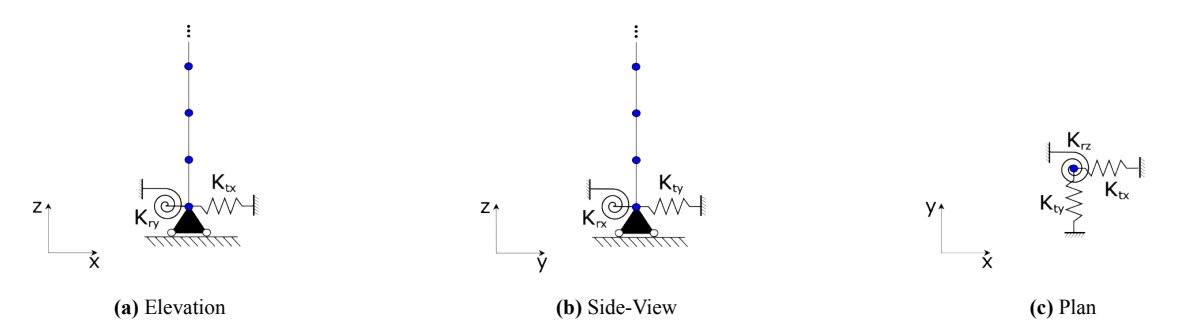


Figure 5.3: Sign Convention for foundational stiffnesses

Table 5.2: Boundary Conditions

Boundary	Туре	Symbol	Value
Translation x	Spring	K_{tx}	$3.1\times10^9\;\mathrm{N/m}$
Translation y	Spring	K_{ty}	$3.1\times10^9~\mathrm{N/m}$
Translation z	Fixed	_	∞
Rotation x	Spring	K_{rx}	$1975\times10^9~\mathrm{Nm/rad}$
Rotation y	Spring	K_{ry}	$1927\times10^9~\mathrm{Nm/rad}$
Rotation z	Spring	K_{rz}	$511\times10^9~\mathrm{Nm/rad}$

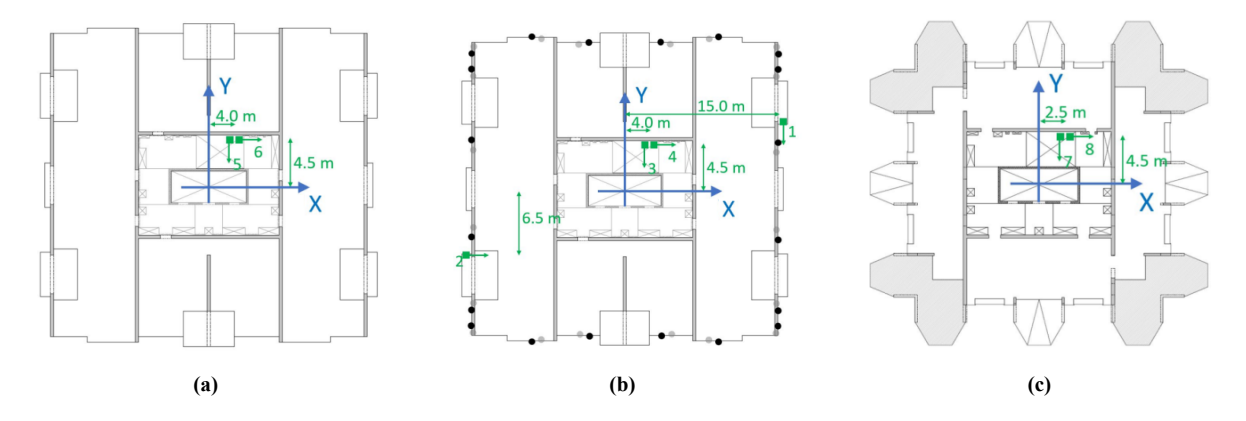


Figure 5.4: Accelerometer layout (green squares) in New Orleans Tower. (a) 15th floor plan (b) 34th floor plan (c) 44th floor plan. Green Arrows indicate measurement direction [5]

sensor location in the direction of measurements, for a fair comparison, it is important to also measure the modal displacements at the sensor locations. For this reason, nodes were added in the sensor locations for obtaining the output of eigenanalysis. These nodes representing the location of sensor measurements are connected to the centre of stiffness at the same level via a rigid beam elements.

5.4. Comparison of Measured and Calculated Modal Properties

When developing any model, it is important to verify the model, ensuring that the developed model accurately represents the original structure, or in this case, the original design model, to the best of the model's ability. In this thesis, the comparison between the first eight natural frequencies and mode shapes is used for the verification purpose. The comparison between the full FE model developed by Besix and the simplified model are outlined in Table 5.4.

Table 5.3: Sensor Positions

S.No.	Measurement Direction	x	y	z
1	x	4	4.5	51.35
2	x	-15	-6.5	114.62
3	x	4	4.5	114.62
4	x	2.5	4.5	147.92
5	y	4	4.5	51.35
6	y	15	6.5	114.62
7	y	4	4.5	114.62
8	y	2.5	4.5	147.92

Table 5.4: Comparison of Detailed FE Model and Simplified FE Model

]	Frequency [Hz]		Error in Simplified Model [%]		
Mode	Measurement	Detailed FE Model	Simplified FE Model	w.r.t. Detailed FE Model	w.r.t. Measurement	
by1	0.281	0.200	0.218	9.00	22.42	
bx1	0.290	0.230	0.237	3.04	18.28	
t1	0.636	0.500	0.961	92.20	51.10	
bx2	1.323	1.250	1.565	25.20	18.29	
by2	1.518	1.020	1.492	46.27	1.71	
t2	2.075	1.550	3.330	114.84	60.48	
bx3	2.778	2.440	3.210	31.56	15.55	
mix	3.558	2.140	3.014	40.84	15.29	

The current simplified model shows good agreement with the detailed FEM model for the first bending modes (by1 and bx1), with errors of 9.0% and 3.0% with the detailed model, respectively. For higher bending modes (bx2, by2, bx3), the discrepancy increases, which may be due to simplifications in the model, such as assumptions on connection stiffness and local properties that start affecting these higher modes.

The torsional modes (t1 and t2) exhibit large errors compared to the detailed FEM model (92.2% and 114.8%), likely due to a lack of information about torsional stiffness at the foundation in the detailed FEM model. In the simplified model, torsional stiffness at the base was derived from pile locations and stiffnesses without directly accounting for soil effects, which could partially explain the observed discrepancies.

While it is important for the simplified model to have a similar frequencies as the detailed FE model, in the end, the two models are simply derived from the same drawings with different assumptions. Without complete information about the detailed model regarding these assumptions and the simplifications made, it becomes difficult to make a conclusive comparison between the two models. In such a case, the comparison with the measurement data provides insight on how well the model represents the real structure.

When comparing with the measurements, the simplified model has similar error levels for all the modes

except the torsional modes and the second bending in y direction. This shows the presence of a consistent error in the model. The high error in torsional mode is likely due to inaccurate assessment of the foundational stiffness, which has many assumptions associated with it (Appendix B). Finally, the second bending mode in y-direction shows a very good agreement with the measurement at only 1.71% mismatch. Similarly, there are also a few modes (by1, bx1, by2) which have better frequency estimation than detailed FE model. This is unexpected as detailed FE model should be more accurate than the simplified models. This counter-intuitive result has also been observed in previous studies (Ritfeld [27]), where simpler models sometimes match measurements better than more detailed FEM models. One possible explanation is that model structure errors in the simplified model partially cancel out model parameter errors, resulting in better agreement with the measured data.

The comparison of the mode shapes for the most common measured mode, the mode from the simplified model and the detailed FE model shows a good match with each other for all modes except the torsional modes and the third bending mode in x-direction. For both the torsional modes, the detailed FE model shows fairly good comparison with the measured modes, while the simplified FE model deviates from both the detailed model and measurement. This is likely due to reasons discussed previously in the mismatch of frequencies. For the mode bx3, while the simplified FE model and the detailed FE model have similar mode shapes, they both significantly differ from the measured mode shape. This suggests the presence of error in both the models, and potentially in the design values themselves.

While the agreement between the simplified FE model and the measurement is a promising result, this also suggests that the mode shapes may not provide a significant information when updating the model.

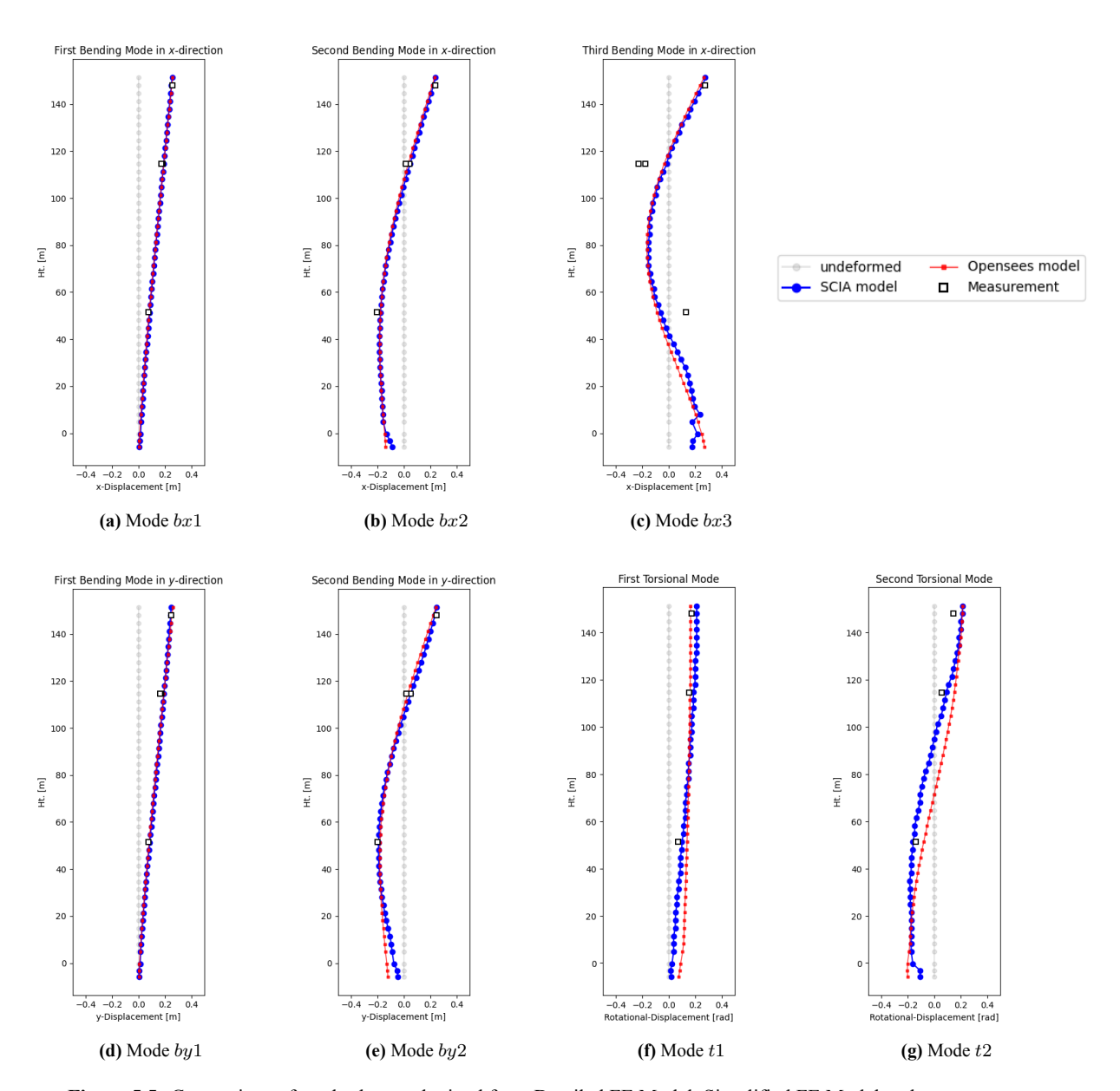


Figure 5.5: Comparison of mode shapes obtained from Detailed FE Model, Simplified FE Model and measurement



Model Updating Configuration and Uncertainty Quantification

This chapter establishes the different settings and configuration to be used for the case study. First, the different candidate parameters are selected in Section 6.1. Then, the appropriate priors are defined in Section 6.2. Section 6.3 describes a sensitivity analysis for updating parameter selection. Section 6.4 discusses the likelihood function formulation. Section 6.5 outlines a synthetic analysis for identifiability of the parameters.

6.1. Candidate Parameters

Based on the created FE model in the previous chapter, it is evident that there are a lot of parameters that control the structure. On the global level, these parameters include the self-weight of concrete, ρ_{conc} , modulus of elasticity of concrete E_{conc} , permanent load, imposed loads, facade loads and the five foundational stiffnesses, K_{tx} , K_{ty} , K_{rx} , K_{ry} , K_{rz} . On the local level, the self-weight, modulus of elasticity, and permanent, imposed and facade loads can be altered for every floor. This leads to countless parameter combinations that can be considered. The choice of sub-structuring, i.e. dividing the structure into smaller sections depends on what is required from the analysis, and what the parameters of interests are. For the current study, substructuring will not be performed, and the analysis will be done on the global scale. Thus, the candidate parameters for updating are ρ_{conc} , E_{conc} , K_{tx} , K_{ty} , K_{rx} , K_{ry} , K_{rz} , permanent load, and imposed loads. The façade load will be left out due to a general high certainty in their determination.

6.2. Prior Selection

For every candidate parameter, we must consider the prior distribution for the parameter that accurately reflects our known information. As discussed in the previous chapter, the principle of maximum entropy provides a rough guideline on what the distributions should be based on the known knowledge. In addition to that there have also been past studies that provide recommendations for the choice of priors.

Table 6.1 lists some of the parameters that are recommended to have a normal or log-normal distributions from the literature. The mean value in the table represents the factor by which the nominal value is multiplied.

From the table above, it is to be noted that the mean value for the distribution is generally centred at nominal value. However, for the self weight of concrete, this recommended mean is 1.05 times the nominal value. The reason for introducing a 5% bias is to cover the conservative over-estimation of self

6.2. Prior Selection 38

Parameter	Distribution	Mean	CV	Reference
Density, $\rho_{\rm conc}$	Normal	1.05	0.04	[26]
Permanent Load	Normal	1.00	0.10	[26]
Modulus of Elasticity, E	Log-normal	1.00	0.15	[26]

Table 6.1: Probabilistic Models for Structural Parameters

weight often performed during design [26]. For the modulus of elasticity, E_{conc} , the prior distribution was refined to a narrower normal distribution with a mean of $1 \times E_{cm}$ and a coefficient of variation of 0.1. This adjustment was made because the long tail of the original log-normal distribution was considered unrealistic for the case study.

For live loads, selecting an appropriate distribution is somewhat more complex. Unlike dead or permanent loads, live loads fluctuate both over time and across different areas of a structure. The values used in structural design are typically based on the worst-case scenarios, which are rarely observed during actual measurements. Consequently, the live loads present during monitoring are expected to be much lower than the design values.

In general, live load is modelled as the sum of two components: the sustained load and the intermittent load. The sustained load represents actions that persist over long periods, such as the weight of furniture, equipment, and the presence of occupants engaged in normal activities. The intermittent load, on the other hand, represents rare and short-duration extreme events, such as large gatherings of people or temporary accumulation of heavy items.

As the occurrence of the intermittent loads are rare, it is unlikely that they are present during measurement campaigns. Therefore, their contribution can be reasonably neglected when defining the prior for live load. This simplification allows the prior of the live load to be taken as equivalent to that of the sustained load.

To model the uncertainty in the sustained load (q), and consequently the live load, gamma distribution is recommended as follows:

$$q \sim \text{Gamma}\left(\mu_q = m_q, \sigma_q = \sqrt{\sigma_V^2 + \sigma_U^2 \frac{A_0}{A}\kappa}\right)$$
 (6.1)

Here, m_q denotes the mean load intensity across the building for a given usage case. The term V is a random variable that captures deviations of the load intensity from the mean value. It accounts for variations in the global and floor-wise spatial averages relative to the mean load m_q . The corresponding standard deviation of this variability is denoted by σ_V .

The term U represents a zero-mean random field with a standard deviation σ_U , and it is stochastically independent of V. The parameters m_q , σ_V , and σ_U depend on the building's usage type. For the New Orleans Tower, which is residential, the adopted values are $300 \,\mathrm{N/m^2}$, $150 \,\mathrm{N/m^2}$, and $300 \,\mathrm{N/m^2}$ for m_q , σ_V , and σ_U , respectively.

The reference area A_0 is typically taken as $10 \, \mathrm{m}^2$, while A represents the tributary area associated with the imposed load effect, which in this case is taken as the floor area of the New Orleans Tower model. The ratio $\frac{A_0}{A}$ can reach a maximum value of 1.

Finally, κ characterizes the shape of the influence surface of the load, where a value of 1 corresponds to a uniform influence and higher values indicate a more localized load effect. Since the current model of the New Orleans Tower applies all the mass-like quantities at a single node (the Center of Mass), the imposed load is assumed to be uniformly distributed across the floor. Accordingly, $\kappa=1$ is adopted.

6.2. Prior Selection 39

Under these assumptions, the standard deviation of the imposed load is calculated as $0.156 \,\mathrm{N/m^2}$. For more details on the probabilistic modelling of live loads, the reader is encouraged to read the sources [26, 7].

The foundational stiffnesses pose a challenge in determining its prior distribution. Unlike other quantities discussed above, the probabilistic model for foundational stiffness differs on case basis. As the soil-structure interaction has been modelled as a set of five global springs, which in-turn was modelled from individual springs that represents individual piles, a lot of factors, such as uncertainty in the foundation material, soil properties, interaction between soil and foundation, as well as interaction between different pile groups, affect the final five global spring stiffnesses. Shirzad-Ghaleroudkhani et al (2018) used a non-informative joint uniform distribution to model the prior uncertainty in the foundational spring stiffnesses along with other parameters [29]. The specific ranges for the uniform distribution were, however, not specified. In the current study, to model the prior distribution of the foundational spring stiffnesses of the New Orleans Tower, first the stiffnesses were increased and decreased to see when the building exhibits a fixed or free boundary conditions. The observation was increasing or decreasing the stiffness by a factor of 10 leads to an almost fixed/free behaviour, while changing it by a factor of 100 leads to a complete fixed/free behaviour. As the behaviour varied fairly smoothly between these factors, the stiffness is parametrized by a term θ_{K_i} in the following manner:

The foundational stiffnesses present a particular challenge when defining their prior distributions. Unlike the other quantities, the probabilistic model for foundation stiffness is highly case-dependent. In this study, the soil-structure interaction is represented by five global springs, each derived from the combined behaviour of multiple springs corresponding to individual piles. Consequently, several factors including uncertainties in foundation material properties, soil characteristics, soil–foundation interaction, and interaction among different pile groups affect the resulting global spring stiffnesses.

Shirzad-Ghaleroudkhani et al. [29] modelled the prior uncertainty of foundational spring stiffnesses, along with other parameters, using a non-informative joint uniform distribution [29]. However, the specific ranges for this uniform distribution were not reported. In the present study, the prior distribution of the foundational spring stiffnesses for the New Orleans Tower was established through a sensitivity analysis. The stiffness values were systematically increased and decreased to identify when the structure exhibited nearly fixed or free boundary behaviour. It was observed that modifying the stiffness by a factor of 10 resulted in an almost fixed or free response, whereas a change by a factor of 100 and higher produced a fully fixed or free type behaviour. As the transition between these behaviours was observed to be smooth, the stiffness is parametrized by a factor $\theta_{K,i}$, defined as follows:

$$K_{i} = K_{i,0} \times 2^{\theta_{K_{i}}} \quad \text{with} \quad K_{i} \in \{K_{tx}, K_{ty}, K_{rx}, K_{ry}, K_{rz}\}$$

$$K_{i,0} = \text{Nominal value of } K_{i}$$

$$\theta_{K_{i}} = \text{Parametrization of } K_{i}$$

$$(6.2)$$

The prior is then defined through each of the θ_{K_i} parameter. As per the recommendation of geotechnical experts, the foundational stiffness is not expected to deviate more than a factor of 2. To account for this, in addition to the previous observation of fixed-free behaviour, a truncated normal distribution was proposed for θ_{K_i} . The distribution is centred around 0, which represents the nominal value of K_i and the standard deviation was chosen such that 1% – tile and 99% – tile are observed at $\theta_{K_i} = -1$ and 1 respectively, corresponding to a factor of 0.5 and 2 to the nominal value. Finally, the distribution was truncated at -10 and 10 which corresponds to a factor of 1024. The prior distributions along with the 1%-tile and 99%-tile values are shown in Figure 6.1.

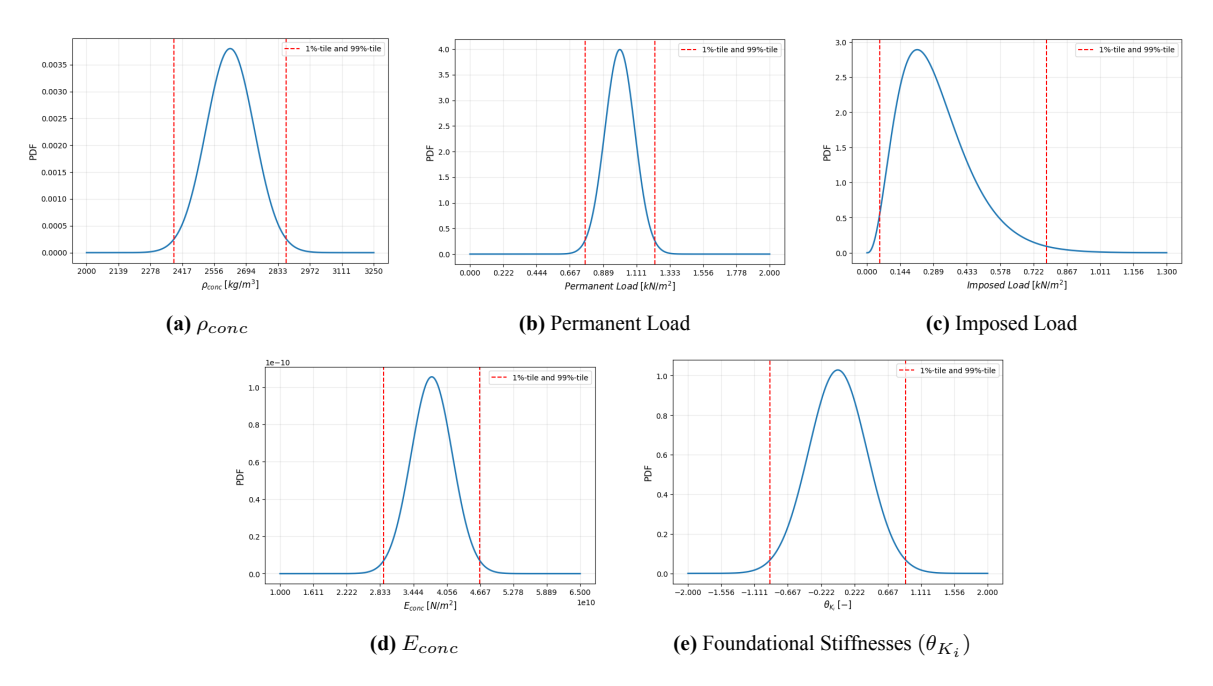


Figure 6.1: Priors for the candidate parameters

6.3. Sensitivity Analysis

When performing model updating, an important consideration is the selection of parameters to be updated. Although the section on candidate parameters identifies a set of variables that govern the model's behaviour, not all of these parameters influence the modal properties to the same extent. Since model updating is a computationally intensive process, it is essential to minimize the number of parameters involved. To achieve this, a sensitivity analysis is typically conducted to identify the parameters that have the greatest influence on the modal properties.

6.3.1. Methodology

In general, sensitivity analysis is performed by varying a parameter of interest within a predefined range, for instance, between factors of 0.1 and 10. However, in Bayesian updating, prior information about the parameters is already available, providing insight into the expected range of their plausible values. It is therefore more consistent to use these priors to define the ranges for sensitivity analysis.

This approach, however, introduces a challenge when comparing different parameters, as the region or range of the sensitivity analysis will not be directly comparable. To address this, the sensitivity analysis is carried out over a uniform percentile interval of the priors. In the present study, each model parameter was evaluated at 30 uniformly distributed points along the percentile scale of its prior, ranging from the 1%-tile to 99%-tile. The corresponding lower and upper bounds for each parameter are listed in Table 6.2. The natural frequencies obtained from these evaluations were then plotted against the nominal values to assess the degree of deviation, providing a measure of how sensitive each frequency is to the parameter under investigation.

6.3.2. Results

Figure 6.2 presents the results of the sensitivity analysis for the global parameters. The first observation is that the permanent load and imposed load parameters have little to no influence on the modal frequencies and can therefore be excluded from the updating process.

Next, it can be observed that variations in $E_{\rm conc}$ affect all the modal frequencies, with the impact becoming more pronounced in the higher modes. This behaviour is expected, as higher modes generally

Parameter	Nominal Value	Lower Bound	Upper Bound	Unit
Density, $\rho_{\rm conc}$	2500	2380	2869	$[\mathrm{kg/m^3}]$
Permanent Load	1	0.767	1.233	$[\mathrm{kN/m^2}]$
Imposed Load	0.525	0.056	0.779	$[\mathrm{kN/m^2}]$
Modulus of Elasticity, ${\cal E}$	37.8	26.4	52.8	[GPa]
Foundation stiffness, k_{tx}	3.1	1.55	6.2	[GN/m]
Foundation stiffness, k_{ty}	3.1	1.55	6.2	[GN/m]
Foundation stiffness, k_{rx}	1975	987.5	3950	$[\mathrm{GNm/rad}]$
Foundation stiffness, k_{ry}	1927	963.5	3854	$[\mathrm{GNm/rad}]$
Foundation stiffness, k_{rz}	511	255.5	1022	$[\mathrm{GNm/rad}]$

Table 6.2: Ranges for Sensitivity Analysis

exhibit greater curvature, which corresponds to higher strain energy. Since the modulus of elasticity directly reflects a material's capacity to store strain energy, changes in $E_{\rm conc}$ are naturally expected to influence modes with higher strain energy more than those with lower strain energy.

The self-weight of the structure, parametrized by $\rho_{\rm conc}$, also influences all the modal frequencies. This is not surprising, as all frequency depends primarily on the stiffness and mass of the system. However, the effect of self-weight is smaller than that of stiffness, with the frequency deviations ranging from approximately -6% to 3%, compared to a minimum range of $\pm 8\%$ for stiffness variations. As including both mass and stiffness parameters would inevitably lead to a correlated solution, due to their similar effects on the natural frequencies, only the parameter with the higher influence (E_{conc}) was chosen.

The five foundational stiffnesses exhibit a selective influence on the natural frequencies. This is logical, for instance, K_{tx} is expected to affect modes involving bending or motion in the x-direction, but not the modes with pure bending in the other directions. Specifically, K_{tx} significantly affects the fourth, fifth, seventh, and eighth frequencies, while K_{ty} affects the fourth, sixth, and eighth frequencies. The fourth and eighth frequencies are influenced by both translational stiffnesses, indicating a potential mode order swap around these frequencies when the translational stiffnesses are varied.

For the rotational foundation stiffnesses, K_{rx} and K_{ry} , the effects are mainly limited to the lower modes, particularly the first bending modes. K_{ry} influences both the first and second frequencies, again suggesting a possible mode switch. The rotational stiffness K_{rz} , which governs torsional behaviour, significantly affects the third, eighth, and ninth frequencies, all of which correspond to torsional or torsion-dominated modes.

When the effects of all foundational stiffnesses are considered together, it is evident that all nine frequencies are influenced by at least one parameter, and each stiffness parameter affects a unique set of frequencies. This suggests that, in principle, all six parameters should be identifiable within the updating scheme.

Based on these observations, the six parameters are selected for the updating procedure, namely $E_{\rm conc}$, K_{tx} , K_{ty} , K_{rx} , K_{ry} , and K_{rz} .

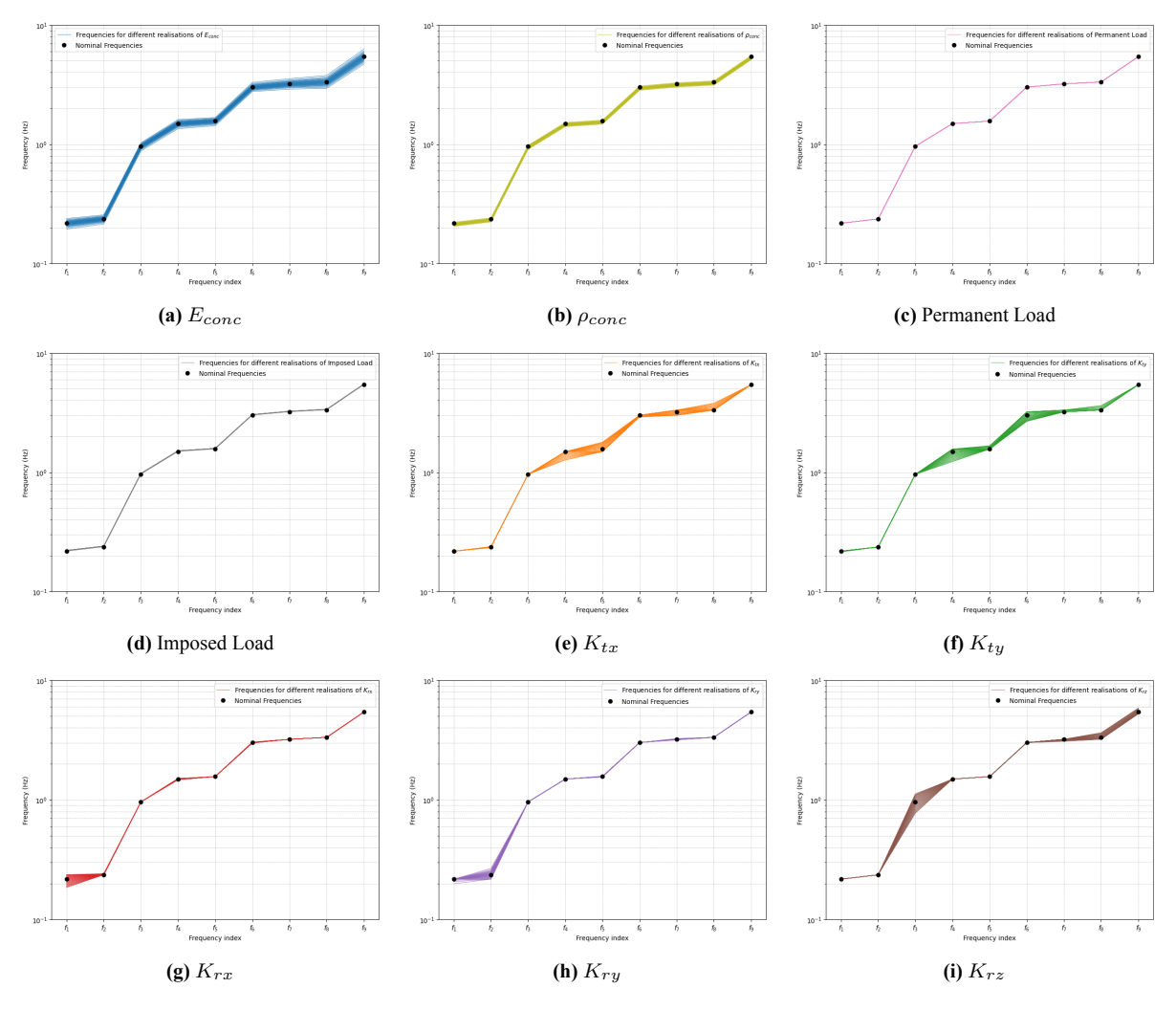


Figure 6.2: Sensitivity analysis results for the candidate parameters.

6.4. Likelihood Function Selection

The likelihood functions described in Section 4.3 will be taken as the likelihood function for the case study. For the frequency, this corresponds to Eq. 6.4 below:

$$\mathbf{f}_E = \mathbf{f}(\boldsymbol{\theta}) + \boldsymbol{\eta}_{f,M} + \boldsymbol{\eta}_{f,E} \tag{6.3}$$

$$p(\mathbf{f}_E|\boldsymbol{\theta}) \equiv P(\boldsymbol{\eta}_{f,M} + \boldsymbol{\eta}_{f,E}|\boldsymbol{\theta}) \tag{6.4}$$

Here, the measurement error $\eta_{f,E}$ is assumed to follow a zero-mean Gaussian distribution, with its standard deviation obtained directly from the measurement data. The model error can similarly be represented as a zero-mean Gaussian term. However, determining its standard deviation, or the coefficient of variation (CV), is more challenging. This error term quantifies the likely deviation of the current model from the real structure, which would require knowledge of the true structural parameters to evaluate. Since the fundamental premise of model updating is that these true values are unknown, alternative approaches are necessary to estimate the model error.

The JCSS probabilistic model code [35] suggests CV values ranging from 0.05 to 0.25 for various finite element analyses. However, guidance specific to dynamic analyses involving frequencies and mode shapes is not provided, and the influence of the level of detail of the FE model is also not addressed. Examining 99% confidence intervals for different CV values yields the frequency ranges shown in

Table 6.3. Based on these intervals, a CV between approximately 0.01 and 0.05 appears reasonable for the model error. While selecting the higher end of this range (CV = 0.05) would make the likelihood function more conservative, it could also create challenges for parameter identifiability. To assess the practicality of using these CV values in the likelihood function, a synthetic study must be conducted.

Table 6.3: Frequencies [Hz] with 99% Confidence Intervals for different Coefficients of Variation. Numbers indicate the half-width of the 99% confidence interval around the nominal frequency f_{nom} .

-			99%-Confidence Interval Half-Width						
	cies [Hz] /	0.25	0.10	0.05	0.025	0.01	0.005	0.003	
$\overline{f_1}$	0.218	0.127	0.051	0.025	0.013	0.005	0.003	0.002	
f_2	0.237	0.138	0.055	0.028	0.014	0.006	0.003	0.002	
f_3	0.961	0.559	0.224	0.112	0.056	0.022	0.011	0.007	
f_4	1.492	0.868	0.347	0.174	0.087	0.035	0.017	0.010	
f_5	1.565	0.910	0.364	0.182	0.091	0.036	0.018	0.011	
f_6	3.014	1.753	0.701	0.351	0.175	0.070	0.035	0.021	
f_7	3.210	1.867	0.747	0.373	0.187	0.075	0.037	0.022	
f_8	3.330	1.937	0.775	0.387	0.194	0.077	0.039	0.023	
f_9	5.428	3.159	1.263	0.631	0.316	0.126	0.063	0.037	
**	erms of entage	58.20%	23.27%	11.63%	5.82%	2.33%	1.16%	0.69%	

For a selected CV for the model uncertainty, the likelihood for a given frequency will be formulated as follows:

$$p(\eta_{f,M} + \eta_{f,E}|\theta) \sim \mathcal{N}\left(\mu = 0, \sigma^2 = \sigma_M^2 + \sigma_E^2\right) \tag{6.5}$$

where.

$$\sigma_M = \text{CV}_{model} \times f_{nom}$$

For the mode shapes, the equation Eq. 6.7 is used.

$$\phi_{E,r} = a_r \Gamma \phi_r(\theta) + \eta_{\phi_r,E} \tag{6.6}$$

$$p(\phi_{E,r}|\boldsymbol{\theta}) \equiv p(\eta_{\phi_r,E}|\boldsymbol{\theta}) \sim \mathcal{N}_m \left(\boldsymbol{\mu} = \mathbf{0}, \boldsymbol{\Sigma} = \boldsymbol{\Sigma}_{\phi_r}\right)$$
(6.7)

The explanations of the various terms are provided in Section 4.3. Note that the bias term is not included here. Comparison of the nominal mode shapes with those observed in the measurements shows that the majority of the measured mode shapes are already close to the nominal ones (Figure 5.5). For the mode shape closest to the mean, the MAC values for almost all modes exceed 90%, indicating that the model bias, though present, is small enough to be neglected, simplifying the likelihood formulation. Furthermore, since the mode closest to the mean achieves an MAC greater than 90%, the mode shapes may not contribute significantly to the likelihood. This suggests that neglecting the model bias in the mode shapes would not substantially affect the updating results.

The total likelihood function is then defined as a combination of the individual likelihood functions, as given in Equation 4.15.

6.5. Synthetic Analysis

6.5.1. Introduction

The goal of the synthetic analysis in this thesis is to assess the feasibility of identifying the parameters under the specified model uncertainty. For this purpose, the synthetic analysis setup is designed to closely

replicate the real-case scenario. By performing the analysis in an idealized context, the study evaluates whether the chosen level of model uncertainty can produce acceptable prediction errors, thereby demonstrating that parameter identification is feasible in the real case.

6.5.2. Model Truth

To perform a synthetic analysis, it is first necessary to define a set of true parameters, which serve as the target values for the study. These "truth" values represent the real, but unknown, parameters of the building under investigation. The advantage of synthetic analysis is that these true values are known a priori, allowing for a direct assessment of the method's effectiveness. Before defining the model truths, the set of parameters to be updated must be selected. This set corresponds to the six parameters identified in the sensitivity analysis. To establish the target values, random scalars were applied to these six nominal parameters. Table 6.4 lists the parameters, the applied scalar values, and the resulting model truths.

Parameters (θ)	Truth Scalar	Target Values
E_{conc}	0.9	34.02 [GPa]
k_{tx}	$2^{0.5}$	4.38 [GN/m]
k_{ty}	$2^{0.4}$	4.09 [GN/m]
k_{rx}	$2^{-0.35}$	1550 [GN/rad]
k_{ry}	$2^{-0.3}$	1565 [GN/rad]
k_{rz}	$2^{-0.97}$	260 [GN/rad]

Table 6.4: Model Truths for the Synthetic Analysis

6.5.3. Data Generation

With the model truths established, the next step in the synthetic analysis is to generate data from these true parameter values. Data generation is a critical component of the synthetic analysis, as poor data generation can produce unusable or misleading results. To ensure that the synthetic data closely reflects the real-case scenario, the methodology outlined in Section 4.3 is adopted. In this approach, errors are systematically introduced to the modal properties to simulate real-world measurement uncertainties. The data generation for the frequencies proceeds according to the following steps:

- 1. Calculate $\mathbf{f}_{model}(\boldsymbol{\theta}_{truth})$. This represents the frequency of the structure with the model bias, as the frequencies are being generated through the FE model.
- 2. Select a single CV_{model} value to be investigated. The set of CV_{model} that were considered under investigation were $\{0, 0.005, 0.01, 0.025, 0.05, 0.10, 0.25\}$
- 3. Using the selected CV_{model} , generate a set of random bias, one for each mode to be considered, from the distribution $\eta_{f,M} \sim \mathcal{N}(\mu=0,\sigma=CV_{model}\times f_{nom})$. Add these biases to the corresponding frequencies. The resulting frequencies now represent the true frequencies of the structure without any model bias.
- 4. From the real data of the New Orleans Tower, calculate the standard deviations of the measured frequencies, $\sigma_{f,E}$. This is done so as to ensure that the generated synthetic data matches the measurement data as much as possible.
- 5. Using the measurement uncertainty, generate a set of 100 random numbers for each frequencies from the distribution $\eta_{f,E} \sim \mathcal{N}(\mu = 0, \sigma = \sigma_{f,E})$. These random numbers represent the measurement errors, and are added to the corresponding frequencies obtained in step 4. This would

result in a set of 100 frequencies, which will become the synthetic measured frequencies.

The data generation for mode shapes follows a similar methodology, with the main difference being a lack of model uncertainty. The steps are as follows:

- 1. Calculate the mode shape from the model at the truth parameters, $\phi_{model}(\theta_{truth})$, restricted to the measurement DOFs, and normalize it to unit norm. This represents the mode shape of the structure with model bias.
- 2. Obtain the covariance matrix of the mode shape for each mode r, Σ_{ϕ_r} , from the measurement data. This represents the uncertainty in the measured mode shapes.
- 3. Using the covariance matrix, generate 100 sets of random errors for each mode from the distribution of measurement uncertainty, $\eta_{\phi_r,E} \sim \mathcal{N}(\mu = 0, \Sigma = \Sigma_{\phi_r})$.
- 4. Add the generated errors to the mode shapes obtained in Step 1. Normalize the resulting mode shape to unit norm to ensure consistency. The resulting set of 100 mode shapes for each mode represent the synthetic measured mode shapes.

6.5.4. Bayesian Updating Settings

For Bayesian updating, the priors for the six parameters, as discussed in Section 6.2, were adopted. Similarly, the likelihood function was constructed following the formulation outlined in Section 6.4. For the model uncertainty, the same $CV_{\rm model}$ used in the data generation was employed in the likelihood function. This approach simulates an ideal scenario in which the likelihood exactly matches the data generation process. In reality, the likelihood is unlikely to perfectly reflect the data generation process; however, choosing the ideal scenario allows assessment of whether Bayesian updating can succeed under optimal conditions and to quantify the deviation from the truth in the final results. This provides two key insights: (1) if the updating produces a very large error, it suggests that the procedure may not be feasible, as it struggles even under ideal conditions, and (2) if the updating produces an acceptable error, it establishes a baseline expectation for the minimum error likely in real-case applications.

The MCMC routine was implemented using the emcee module in Python. A total of 60 walkers were employed, and the algorithm was allowed to run for a maximum of 30,000 steps. If the chains converged and stabilized satisfactorily before reaching the maximum number of steps, the algorithm was terminated early. The initial values for the different walkers were taken as random samples from the prior distribution. Apart from this, the default settings of the emcee module were used.

6.5.5. Results

The synthetic analysis was done by varying the model uncertainty in both the data generation and the likelihood function. The updating for all the different model uncertainty was successful, in that the solution converged to a set of parameter values. The converged solution was then compared with the model truth (Table 6.4), to see the accuracy and quality of the updated parameters.

The results of the synthetic analysis are shown in Figure 6.3. From the figure, it can be seen that increasing the model uncertainty in the generated data leads to an increase in error of the updated parameter. This is an expected result, as higher model uncertainty corresponds to a lower quality of model, and thus, poorer representation of the real structure. Despite this, the error does not significantly increase until the CV_{model} value of 0.025. For the CV_{model} value of 0.05, the error in parameter estimation is quite high, particularly for K_{tx} and K_{ty} . This suggests that if the model uncertainty happens to be in this order, the updating process would not be able to reasonably identify these two parameters.

The model uncertainty of $CV_{model} = 2.5\%$ does not have significant error in the parameter estimation. The highest error seen in this run is for K_{tx} at the parameter prediction error of 6.35%. This error corresponds to an error band of $\pm 280 \times 10^9$ N/m. Table 6.5 outlines the error bands for different

parameters considering the error observed in the run, and also if the maximum error was taken as the expected error for all the parameters. The error bands for various parameters seem reasonable enough for the identification of the parameters to be feasible. Similarly, all the model uncertainties lower than 2.5% also show feasibility for the identification of these parameters.

From the Table 6.3, it was concluded that the model uncertainty of 0.01-0.05 is a reasonable choice for the model uncertainty, based solely on the expected deviation in the predicted frequency by the model. It is preferred to choose a higher uncertainty than the lower one, given that the said uncertainty does not interfere with the feasibility of parameter identification. The main reason for this is due to the fact that the true model bias is unknown. Based on this, the model uncertainty of $CV_{model}=2.5\%$ is chosen for updating.

While the choice of a model uncertainty level of 2.5% results in the expected error bands presented in Table 6.5, it is important to recognize that these values may not represent the actual or true error bounds. Since the true level of model uncertainty—and consequently the model bias—is unknown, the real bias in the estimated parameters could be larger than those indicated in the table. Moreover, as the current analysis considers only a single instance of ground truth values and one specific realization of model bias for each frequency, the results cannot be generalized to all possible cases. A more comprehensive assessment would require multiple synthetic studies incorporating different realizations of the noise corresponding to the assumed model uncertainty level.

Nevertheless, if the assumed model uncertainty accurately reflects the true uncertainty, the true parameter values are still expected to lie within the estimated error bands.

In other words, regardless of the true model uncertainty, the updated parameter will, at minimum, have the specified error (as expressed in percentages) summarized in Table 6.5.

Parameters	Truth	Parameter Error	Error Band
E_{conc} [GPa]	34.02	1.38%	± 0.47
K_{tx} [GN/m]	4.38	6.35%	± 0.28
K_{ty} [GN/m]	4.09	5.15%	± 0.21
K_{rx} [GNm/rad]	1550	2.14%	±33.17
K_{ry} [GNm/rad]	1565	3.82%	±59.82
K_{rz} [GNm/rad]	260	4.43%	± 11.54

Table 6.5: Summary of parameter truth values, errors, and error bands (for CV = 2.5%).

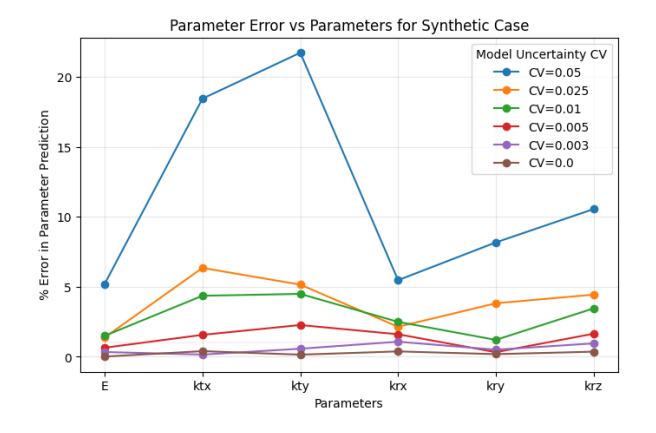


Figure 6.3: Results of Synthetic Analysis

6.6. Conclusion 47

6.6. Conclusion

This chapter started with a focus on defining a set of candidate parameters and their priors for updating. A sensitivity analysis was performed to detect the effect of parameters of the frequencies. It was revealed that the stiffness properties had a larger effect on the frequencies as compared to the mass-like properties. Thus, the six stiffness properties were chosen for updating. This analysis also served as a confirmation that the first seven frequencies were influenced by at least one of the selected parameters, implying that these parameters should be identifiable.

Synthetic analysis was carried out under ideal setups (i.e., when the likelihood and the data generation process matched) to ascertain parameters' identifiability and select a suitable model uncertainty (CV_{model}) . It was found that the higher the model uncertainty in the data, the larger the error of the updated parameters. Considering the error band in the frequency, as well as the feasibility of parameter identification, the $CV_{model}=2.5\%$ was chosen for the model uncertainty.

Parameter Identification of New Orleans Tower

This chapter presents the results of the case study on the New Orleans Tower, including a detailed discussion of the updated modal properties, comparison of updated parameters, evaluation of the posterior probability distributions, and assessment of computational performance.

7.1. Introduction

The analyses with the real measurement data is done through four separate analyses conducted under different settings to examine their influence on the results. The four considered cases are as follows:

- Case 1: Using only the first two bending modes in each direction, i.e., $\{bx1, bx2, by1, by2\}$. This case aims to compare the performance of the currently developed Bayesian updating routine with the previously employed deterministic updating method from the literature.
- Case 2: Using the first three bending modes in the x-direction and the first two bending modes in the y-direction, i.e., $\{bx1, bx2, bx3, by1, by2\}$. This case investigates the effect of model complexity on fitting the third bending mode, which posed challenges in the previous updating.
- Case 3: Using the first three bending modes in the x-direction, the first two bending modes in the y-direction, and the first torsional mode, i.e., $\{bx1, bx2, bx3, by1, by2, t1\}$. This case examines the effect of including a torsional mode in the updating scheme.
- Case 4: Using the first three bending modes in the x-direction, the first two bending modes in the y-direction, and the first two torsional modes, i.e., $\{bx1, bx2, bx3, by1, by2, t1, t2\}$. This case further investigates the effect of adding torsional modes to the updating procedure.

7.2. Bayesian Updating Settings

For Bayesian updating, the six parameters, E_{conc} , K_{tx} , K_{ty} , K_{rx} , K_{ry} and K_{rz} were considered. For Cases 1 and 2, as the torsion mode is excluded from the analysis, the rotational foundation stiffness corresponding to torsion, K_{rz} , was excluded from updating. For Cases 3 and 4, all the six parameters were included.

The priors for the six parameters as discussed in section 6.2 were adopted. Similarly, the likelihood function was constructed based on the formulation of section 6.4. The model uncertainty was selected as $CV_{model} = 0.025$. Of the total 126 available realization of each measured frequency and mode shapes, 100 realizations were used for model updating, and the remaining 26 realization were used to

compute the error metrics after updating.

For MCMC, 60 walkers were chosen and it was allowed to run until convergence, based on the auto-correlation criteria recommended by the <code>emcee</code> documentation [10]. The parameter set in each walker was initialised to a random value sampled from the prior distribution. Upon convergence, four times the maximum auto-correlation length was taken as the burn-in period, and the half of the maximum auto-correlation length was taken for thinning. If the chosen burn-in period appeared short, then it was increased as required.

7.3. Results

The Bayesian updating routine was able to successfully run and converge to a solution for all the four cases. These results of the cases are discussed in the respective sections below.

Case 1

The updating results for the frequencies (Table 7.1) indicate that the updated model successfully fitted the four updated modes. However, the frequency errors for the remaining modes increased. This suggests that the updated parameters may have overfitted the data.

Mode	Measured	Predicted	Nominal Error	Prediction Error	95% Credible Interval	MAC
	[Hz]	[Hz]	[%]	[%]		[%]
by1	0.281	0.283	22.40	0.86	[0.279, 0.286]	98.3
$\overline{\text{bx1}}$	0.290	0.290	18.30	0.16	[0.288, 0.296]	96.8
t1	0.636	1.018	51.22	60.19	[1.007, 1.043]	97.7
$\underline{\mathbf{bx2}}$	1.323	1.340	18.29	1.29	[1.314, 1.353]	94.6
by2	1.518	1.519	1.75	0.08	[1.503, 1.557]	97.8
$\overline{t2}$	2.075	3.738	60.48	80.17	[3.202, 3.326]	85.4
bx3	2.778	3.348	15.56	20.51	[3.263, 3.472]	27.3
mixed-bending	3.558	3.246	15.29	8.75	[3.627, 3.880]	7.9

Table 7.1: Results for Case 1: Frequencies and mode shapes

The corner plot in Figure 7.1a further supports this, showing strong correlations between the parameters. The combination of these correlations and the wide credible intervals suggests that multiple parameter sets can provide a reasonable fit to the data. This indicates redundancy in the parameter set and/or insufficient data, implying that the maximum a-posteriori (MAP) estimate may not correspond to the true parameter values. Interestingly, correlations are observed between all parameters. The negative correlation between E_{conc} and the foundation stiffnesses is expected, as increasing either parameter leads to higher natural frequencies. The indirect correlations among the different foundation stiffnesses arise from their shared dependence on E_{conc} . This implies that modes insensitive to a particular parameter can still help reduce its uncertainty, since all modes are influenced by E_{conc} . A comparison of stiffness

Table 7.2: Comparison of stiffness parameters acr	oss Moretti et al., Ritteld, and Case 1.
--	--

Parameter	Moretti et al.	Ritfeld	Case 1
K_{tx}	2.20×10^{9}	2.80×10^{9}	1.62×10^{9}
K_{ty}	2.85×10^{9}	5.70×10^{9}	2.56×10^9
K_{rx}	3.07×10^{12}	2.14×10^{12}	5.62×10^{12}
K_{ry}	11.1×10^{12}	2.89×10^{12}	3.76×10^{12}

parameters across studies (Table 7.2) shows large differences between this work and previous analyses by Moretti and Ritfeld. Since Bayesian updating reveals the existence of multiple plausible solutions,

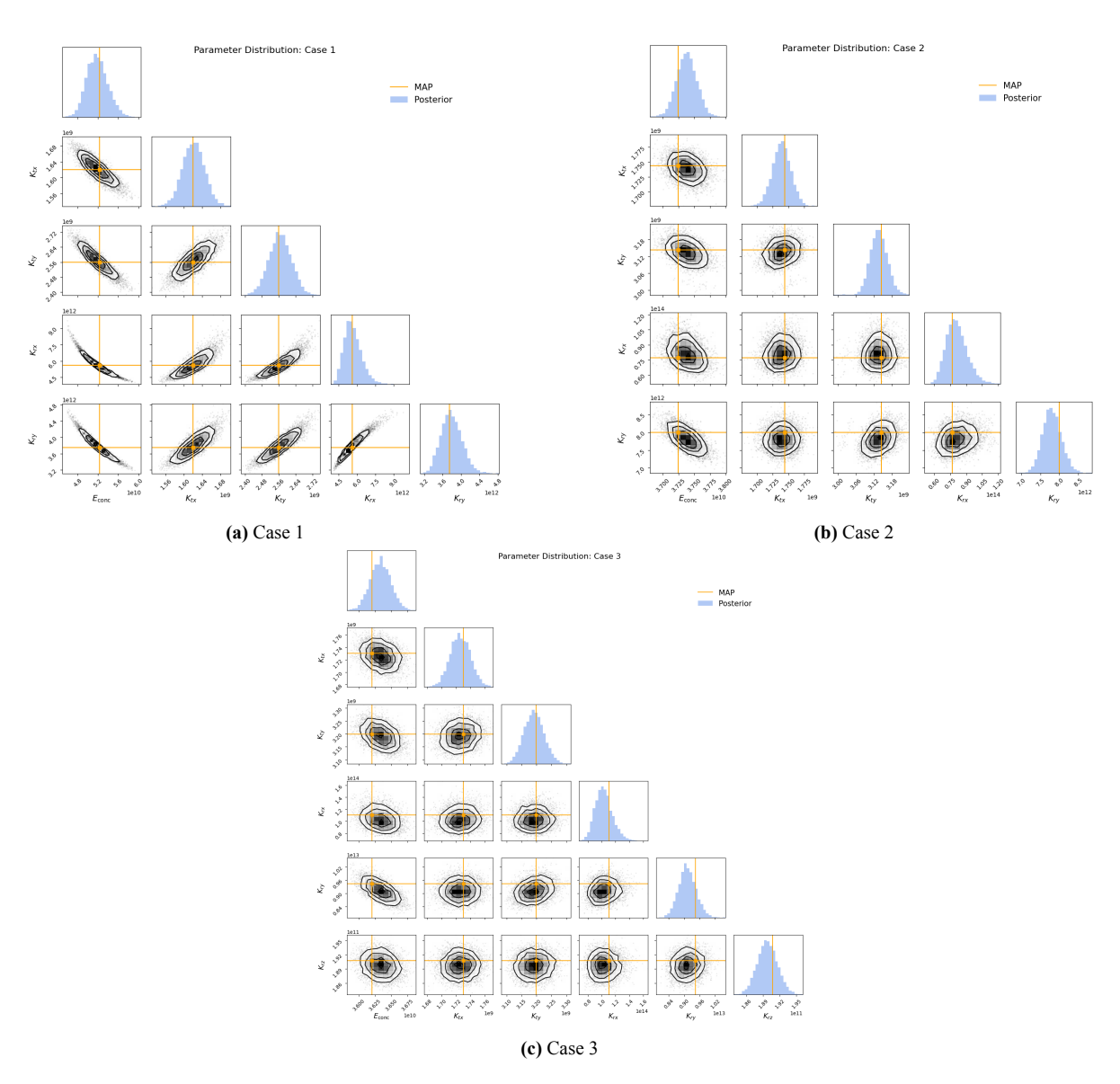


Figure 7.1: Corner plots of the updated parameters for Case 1 through Case 3.

these differences do not imply error, but rather emphasize that the current parameter set is insufficiently informative. To improve identifiability, either fewer parameters should be updated or additional data, such as more modes, should be used.

Case 2

In this case, the third bending mode in the x-direction (bx3) was included in the updating process. This resulted in reduced parameter correlations (Figure 7.1b), indicating improved generalization compared to Case 1. Moreover, the prediction errors for the unupdated modes are comparable to the nominal error, suggesting that overfitting did not occur in this case (Table 7.3).

While the frequency error for bx3 decreased, it remained higher than for lower modes, and the MAC value stayed low. This indicates that the current model still cannot fully capture this mode, likely due to missing parameters, possibly related to the lower part of the tower, where the mode shape mismatch is most visible (Mode shape similar to Figure 7.4e). Nevertheless, the inclusion of bx3 enhanced the overall parameter identifiability by providing new and unique information, as reflected by the reduced parameter correlations.

Mode	Measured	Predicted	Nominal Error	Prediction Error	95% Credible Interval	MAC
	[Hz]	[Hz]	[%]	[%]		[%]
by1	0.281	0.274	22.40	2.33	[0.272, 0.278]	98.5
bx1	0.290	0.289	18.30	0.08	[0.285, 0.293]	88.5
t1	0.636	0.956	51.22	50.40	[0.94 0.968]	97.9
$\underline{\mathbf{b}}\mathbf{x}2$	1.323	1.309	18.29	1.06	[1.294, 1.332]	96.7
by2	1.518	1.544	1.75	1.67	[1.508, 1.562]	93.9
$\overline{t2}$	2.075	3.333	60.48	62.58	[3.258, 3.372]	81.6
bx3	2.778	3.055	15.56	9.98	[3.032, 3.077]	35.1
mixed-bending	3.558	3.055	15.29	14.14	[3.011, 3.139]	12.8

Table 7.3: Results for Case 2: Frequencies and mode shapes

Table 7.4 compares the frequency prediction errors across studies. Unlike in previous analyses, the inclusion of bx3 here did not degrade the fit of lower modes, and the highest frequency error was also reduced. This suggests that the current modelling approach has a better performance than previously employed analytical beam models.

Mode	Moretti et al.	Ritfeld	Case 2
	[CRPS %]	[CRPS %]	[CRPS %]
by1	1.42	0.00	2.86
bx1	13.06	17.18	0.54
bx2	0.07	0.00	1.57
$\mathbf{by2}$	1.38	0.00	0.74
bx3	12.27	0.07	7.76

Table 7.4: Comparison of Errors in Frequencies

Case 3

This case introduces the first torsional mode and includes K_{rz} in the updating. Table 7.5 shows that the frequency errors decreased for all included modes, with by1, t1, and bx3 remaining slightly higher but still within commonly adopted limits ($\approx 8-9\%$), as observed in previous studies for torsional and higher bending modes. The second torsional mode (t2) improved notably, from 60.48% to 41.80% error, indicating better generalization.

Mode	Measured	Predicted	Nominal Error	Prediction Error	95% Credible Interval	MAC
	[Hz]	[Hz]	[%]	[%]		[%]
by1	0.281	0.271	22.40	3.49	[0.268, 0.275]	99.6
$\underline{\mathbf{bx1}}$	0.290	0.288	18.30	0.70	[0.285, 0.293]	97.5
$\underline{\mathbf{t1}}$	0.636	0.681	51.22	7.09	[0.674, 0.695]	97.5
$\underline{\mathbf{b}}\mathbf{x}2$	1.323	1.298	18.29	1.84	[1.285, 1.325]	98.6
$\underline{\text{by2}}$	1.518	1.537	1.75	1.25	[1.505, 1.559]	95.7
t2	2.075	2.942	60.48	41.80	[2.924, 2.971]	88.3
$\underline{\mathbf{bx3}}$	2.778	3.042	15.56	9.51	[2.966, 3.095]	34.4
mixed-bending	3.558	3.054	15.29	14.15	[3.010, 3.120]	25.5

Table 7.5: Results for Case 3: Frequencies and mode shapes

Interestingly, Figure 7.2 shows that, even though the higher modes were not included in the updating, their frequency uncertainties are reduced to a level comparable with the measured values. This suggests that the parameter uncertainty cannot be further reduced with the available data.

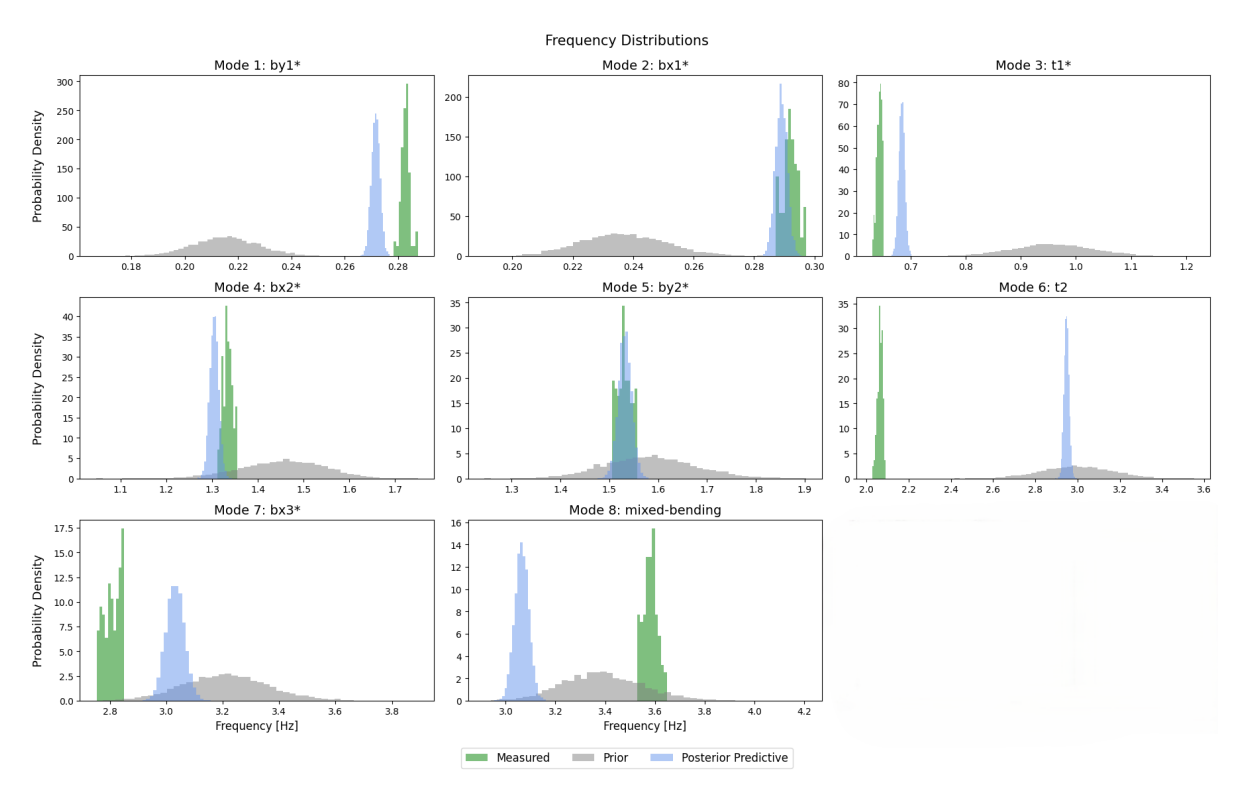


Figure 7.2: Frequency Distribution Comparison for Case 3 (* denotes modes used in the updating process)

The MAC values indicate good agreement for the first five modes, while the higher modes show notably lower values. The measured and predicted mode shapes are presented in Figure 7.4, with clear mismatches observed for the torsional modes and the third bending mode (bx3). For the torsional modes, the predicted displacements in the x and y directions at sensor locations vary little, but the derived rotation angle θ shows significant deviation. The bottom sensors, particularly in the x direction, exhibit larger errors than the upper sensors. For bx3, a pronounced mismatch occurs at the bottom sensor, and because the modes are normalized, this propagates to the top to maintain a unit norm. Overall, these mode shapes suggest that the bottom part of the tower may not be accurately represented in the current model.

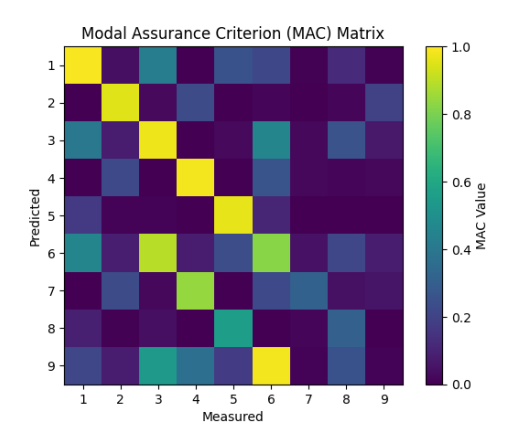


Figure 7.3: MAC Matrix for updated results

The corner plot (Figure 7.1c) reveals a weak correlation between E_{conc} and K_{ry} . However, since the correlation spans a narrow interval for E_{conc} but not for K_{ry} , K_{ry} may not be considered unique.

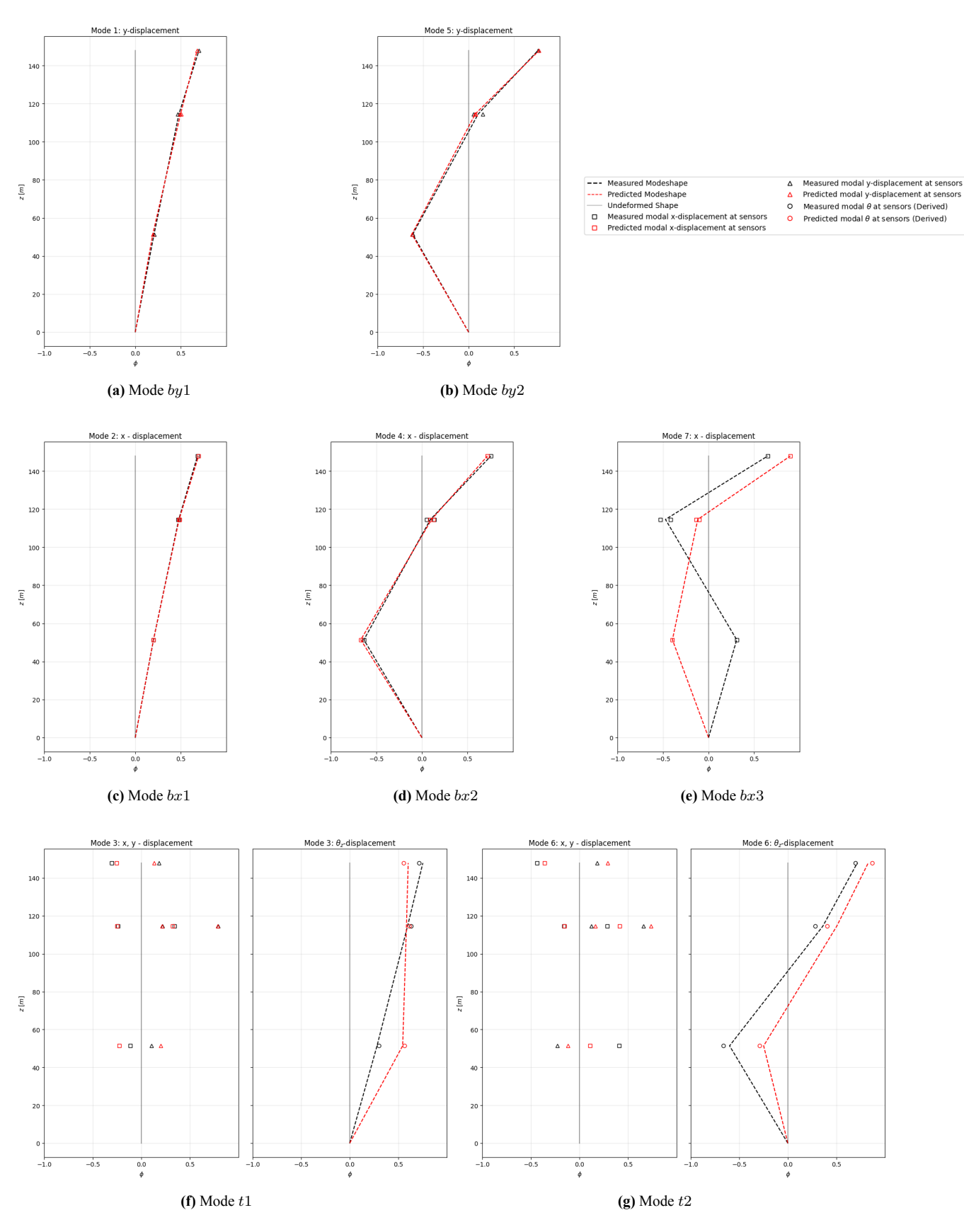


Figure 7.4: Measured and Predicted modes for Case 3

Case 4

In the final case, the second torsional mode was added to the updating. Despite this, t2 retained a large frequency error (Table 7.6), and the fit for by1 showed significant deterioration. Although bx3 improved considerably, these benefits do not outweigh the poorer performance of the lower modes. The updated parameters therefore likely deviate from the true physical values.

Mode	Measured	Predicted	Nominal Error	Prediction Error	95% Credible Interval	MAC
	[Hz]	[Hz]	[%]	[%]		[%]
by1	0.281	0.248	22.40	11.67	[0.245, 0.253]	99.1
$\underline{\text{bx1}}$	0.290	0.282	18.30	2.65	[0.275, 0.286]	96.8
$\underline{\mathbf{t1}}$	0.636	0.676	51.22	6.30	[0.664, 0.728]	97.8
$\underline{\mathbf{b}}\mathbf{x}2$	1.323	1.313	18.29	0.77	[1.219, 1.330]	97.7
$\underline{\text{by2}}$	1.518	1.512	1.75	0.42	[1.490, 1.544]	95.9
$\underline{\mathbf{t2}}$	2.075	2.714	60.48	30.83	[2.696, 2.807]	86.0
$\underline{\mathbf{bx3}}$	2.778	2.872	15.56	3.40	[2.789, 2.936]	38.7
mixed-bending	3.558	3.067	15.29	13.78	[2.982, 3.113]	27.7

Table 7.6: Results for Case 4: Frequencies and mode shapes

The failure to accurately fit t2 suggests missing parameters or limitations in the available data. As noted by Bronkhorst et al.[4], the second torsional mode is difficult to distinguish experimentally from the first, which is also evident in the updated MAC matrix shown in Figure 7.3. Consequently, the second torsional mode may contribute little additional information to the updating scheme, resulting in minimal improvement compared to the previous case.

The posterior distributions (Figure 7.5) exhibit bi-modal behaviour, showing that the Bayesian approach successfully captured multiple local optima in the parameter space. This is reflected in bimodal frequency distributions, particularly for t1, bx2, and t2, though only the main peak values are reported in Table 7.6.

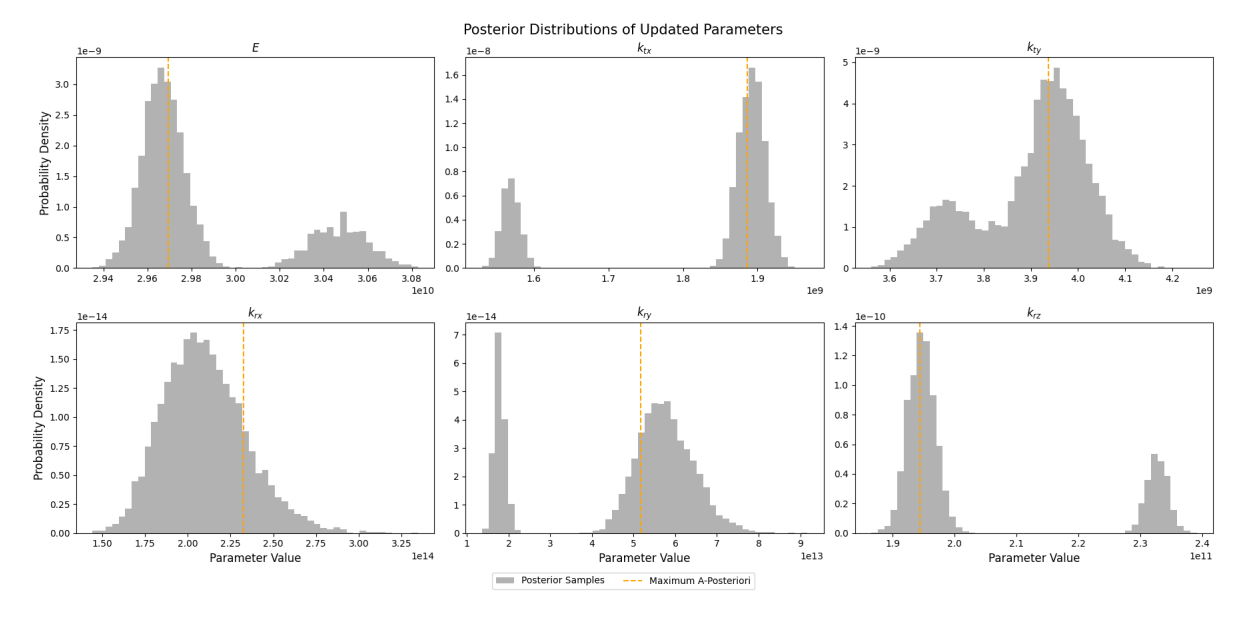


Figure 7.5: Posterior distribution of parameters for Case 4

7.3.1. Comparison of Updated Parameters

The four updating cases reveal distinct trends in parameter identification and model performance. In Case 1, although the updated parameters fit the selected modes well, errors in the remaining modes

increased, indicating overfitting and a lack of unique solutions. Case 4, which included all modes up to the second torsional mode, also exhibited limitations: while some modes improved, others (notably t2 and by1) showed increased errors. This suggests that the updated parameters in these cases do not reliably reflect the true structural properties.

Cases 2 and 3 show more consistent and credible parameter estimates. Including additional modes in Case 2 reduced correlations among parameters, while Case 3, which incorporated the first torsional mode and its associated stiffness K_{rz} , further improved parameter identification. For these cases, $E_{\rm conc}$, K_{tx} , and K_{ty} converge to similar values with narrow 95% credible intervals, indicating a significant reduction in uncertainty and likely proximity to the true values. The torsional stiffness K_{rz} , updated in Cases 3 and 4, shows similar MAP values and overlapping intervals. This also suggests that the obtained value is likely close to true value. The large error in the first bending mode in Case 4 appears to have occurred from the E_{conc} trying to compensate for the missing parameter while trying to fit t2.

The rotational foundation stiffnesses, K_{rx} and K_{ry} , exhibit substantial variation across cases and large deviations from nominal values. The wide credible intervals for K_{rx} in all cases indicate that this parameter was not identified. In contrast, K_{ry} shows narrower intervals (except Case 4), implying some improvement in uncertainty, although its large deviation from the nominal value warrants caution.

Param	Unit	Nominal	Case 1	Case 2	Case 3	Case 4
$E_{\rm conc}$	$\times 10^9 \mathrm{N/m^2}$	37.8	52.3	37.3	36.2	29.6
K_{tx}	$\times 10^9 \mathrm{N/m}$	3.10	1.62	1.75	1.73	1.90
K_{ty}	$\times 10^9 \mathrm{N/m}$	3.10	2.56	3.14	3.21	3.98
K_{rx}	$\times 10^{12} \mathrm{Nm/rad}$	1.98	5.62	75.2	106	219.9
K_{ry}	$\times 10^{12} \mathrm{Nm/rad}$	1.92	3.76	7.94	9.34	55.63
K_{rz}	$\times 10^9 \mathrm{Nm/rad}$	511	_	_	190	196.5

Table 7.7: Nominal and MAP values for different cases

Table 7.8: Credible intervals (95%) for prior and posterior distributions across different cases.

Param	Unit	Prior	Case 1	Case 2	Case 3	Case 4
$E_{ m conc}$	$\times 10^9 \mathrm{N/m^2}$	[30.4, 45.2]	[48.1, 56.2]	[37.1, 37.7]	[36.0, 36.6]	[29.5, 29.9]
K_{tx}	$\times 10^9 \mathrm{N/m}$	[1.83, 5.25]	[1.57, 1.67]	[1.71, 1.77]	[1.70, 1.75]	[1.86, 1.93]
K_{ty}	$\times 10^9 \mathrm{N/m}$	[1.83, 5.25]	[2.46, 2.67]	[3.08, 3.19]	[3.13, 3.26]	[3.83, 4.10]
K_{rx}	$\times 10^{12} \mathrm{Nm/rad}$	[1.17, 3.35]	[4.50, 7.34]	[64.1, 103]	[82.1, 131]	[170, 266]
K_{ry}	$\times 10^{12} \mathrm{Nm/rad}$	[1.14, 3.27]	[3.39, 4.28]	[7.35, 8.32]	[8.50, 9.82]	[45.9, 72.4]
K_{rz}	$\times 10^9 \: \mathrm{Nm/rad}$	[302, 866]	_	_	[186, 193]	[191, 199]

A further investigation on the log-likelihood and the log-posterior values around the Case 3 MAP solution (Figure 7.6) confirms these observations: for most parameters, there is a well defined peak in the log-likelihood plot and the predicted values align with the likelihood maxima, indicating that the data dominates the posterior. For K_{rx} , the likelihood is nearly flat implying that the priors strongly influence the posterior. Since the selection of the prior is usually subjective (especially in the current study, where the prior is based on engineering judgement), the resulting estimate also inherits this subjectivity. Consequently, the predicted K_{rx} is likely unreliable.

Nevertheless, the plateau in the likelihood indicates that beyond a certain point, the frequencies and mode shapes show negligible sensitivity, allowing K_{rx} to be idealized as a fixed support without significant error. For K_{ry} , the data suggests that the predicted value may be close to reality, but the associated uncertainty is higher than for other parameters, as reflected in the credible intervals. However, as K_{ry} also showed correlation with E_{conc} for all the cases, it is difficult to conclusively ascertain if the parameter has been reliably identified.

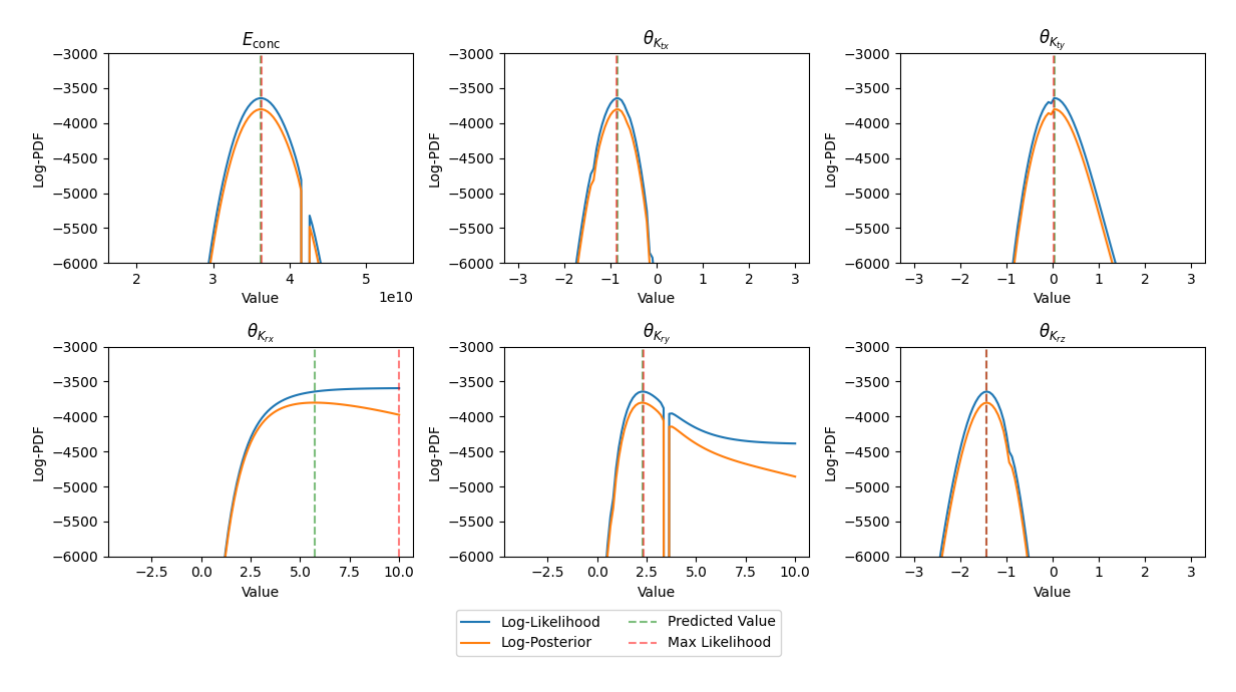


Figure 7.6: Log-Likelihood and Log-Posterior around the predicted value of Case 3

7.3.2. Computational speed

All computations for this research were performed on a laptop equipped with an AMD Ryzen 7 PRO 5500U processor (8 cores, 16 threads, base frequency 1.9 GHz) with integrated Radeon Graphics and 16 GB DDR4 RAM operating at 3200 MT/s. The operating system used was Windows 11 (64-bit).

Table 7.9 summarizes the computational performance for the four cases analysed, including the number of steps required for convergence, the total computation time, and the average time per 1000 steps and per 10,000 model evaluations.

Case	No. of steps to convergence	Time to convergence [min]	Average time taken [min per 1000 steps]	Average time taken [min per 10,000 model computations]
Case 1	5000	197	39	6.6
Case 2	6000	211	35	5.9
Case 3	6150	257	42	7.0
Case 4	16200	773	48	8.0

Table 7.9: Convergence Time for Different Cases

The analyses exhibited a consistent computational efficiency across the first three cases, averaging approximately 40 minutes per 1000 steps. These runs required between 5,000 and 6,150 steps, achieving convergence within roughly 3 to 4.5 hours (197 to 257 minutes).

In contrast, Case 4 required substantially more computational effort, taking 16,200 steps and 773 minutes (approximately 13 hours) to converge. This increased computational demand can be attributed to the bi-modal nature of the posterior distribution observed for this case. The existence of two distinct peaks in the posterior indicates that the Bayesian updating process identified multiple local maxima. Consequently, the MCMC sampler was required to explore two separate regions of the parameter space, which increased the autocorrelation length of the chains and delayed convergence. This demonstrates the computational cost associated with exploring complex, multi-modal posteriors in Bayesian inference.

7.4. Conclusion 57

Overall, the simplified FE model demonstrated satisfactory computational performance, completing approximately 10,000 model evaluations in 68 minutes. Each model evaluation involved building the model from scratch, performing eigenvalue analysis, computing the frequency and mode shape errors, and evaluating the log-posterior based on these discrepancies.

7.4. Conclusion

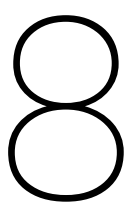
For the analysis with the measured data, four distinct cases were investigated by varying the number and type of modes included in the updating procedure:

- Case 1 (First two bending modes in x and y): The major characteristic of this case was overfitting to the data, as errors in modes which were not included in the updating increased significantly. Additionally, the updated distributions revealed strong correlations between the parameters, indicating redundancy in the selected parameters non-uniqueness of the solution. Due to the non-uniqueness, a conclusive comparison with the previous studies was not possible.
- Cases 2 (Including third bending mode in x): The addition of the third bending mode (bx3) led to a correlation level that was substantially lower than that of Case 1, thus indicating that the model had better generalization properties. However, the model was not able to explain the bx3 mode completely, which hinted at missing parameters or certain model limitations. A comparison with the previous studies revealed that the current approach has better results, particularly as the estimation of the lower modes were not affected by the inclusion of the higher mode.
- Case 3 (Including the first torsional mode t1): This case showed the most promising results of balancing between model generalization and data fitting. The errors of frequency for by1 and t1 were pretty close to the acceptable range of 8% to 9% cited in the literature. The error in bx3 mode was comparable to the previous case, reinforcing the previous claim of model limitations.
- Case 4 (Including the second torsional mode t2): While this analysis was able to reduce the error for t2 mode and even bx3 mode as compared to the previous case, the error in t2 was still significantly high (30.7%). Furthermore, the case leads to an increase in the first mode, by1, at 11.7%. As the first mode is usually much more important for different analysis than the higher modes, this updating case was deemed as unsuccessful. Interestingly, this case revealed a bi-modal distribution in the updated parameters, demonstrating the Bayesian updating routine's ability to detect local maxima in the posterior distribution.

The updated Maximum A, Posteriori (MAP) values for parameters E_{conc} , K_{tx} , and K_{ty} were similar across the two better cases (Case 2 and Case 3) meaning that these values most likely represent the true properties of the structure.

Specifically, the rotational stiffnesses K_{rx} and K_{ry} , in particular, were very different and had a large range of credible intervals in all analyses. Likelihood function analysis showed that the function for K_{rx} was characterized by a large flat area with no distinct peak, making the solution highly dependent on the prior distribution. This suggested that for these parameters, the choice of priors are critical in their identifiability through Bayesian model updating.

In conclusion, Case 3 provided the best balance for updating the simplified FE model of the New Orleans Tower, successfully incorporating the first torsional mode and demonstrating the utility of Bayesian updating in revealing parameter uncertainty, correlation, and model limitations. The results suggest that while the current approach improves accuracy and generalization compared to previous studies, further improvement would require addressing potential missing parameters, such as connection stiffnesses, that may be relevant for higher-order bending and torsional modes



Discussions

In this study, various analyses were performed to check the effectiveness of using Bayesian Model Updating on a Simplified FE Model of the New Orleans tower. The analyses covered several aspects of both Bayesian model updating, and the simplified FE Model, which are discussed in the following sections.

8.1. Uncertainty Quantification

Bayesian model updating requires well-defined prior and likelihood functions that describe prior knowledge of the structure and the data generation process. Ideally, these functions should yield the true parameters that reproduce the real structural behaviour; however, several practical challenges prevent such idealization.

For the priors, the literature provides structure-independent guidelines, which can be refined to reflect the knowledge of the specific structure. While parameters directly representing material or loading properties are relatively straightforward to define, derived quantities present a greater challenge. In this study, this difficulty arose in defining the foundation stiffnesses, which were derived from the properties of the supporting piles. Their priors can either be too broad, leading to non-physical results, or too narrow, requiring detailed information that may not always be available. Since derived parameters typically exhibit higher uncertainty, their priors become both more important and harder to specify. In this work, these priors were defined based on engineering judgement, providing a reasonable but general representation.

Despite these challenges, the likelihood exploration around the converged solution showed that with sufficient, high-quality data, the results are not strongly dependent on the choice of prior. A smooth prior that adequately spans the plausible parameter space is often sufficient.

Similar challenges arise in defining the likelihood function, which represents the probability of obtaining the measured data given the model and its parameters. This requires quantifying both measurement and model uncertainties. While measurement uncertainty is often modelled as white noise for simplicity, the true error may exhibit coloured characteristics, necessitating more complex formulations. The quantification of model uncertainty poses a far greater challenge as the model bias, reflecting the deviation between the model and reality, cannot be evaluated directly when the true model and parameters are unknown.

In this research, a synthetic analysis was used to estimate an appropriate level of model uncertainty. However, the adopted value remains an assumption, and the true model bias may differ. Consequently,

the resulting parameter estimates may deviate from reality.

8.2. Parameter Identification

Bayesian updating was performed using measured data across multiple cases, each employing a different combination of modal information. The results demonstrated the method's capability to reproduce measured behaviour. Case 1 highlighted a key advantage of Bayesian updating over deterministic methods - its ability to reveal parameter correlations and thereby indicate parameter redundancy and non-uniqueness in solutions and overfitting. Furthermore, Bayesian updating yields full posterior distributions, thereby capturing uncertainty and revealing which parameters are weakly informed by the data (those with wide posterior spreads).

Case 2 examined the influence of increasing model complexity from the uniform Euler–Bernoulli and discrete Timoshenko beam models to the simplified FE model. The proposed FE model effectively resolved a major issue seen in the previous models, the influence of the third bending mode (bx3) on the first bending mode (bx1), while maintaining low overall error. This improvement results from the model's ability to capture bending in both directions simultaneously. Two main reasons explain this improvement:

- By including both directions simultaneously, all modes contribute to the updating of E_{conc} . In previous models, only modes corresponding to one direction influenced the stiffness in that same direction. Consequently, the updated E_{conc} is expected to be more accurate.
- Because the model incorporates all six parameters together (rather than treating each direction separately), the stiffness in one direction can influence that in the other through E_{conc} , which is affected by all frequencies. Hence, even modes that do not directly depend on a given stiffness can influence it indirectly. This coupling represents one of the key advantages of the current model formulation.

The case also revealed another advantage of using Bayesian updating, wherein the addition of modes may have significant improvement in removing parameter redundancy and reducing the correlation in the obtained solution, which cannot be detected in the deterministic model updating. This becomes especially crucial, when the error of the added mode itself does not improve.

Adding the first torsional mode and its corresponding stiffness (K_{rz}) improved the prediction of the first torsional frequency without significantly affecting the others. The second torsional mode also improved. The success in matching the first torsional mode confirms the dominant influence of K_{rz} on torsional behaviour.

In Case 4, the inclusion of the second torsional mode further reduced its error; however, the final discrepancy remained significantly higher than that of the other modes. This outcome, together with the findings from Case 3, suggests the presence of a missing parameter in the model or an underlying modelling inadequacy.

8.3. Model Inadequacy

A reasonable hypothesis can be made regarding the nature of the missing parameter or model inadequacy. Based on the mode shapes (Figure 7.4), most discrepancies occur in the lower floors. The torsional modes show slightly larger errors in the x-direction, and the third bending mode (bx3) displays significant mismatch in the same direction. These observations suggest that the source of error lies in the lower part of the structure and likely in the x-direction.

In the current model, the tower is idealized as a slender structure with a cross-section of $28.8, m \times 32.3, m$ at the base, neglecting the adjoining low-rise structure (Figure 8.1). This portion likely provides

additional stiffness in the x-direction, accounting for the observed discrepancies.



Figure 8.1: New Orleans Tower with the Low-rise building

Another possible source of error is the assumption of perfectly rigid connections. Relaxing this assumption and introducing connection stiffnesses as updating parameters may provide valuable insight into whether the rigid connection assumption is justified.

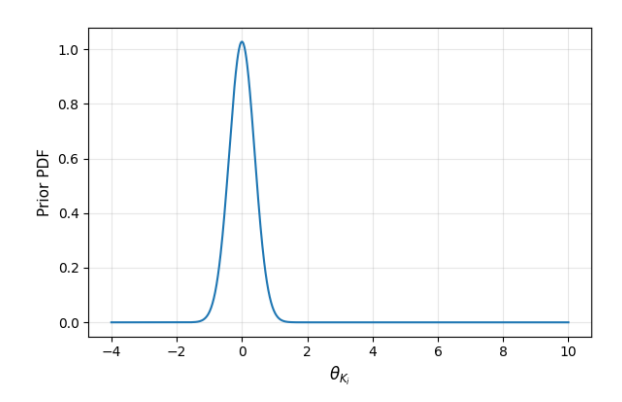
8.4. Investigation of Log-Likelihood and Log-Posterior

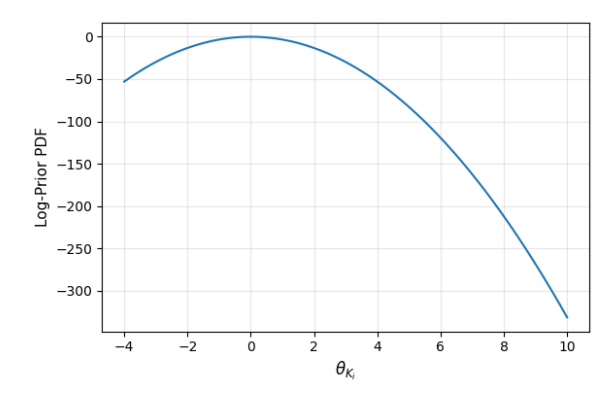
Analysis of the updated parameters revealed a decrease in uncertainty for all parameters except K_{rx} . The log-likelihood function indicated a broad plateau rather than a sharp peak, suggesting that this parameter is weakly informed by the data and highly influenced by its prior. Testing different priors can confirm this: if the posterior is highly sensitive to the prior, the data do not provide sufficient information to identify the parameter. In such cases, it is advisable to gather more data or exclude the parameter from updating.

The examination of the likelihood function also highlights an important feature of Bayesian model updating. Although Bayesian methods are sometimes criticized for their subjectivity due to prior selection [9], Figure 7.6 demonstrates that as the amount and quality of data increase, the subjective influence of the prior diminishes. Hence, with reliable data and a well-chosen prior, Bayesian updating produces consistent, objective, and scientifically reliable results.

8.5. Rotational Foundation Stiffness

Finally, it should be noted that, while K_{rx} was deemed unidentifiable, the data strongly suggests that this stiffness is significantly higher than what might typically be expected based on engineering judgement. A similar observation applies to K_{ry} , with the difference that the data constrains it to a more specific value. It is important to note that the priors reflect the engineering judgement, assigning extremely low probabilities to these high values (Figure 8.2). Nevertheless, the posterior converges to these high values due to strong support from the data, as reflected in the likelihood function. (Figure 7.6) The exact reason for this behaviour is not fully known, but several plausible explanations can be considered:





- (a) Prior distribution of all the foundational stiffnesses θ_{K_i}
- **(b)** Log-prior distribution of all the foundational stiffnesses θ_{K_i}

Figure 8.2: Prior and log-prior distributions of all the foundational stiffnesses θ_{K_i}

- 1. K_{rx} and K_{ry} directly influence only the first bending modes, by1 and bx1, respectively. Since only one mode directly constrains each of these parameters, whereas other parameters are influenced by multiple modes, there may simply be insufficient modal information to accurately infer these rotational stiffnesses.
- 2. Other modes also influence the rotational stiffnesses indirectly through E_{conc} . Since E_{conc} is constrained by all the parameters, it is relatively well-determined. However, this also means that fitting the first bending modes places a disproportionately high influence on the rotational stiffnesses. Consequently, if the current updating scheme is missing any parameter that affects these first bending modes, the rotational stiffnesses may compensate significantly to achieve a fit, which could explain their elevated values.
- 3. In line with the previous point, the adjoining low-rise structure may contribute significant rotational stiffness that is not explicitly modelled. This could manifest as high rotational stiffnesses in the updated results.
- 4. Similarly, compensatory effects from model inadequacies affecting higher bending modes may influence E_{conc} , which in turn forces the rotational stiffnesses to adjust. For instance, in Case 4, the second torsional mode led to compensatory adjustments in E_{conc} . If a similar effect occurs in Case 2 (and by extension Case 3) with the introduction of bx3, the first bending modes, being primarily sensitive to rotational stiffness, may drive K_{rx} and K_{ry} to higher values. Additionally, as other modes do not affect these stiffnesses, the first bending modes are free to drive the values of K_{rx} and K_{ry} to unreasonable values. This appears to be the most plausible explanation, particularly considering the notable reduction in uncertainty for E_{conc} between Case 1 and Case 2.
- 5. Finally, it is also possible that the structure genuinely has such high rotational stiffnesses. Verifying this outcome would require further investigation on the identification of these stiffnesses, preferably using methods other than model updating.

A study by Carranza [6] on the frequency dependence of the foundational stiffness reports that the stiffness corresponding to K_{rx} is approximately $5-6\times10^{12}$ Nm/rad in the frequency range 0-1 Hz. The mode by1 falls within this range, which aligns with the result for K_{rx} in Case 1, but not with the results of the other cases.

Similarly, the study also reports that K_{ty} has a value of $3-3.5\times10^9~\mathrm{N/m}$ in the frequency range $0-0.5~\mathrm{Hz}$. This corresponds well with the results of Case 2 and Case 3, where K_{ty} was $3.14\times10^9~\mathrm{N/m}$ and $3.21\times10^9~\mathrm{N/m}$, respectively. However, the frequencies influencing this stiffness in these cases

lie outside the reported range, where the foundational stiffness is significantly lower.

Taken together, these observations suggest that the stiffnesses corresponding to the static case have been reasonably identified across the different cases. Nevertheless, it remains unclear whether this agreement is coincidental or a true reflection of the effectiveness of the model updating and the data.

9

Conclusion

The goal of this thesis was to enhance the accuracy and reliability of structural parameter estimation in high-rise buildings by applying a vibration-based Bayesian Finite Element (FE) model updating approach. This methodology aimed to build up on the previous studies by incorporating previously unused modal data, such as torsional, as well as incorporating the uncertainty present in the data. This work successfully utilized a Simplified (3D) FE model of the New Orleans Tower, a lumped-mass stick model that accounts for torsional deformations, as well as coupling between different directions. The research addressed the main question: "How can Bayesian model updating, combined with a simplified FE model, be effectively utilized to enhance the accuracy and reliability of structural parameter estimation in high-rise buildings?" A set of sub-questions were derived to answer this research question. This section will provide the specific answers to these questions presented in the introduction.

9.1. Simplified FE Modelling Approach

The research sub-questions related to the modelling choice are addressed in this section.

How should the updating parameters be determined?

The selection of updating parameters was guided by a sensitivity analysis conducted to evaluate their influence on the natural frequencies. In Bayesian model updating, prior distributions must be defined for all parameters to be updated. By first establishing priors for the candidate parameters, reasonable parameter bounds can be identified for the sensitivity analysis. This approach ensures that extreme or physically unrealistic parameter values do not bias the results or affect the conclusions drawn from the sensitivity analysis.

What effect does increasing model complexity have on the model updating results?

By increasing the model complexity from the previously used analytical beam model to the current simplified FE model, the third bending modes could be included without introducing compensatory errors in the lower modes. The 3D representation also enabled the incorporation of torsional modes, thereby providing a more complete description of the building's dynamic behaviour.

The use of a 3D model improved the updating results in two key ways. First, unlike the previous approaches that employed two uncoupled models for the x and y directions, the current model captures the behaviour of both directions within a single model. This allows more modes to directly influence certain parameters, such as E_{conc} . Second, when parameters like E_{conc} , which affect all natural frequencies, are included in the updating process, modes that are not directly dependent on a particular parameter can still contribute indirectly to improving its estimation through their shared dependence on

 E_{conc} . This coupling effect is evident in the reduced uncertainty of K_{ty} from Case 1 to Case 2, where the only difference was the inclusion of mode bx3, which itself is not directly dependent on K_{ty} .

What effect does including torsional modes have on the model updating results?

The first torsional mode was successfully incorporated into the model updating without causing any significant impact in the results of the other modes, demonstrating the model's capability to capture torsional behaviour. The second torsional mode, however, could not be successfully incorporated. This limitation is likely due to an missing features in the model or missing updating parameters, rather than an inherent shortcoming of the simplified FE modelling approach.

Computational Speed

The model updating showed a reasonable speed for updating the model, which lasted on average of about 6-8 minutes per 10,000 model computations. For the updating to complete, the best run took about 3 hours to complete while the longest run took about 13 hours. The updating can be optimized further to improve these speeds, especially if parallelization could be achieved, which should significantly reduce the computational time.

9.2. Bayesian Model Updating

The research sub-questions related to the Bayesian model updating approach are addressed in this section.

How should the prior probabilities be defined to best reflect the initial knowledge about the structural properties, including correlation?

For the choice of priors, a combination of guidance from the literature, such as the JCSS Probabilistic Code [35] and the reliability background of the Eurocodes [26], can serve as a starting point. When available information is limited, the principle of Maximum Entropy can be applied to define the prior distribution in a way that introduces the least bias. These suggested priors can subsequently be adjusted based on additional information as it becomes available. Similarly, in the absence of information about correlations, the Maximum Entropy principle recommends assuming no correlation between parameters, providing a neutral starting point for the Bayesian updating process.

To what extent does the definition of the priors affect the posterior distribution?

While priors influence the posterior distribution, it was observed that with a large and high-quality dataset, their effect becomes less critical. This indicates that a smooth prior covering the likely region of the solution is generally sufficient. In the present case study, a dataset of 100 points was adequate to reasonably constrain most parameters. Conversely, if the posterior remains sensitive to the choice of prior despite using a large dataset, this may indicate that the parameter is not identifiable with the available data, highlighting the potential subjectivity introduced by the priors.

What likelihood function/model should be used?

The likelihood function provides a measure of how likely a given set of measurements is, given the current parameter values in the model. While some authors have used error metrics, such as percentage error or the Modal Assurance Criterion (MAC), to construct the likelihood, a more rigorous definition is obtained by considering an assumed data generation process. This process links the real structure and the model while accounting for expected errors. When these errors are treated as random variables with assumed distributions, the likelihood of a parameter being the true value becomes equivalent to the probability of observing the mismatch between measured and predicted dynamic properties for the same parameter set.

Defining the likelihood in this way incorporates contributions from both measurement and model uncertainties. While measurement uncertainties can often be reasonably estimated, quantifying model

uncertainty remains a significant challenge. This is because little to no information is usually available on the characteristics of these uncertainties, and their quantification requires knowledge of the true structural parameters. However, by definition, the model updating process does not have access to the true parameters, which creates an inherent difficulty in accurately characterizing model uncertainty.

What insights can be derived from the updating results?

The Bayesian updating results provide uncertainty estimates of the updated parameters in the form of a joint posterior distribution. Analysing this distribution offers several insights into the model behaviour and the quality of the obtained solutions that may not be evident in deterministic approaches. Key insights include:

- Parameter Redundancy and Overfitting Detection: The Bayesian model updating revealed
 instances of overfitting caused by parameter redundancy through the presence of strong correlations among parameters. Such correlations, particularly when associated with wide uncertainty
 bounds, indicate that certain parameters may be redundant or that the available data are insufficient to constrain them effectively.
- Improvement in Correlation: The Bayesian approach can identify modal data that enhance the solution by reducing parameter correlation and overall uncertainty, even when these modes do not directly improve the frequency prediction error. This was evident in Case 2, where the inclusion of mode bx3 introduced additional independent information that mitigated overfitting observed in Case 1. Deterministic methods might overlook the value of such modes, as they typically assess performance only based on prediction accuracy.
- Parameter Identifiability: The Bayesian updating results can also reasonably check the identifiability of the updated parameters. The updated parameter showing a higher credible interval than the prior hints at the non-identifiability of a parameter, as it implies that less information is known about the parameter than what was started with. The investigation on the behaviour of the log-likelihood function around the predicted value revealed that if a parameter is not identifiable by the available data, then its converged value should be highly sensitive to the choice of prior.
- Multiple Solution Detection: Bayesian model updating demonstrated the capability to detect
 multi-modal posterior distributions, revealing the presence of multiple plausible solutions. Moreover, it quantifies the relative likelihood of each solution through the inherent probabilistic formulation of the posterior. Sampling-based methods, such as Markov Chain Monte Carlo (MCMC),
 further enhance this process by exploring the entire solution space, thereby capturing the true
 shape of the posterior distribution and providing deeper insight into the range and nature of potential solutions.

Mode Matching

The current research also developed a novel mode-matching method that pairs measured and model modes using the modal participation mass ratio (MPM). This approach provides an objective quantification of the contribution of each mode to the total dynamic response of the structure in a given direction (e.g., x, y, z, or θ). By considering both the directional influence and the relative order of the modes, this method enables robust pairing of modes even when measurements are sparse. Such robustness is particularly important for higher modes, which are often difficult to distinguish from lower modes in cases with limited spatial measurements.

9.3. Limitations and Recommendations

The results and findings of this research also highlight key limitations of the current approach. The case study indicates model inadequacy, particularly in capturing torsional and higher bending modes. One possible reason for this inadequacy is the omission of the adjoining low-rise building in the model.

The observed mode shapes suggest that the influence of surrounding structures cannot be ignored for higher bending (and potentially torsional) modes. Therefore, a recommendation for future work is to investigate this effect and determine the conditions under which the influence of adjoining structures can be safely neglected.

Similarly, another potential source of the model inadequacy, and the limitation of the current modelling approach is the assumption of rigid connection between all structural elements (beams, columns, shear walls and slabs). The connection stiffness can have a significant influence on the torsional (and potentially higher bending) modes. Investigating the effect of connection stiffness on these modes would provide valuable insight into the conditions under which the assumption of rigid connections is valid.

For the results of model updating, it was observed that the rotational stiffnesses converged to values significantly higher than expected. This raises questions regarding the validity of the current study. While several possible explanations have been proposed, the underlying mathematical reason appears to be that the reduction in uncertainty of E_{conc} , combined with the value at which it converged, led to the significant increases in the estimated rotational stiffnesses. Therefore, a dedicated study aimed at accurately identifying either the modulus of elasticity of the building or the rotational foundation stiffness with high confidence is recommended. Although model updating could be extended with additional data or refined model features, an independent investigation focusing on one of these two parameters would be valuable for verifying the present results.

Focusing on the Bayesian model updating aspect, a big challenge and limitation in the current study was the choice of model uncertainty. The current study employed a rudimentary method for determining an appropriate value, which relied on running a synthetic analysis to determine the identifiability of the parameter under assumed model uncertainty. A more rigorous approach may be used in future works to address this issue. For this, Bayesian model class selection can be used by varying the model uncertainty between different models and selecting the most promising value. Alternatively, the model uncertainty itself may be chosen as one of the parameter to be updated.

The final limitation relates more to the data rather than the methodology of the current study. The measurements were obtained using a set of four sensors in each direction. While this sparse sensor configuration was sufficient to identify the global modes, the limited sensor coverage near the lower floors and the base of the tower made it difficult to accurately estimate the behaviour of the foundation. It was observed that variations in foundational stiffness often had minimal effect on the mode shapes at the sensor locations. Additional sensors near the base would have provided critical information for improving the estimation of foundational stiffness. Therefore, a recommendation for future work is to prioritise additional sensor placement on the lower floors, particularly when identification of foundational stiffness is a key focus of the study.

References

- [1] Angelo Aloisio et al. "Dynamic identification and model updating of an eight-storey CLT building". In: *Engineering Structures* 213 (2020), p. 110593.
- [2] Onur Avci et al. "Operational modal analysis and finite element model updating of a 230 m tall tower". In: *Structures*. Vol. 37. Elsevier. 2022, pp. 154–167.
- [3] A. J. Bronkhorst et al. "Identification of the modal and structural properties of a high-rise scale model". In: *Proceedings of ISMA2024 including USD2024*. 2024.
- [4] AJ Bronkhorst and CPW Geurts. "Long-term vibration and wind load monitoring on a high-rise building". In: *Proceedings ISMA*. 2020.
- [5] AJ Bronkhorst, D Moretti, and CPW Geurts. "Identification of the dynamic properties of the residential tower New Orleans". In: *Experimental Vibration Analysis for Civil Engineering Structures: Select Proceedings of the EVACES 2021*. Springer, 2022, pp. 469–479.
- [6] A. Carranza Neurohr. "Wind-Induced Dynamic Response of High-Rise Buildings: The Effects of Soil-Structure Interaction and a Comparison with the Eurocode Approach". Public defense on August 25, 2022. Student number: 5215307. Master of Science Thesis (Civil Engineering). Delft, The Netherlands: Delft University of Technology, Aug. 2022. URL: http://repository.tudelft.nl/.
- [7] Luis GL Costa and André T Beck. "A critical review of probabilistic live load models for buildings: Models, surveys, Eurocode statistics and reliability-based calibration". In: *Structural Safety* 106 (2024), p. 102411.
- [8] Yu-Xia Dong et al. "Bayesian model updating of a 250 m super-tall building utilizing an enhanced Markov chain Monte Carlo simulation algorithm". In: *Case Studies in Construction Materials* 21 (2024), e03650.
- [9] Suzana Ereiz, Ivan Duvnjak, and Javier Fernando Jiménez-Alonso. "Review of finite element model updating methods for structural applications". In: *Structures*. Vol. 41. Elsevier. 2022, pp. 684–723.
- [10] D. Foreman-Mackey et al. "emcee: The MCMC Hammer". In: *PASP* 125 (2013), pp. 306–312. DOI: 10.1086/670067. eprint: 1202.3665.
- [11] Jonathan Goodman and Jonathan Weare. "Ensemble samplers with affine invariance". In: *Communications in applied mathematics and computational science* 5.1 (2010), pp. 65–80.
- [12] Ward Heylen and Paul Sas. "Modal analysis theory and testing". In: (2006).
- [13] Jun Hu and Jia-Hua Yang. "Operational modal analysis and Bayesian model updating of a coupled building". In: *International Journal of Structural Stability and Dynamics* 19.01 (2019), p. 1940012.
- [14] Edwin T Jaynes. "Information theory and statistical mechanics". In: *Physical review* 106.4 (1957), p. 620.
- [15] Edwin T Jaynes. "Information theory and statistical mechanics. II". In: *Physical review* 108.2 (1957), p. 171.
- [16] Tom de Jonge. Simulation-Efficient Structural Health Monitoring via Graph Neural Networks and Amortized Bayesian Inference. 2025.

References 68

[17] Korkut Kaynardağ and Serdar Soyöz. "'Structural Health Monitoring Of A Tall Building". In: Second European Conference On Earthquake Engineering And Seismology. 2014, pp. 25–29.

- [18] Heung Fai Lam, Jun Hu, and Mujib Olamide Adeagbo. "Bayesian model updating of a 20-story office building utilizing operational modal analysis results". In: *Advances in Structural Engineering* 22.16 (2019), pp. 3385–3394.
- [19] Pei Liu et al. "Bayesian model updating of a twin-tower masonry structure through subset simulation optimization using ambient vibration data". In: *Journal of Civil Structural Health Monitoring* 11.1 (2021), pp. 129–148.
- [20] Y Liu et al. "Lumped-mass stick modeling of building structures with mixed wall-column components". In: *Proc. 15th World Conf. Earthq. Eng.(WCEE)*. 2012, pp. 19624–19633.
- [21] Adolphus Lye, Alice Cicirello, and Edoardo Patelli. "Sampling methods for solving Bayesian model updating problems: A tutorial". In: *Mechanical Systems and Signal Processing* 159 (2021), p. 107760.
- [22] E. Marchelli. Reducing the uncertainty in dynamic models of high-rise buildings by means of parameter identification. 2023.
- [23] Davide Moretti, A.J. Bronkhorst, and Chris Geurts. *Identification of the structural properties of a high-rise building*. 2023.
- [24] Yuxin Pan et al. "Model updating and seismic response of a super tall building in Shanghai". In: *Computers & Structures* 239 (2020), p. 106285.
- [25] Phoebe. "Phoebe 2.4 Documentation". URL: https://www.phoebe-project.org/docs/2.4/tutorials/emcee.
- [26] Reliability background of the Eurocodes Support to the implementation, harmonization and further development of the Eurocodes. Publications Office of the European Union, 2024. DOI: doi/10.2760/9482837.
- [27] I.S. Ritfeld. *Identification of structural properties of high-rise buildings*. 2024.
- [28] IS Ritfeld, AJ Bronkhorst, and D Moretti. "Beam Model Updating Based on In-Situ Measured Modal Properties of a High-Rise Building". In: *International Conference on Experimental Vibration Analysis for Civil Engineering Structures*. Springer. 2025, pp. 521–531.
- [29] Nima Shirzad-Ghaleroudkhani et al. "Bayesian identification of soil-foundation stiffness of building structures". In: *Structural Control and Health Monitoring* 25.3 (2018), e2090.
- [30] Minjie Zhu Silvia Mazzoni. *Openseespy Documentation*. 2019. URL: https://openseespydoc.readthedocs.io/en/latest/index.html (visited on 04/26/2025).
- [31] Ellen Simoen. "Uncertainty Quantification in Finite Element Model Updating". PhD thesis. KU Leuven, 2013.
- [32] Ellen Simoen, Guido De Roeck, and Geert Lombaert. "Dealing with uncertainty in model updating for damage assessment: A review". In: *Mechanical Systems and Signal Processing* 56 (2015), pp. 123–149.
- [33] E Taciroglu, S Farid Ghahari, and F Abazarsa. "Efficient model updating of a multi-story frame and its foundation stiffness from earthquake records using a Timoshenko beam model". In: *Soil dynamics and earthquake engineering* 92 (2017), pp. 25–35.
- [34] Michael W Vanik, James L Beck, and Siu-Kui Au. "Bayesian probabilistic approach to structural health monitoring". In: *Journal of Engineering Mechanics* 126.7 (2000), pp. 738–745.
- [35] Ton Vrouwenvelder et al. *The JCSS probabilistic model code*. STRUCTURAL SAFETY VOL. 19, No. 3, 1997, 2001.

References 69

[36] JR Wu and QS Li. "Finite element model updating for a high-rise structure based on ambient vibration measurements". In: *Engineering Structures* 26.7 (2004), pp. 979–990.



Mass moment of inertia

Derivation of Mass Moment of Inertia of a prism with a constant cross-sectional area along its axis

The derivation for the mass moment of inertia around the centroidal axis, for any arbitrary cross-sectional prism is given below. This is relevant as columns can be considered as prisms with a constant cross-sectional area. This derivation can also be extended to slabs and shear walls, which are essentially as rectangular prisms (i.e. cuboids). The mass moment of inertia for a given body is defined as:

$$I_c = \int_M r^2 \, dm \tag{A.1}$$

Given that $m = V \rho$, for constant density ρ over the element, we get the relation:

$$dm = \rho \, dV \tag{A.2}$$

$$dm = \rho \, dx \, dy \, dz \tag{A.3}$$

Additionally, if we consider z to be in the direction of the axis of the prism, then r becomes independent of z. The sign convention for the prism is depicted in Figure A.1

Substituting in the original integral,

$$\begin{split} I_{c,||} &= \int \int \int r^2 \rho \, dx \, dy \, dz \\ &= \rho \int \underbrace{\int \int r^2 \, dx \, dy}_{I_{A,zz}} \, dz \\ &= \rho \int_0^H I_{A,zz} \, dz \\ &= \rho I_{A,zz} \int_0^H dz \qquad \text{(Constant cross-sectional area)} \\ I_{c,||} &= \rho H I_{A,zz} \end{split} \tag{A.4}$$

This result is valid for any prism-like object with a constant density and a constant cross-section along the z-direction, with H being the height/length quantity along the same direction. The term $I_{A,zz}$ represents the polar (area) moment of inertia of the cross-section of prism perpendicular to its axis.

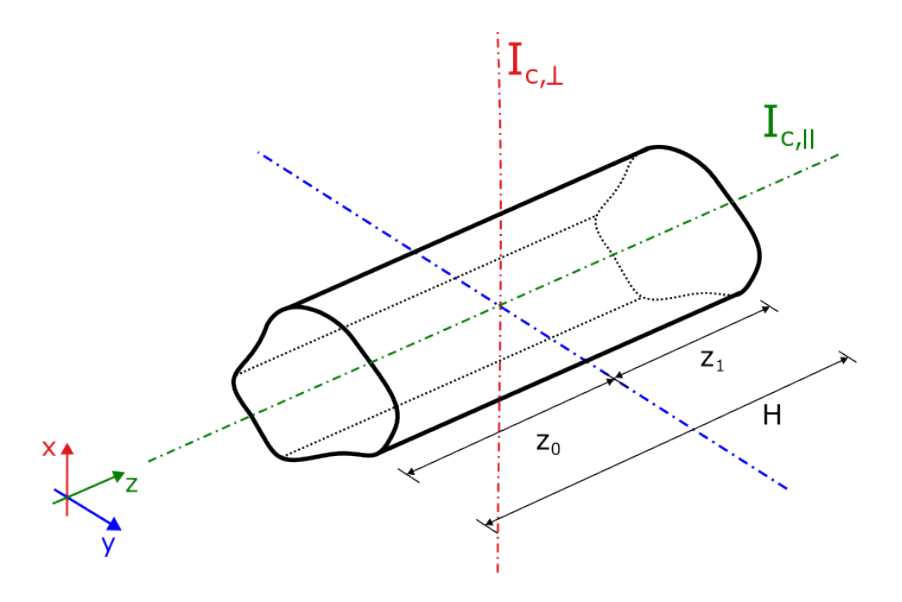


Figure A.1: A prism of arbitrary area A

Derivation of Moment of Inertia of a prism with a constant cross-sectional area perpendicular to its axis

The derivation for the mass moment of inertia around the centroidal axis, for any arbitrary cross-sectional prism is given below. This is mainly relevant for beams when considering the rotational mass for torsion, as beams can be considered as prisms with a constant cross-sectional area. The general equation for mass moment of inertia is again the same:

$$I_{c,\perp} = \int_{M} r^2 \, dm \tag{A.5}$$

Here, r^2 has two components, one in y direction and one in z direction, which makes this:

$$r^2 = y^2 + z^2 (A.6)$$

Given that $M = V \rho$, and considering a constant density ρ along the length of the element,

$$dm = \rho \, dA \, dz \tag{A.7}$$

Substituting this in the original integral, we get

$$I_{c,\perp} = \int_{-z_0}^{z_1} \int_A \rho(y^2 + z^2) \, dA \, dz$$

$$= \rho \int_{-z_0}^{z_1} \underbrace{\int_A y^2 \, dA \, dz}_{I_{A,xx}} + \rho \int_{-z_0}^{z_1} z^2 \int_A dA \, dz$$

$$= \rho I_{A,xx} \int_{-z_0}^{z_1} dz + \rho A \int_{-z_0}^{z_1} z^2 \, dz$$

$$= \rho I_{A,xx} (z_1 + z_0) + \frac{\rho A}{3} (z_1^3 + z_0^3)$$

$$I_{c,\perp} = \rho I_{A,xx} H + \frac{\rho A}{3} (z_1^3 + z_0^3)$$
(A.8)

The term $I_{A,xx}$ represents the area moment of inertia (with axis in x-direction) for the cross section of prism perpendicular to its axis.

Parallel Axis Theorem

For completeness, the derivation of parallel axis theorem is also provided here.

Consider a body with the centre of mass at (x_m, y_m, z_m) . It is required to calculate the mass moment of inertia about a vertical axis passing through the location $(x_m + \Delta x, y_m + \Delta y)$. If (x, y) represents the distance of an infinitesimal element from the centre of mass, then the mass moment of inertia about this shifted axis is given by the following equation:

$$I = \int_{M} r^{2} dm$$

$$= \int_{M} \left((x - \Delta x)^{2} + (y - \Delta y)^{2} \right) dm$$

$$= \int_{M} \left(x^{2} - 2x \Delta x + \Delta x^{2} + y^{2} - 2y \Delta y^{2} + \Delta y^{2} \right) dm$$

$$= \underbrace{\int_{M} (x^{2} + y^{2}) dm - 2\Delta x}_{I_{cm}} \underbrace{\int_{M} x dm - 2\Delta y}_{=0} \underbrace{\int_{M} y dm}_{=0} + \int_{M} \left(\Delta x^{2} + \Delta y^{2} \right) dm$$

$$= I_{cm} + M \left(\Delta x^{2} + \Delta y^{2} \right)$$

$$= I_{cm} + \rho V \left(\Delta x^{2} + \Delta y^{2} \right)$$
(A.9)

As no assumptions about the cross-section was done at any point in the derivation, the result is general, and can be used without the loss of accuracy.

Torsional Foundational Stiffness Determination

B.1. Approach

Let us consider an arbitrary pile located at the polar coordinates (r, θ) . Let the centre of torsion be at the origin, i.e. at (0,0). The location of the pile in the Cartesian plane will be (x,y), which is related to its polar coordinates through the following two relations

$$x = r \cdot \cos \theta$$

$$y = r \cdot \sin \theta$$
(B.1)

Let $\delta\theta$ be a small torsional displacement of the pile cap. Due to this, the new polar coordinates of the displacement pile will be at $(r, \theta + \delta\theta)$ In Cartesian plane, this would be $(x + \delta x, y + \delta y)$. Relating the two coordinates, we get the following equations:

$$x + \delta x = r \cdot \cos(\theta + \delta \theta)$$

$$y + \delta y = r \cdot \sin(\theta + \delta \theta)$$
(B.2)

The expression for δx and δy can now be isolated using equations B.1 and B.2.

$$\delta x = r \cdot \left(\cos(\theta + \delta \theta) - \cos \theta \right)$$

$$\delta y = r \cdot \left(\sin(\theta + \delta \theta) - \sin \theta \right)$$
(B.3)

Applying Trigonometric identities, we get:

$$\delta x = r \cdot \left(\cos \theta \cos \delta \theta - \sin \theta \sin \delta \theta - \cos \theta \right)$$

$$\delta y = r \cdot \left(\sin \theta \cos \delta \theta + \cos \theta \sin \delta \theta - \sin \theta \right)$$
(B.4)

Given that $\delta\theta$ is assumed to be a small torsional displacement, small angle approximation may be used, which approximates $\sin \delta\theta \approx \delta\theta$ and $\cos \delta\theta \approx 1$. This simplifies the expressions into:

$$\delta x = -r \cdot \sin \theta \cdot \delta \theta$$

$$\delta y = r \cdot \cos \theta \cdot \delta \theta$$
(B.5)

B.1. Approach

Using Eq. B.1, the above expression can be further simplified as;

$$\delta x = -y \cdot \delta \theta
\delta y = x \cdot \delta \theta$$
(B.6)

Now, let the equivalent torsional stiffness of the foundation be denoted by K_{rz} . The strain energy U_{tor} stored in the foundation under an applied torsional displacement $\delta\theta$ is given as:

$$U_{tor} = \frac{1}{2} K_{rz} \, \delta\theta^2 \tag{B.7}$$

At this step, a few assumptions are introduced to simplify the calculation of the equivalent torsional stiffness. These assumptions are listed below:

- 1. The pile cap (foundation slab) is assumed to undergo a rigid body rotation. In other words, every part of the pile cap undergoes the same rotation $\delta\theta$. Thus, the pile cap does not provide any rotational stiffness, and consequently, does not store any strain energy.
- 2. The piles themselves are assumed to not undergo any torsional rotation. Thus, the piles do not store strain energy in the form of torsional displacement. This simplification was done as the details for the torsional stiffness of an individual pile was not available.
- 3. The effect of soil surrounding the pile cap and the basement is not considered, due to lack of information in these regards.
- 4. The effect of soil in between the piles are assumed to be considered within the lateral stiffness of the piles provided by the designer.

Under these assumptions, the torsional strain energy is stored entirely in the piles due to their lateral stiffnesses in the x and y directions. Thus, for a pile plan consisting of n_p piles, the strain energy due to the torsional displacement $\delta\theta$ is given as:

$$U_{piles} = \sum_{i=1}^{n_p} \left(\frac{1}{2} k_{px,i} \, \delta x_i^2 + \frac{1}{2} k_{py,i} \, \delta y_i^2 \right)$$
 (B.8)

where

 $k_{px,i}$: translational stiffness of i^{th} pile in x direction

 $k_{py,i}$: translational stiffness of i^{th} pile in y direction

 δx_i : displacement of i^{th} pile in x direction due to $\delta \theta$

 δy_i : displacement of i^{th} pile in y direction due to $\delta \theta$

Given the assumptions, $U_{tor} = U_{piles}$. Using this, along with the substitution of B.6, we get the following expressions:

$$\frac{1}{2}K_{rz} \,\delta\theta^2 = \sum_{i=1}^{n_p} \left(\frac{1}{2} k_{px,i} \, (-y_i \cdot \delta\theta)^2 + \frac{1}{2} k_{py,i} \, (x_i \cdot \delta\theta)^2 \right)$$

$$K_{rz} = \sum_{i=1}^{n_p} \left(k_{px,i} \, y_i^2 + k_{py,i} \, x_i^2 \right) \tag{B.9}$$

where

 (x_i, y_i) : coordinates of the i^{th} pile

Equation B.9 is the required expression for the determination of equivalent torsional stiffness of the foundation.

B.2. Values for the New Orleans Tower

For the New Orleans Tower, 316 piles depicted in Figure B.1 were considered. Each of the pile was assumed to have stiffness as follows:

$$k_{px} = 10 \text{ MN/m} \tag{B.10}$$

$$k_{py} = 10 \text{ MN/m} \tag{B.11}$$

Using Eq. B.9, the torsional stiffness was calculated as

$$K_{rz} = 5.11 \times 10^{11} \text{ Nm/rad.}$$
 (B.12)

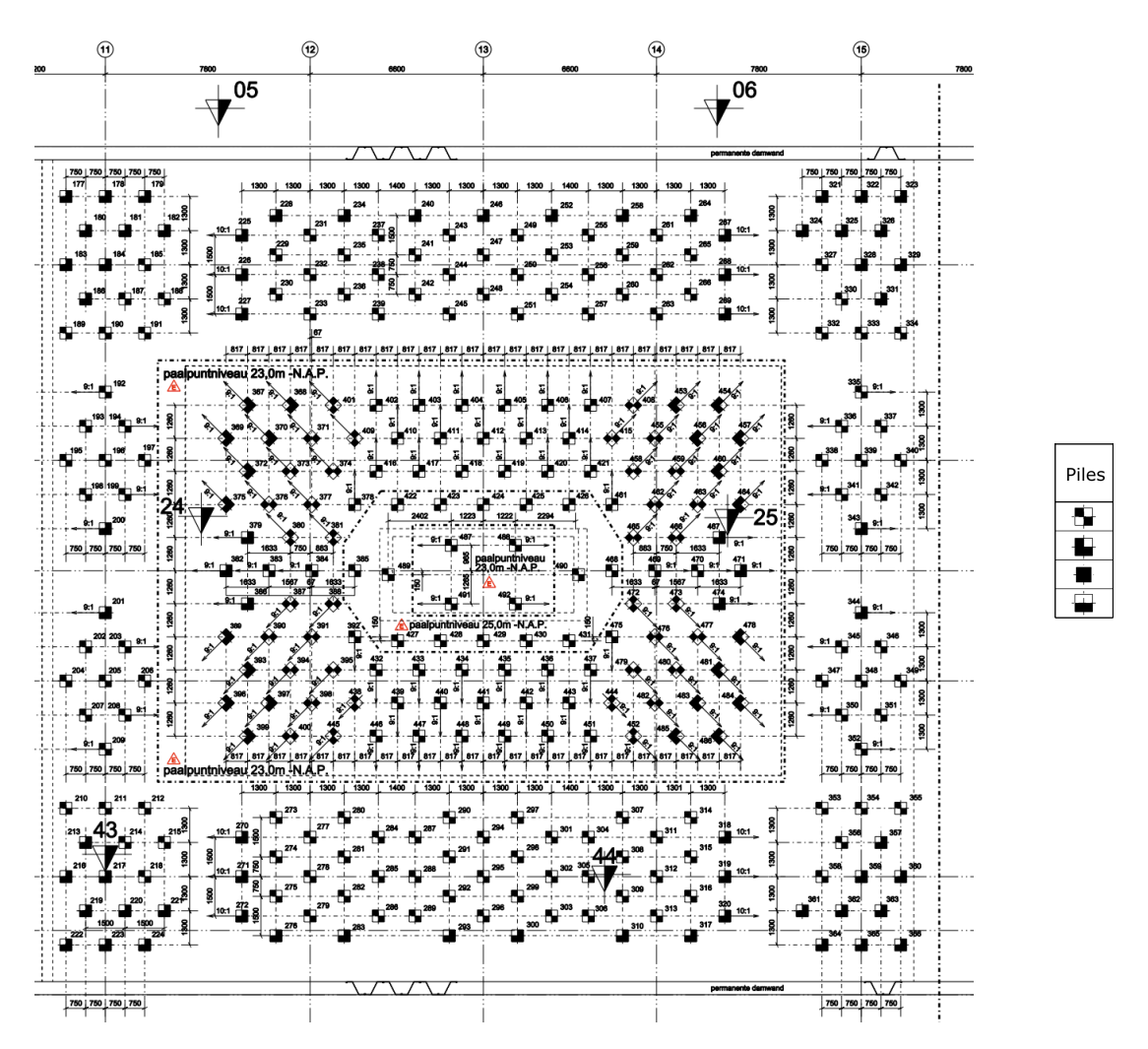


Figure B.1: Pile Plan for New Orleans Tower



Mode Matching

In this appendix the mode matching algorithm is described. The developed mode matching algorithm is based on the use of modal participation mass ratio to classify and match modes. The modal participation mass (MPM) is a quantity that measures the total mass that is mobilized in a given mode of vibration. The modal participation mass is defined as:

$$MPM_{ij} = \frac{\left(\phi_{i}^{T}MT_{j}\right)^{2}}{gm_{ii}}$$
 (C.1)

where,

M = Mass Matrix

 $gm = \phi^T M \phi =$ Generalised Mass Matrix

T = Directional matrix

When the directional matrix, T is defined as follows, the modal participation mass accounts for the three translational and three rotational directions [30].

$$\boldsymbol{T}_{nj} = \begin{pmatrix} 1 & 0 & 0 & 0 & d_z & -d_z \\ 0 & 1 & 0 & -d_z & 0 & d_x \\ 0 & 0 & 1 & d_y & -d_x & 0 \\ 0 & 0 & 0 & 1 & 0 & 0 \\ 0 & 0 & 0 & 0 & 1 & 0 \\ 0 & 0 & 0 & 0 & 0 & 1 \end{pmatrix} \begin{pmatrix} e_1 \\ e_2 \\ e_3 \\ e_4 \\ e_5 \\ e_6 \end{pmatrix}$$
(C.2)

where,

$$e_p = \begin{cases} 1, & p = j \\ 0, & p \neq j \end{cases}$$

 $d_x, d_y, d_z =$ distance of node n from the centre of mass in the three directions

The modal participation mass can be expressed as the percentage of the total mass for translational directions, and the total rotational mass for the rotational mass. This would lead to a modal participation mass

ratio which is a $n_{modes} \times 6$ matrix. The columns of this matrix represent the percentage of total mass activated in the three translational (M_x, M_y, M_z) and three rotational directions (RM_x, RM_y, RM_z) . These six columns can be easily translated to the different mode types - activation of M_x and RM_y corresponds to bending in x, M_y and RM_x to bending in y, RM_z to torsional and M_z to axial type deformation. Thus, based on which mass is activated for a given mode, a reasonable guess on whether the mode is bending in x, bending in y, torsion, axial, or a mixed mode can be made. When this information is supplemented with the order at which all the modes appear, the mode matching can be made with the measured mode easily just based on the order and type.

The proposed algorithm for mode matching requires a few assumptions and conditions to be true for it to work. The first requirement is that the order of the measured modes is known a-priori. This means that the measured modes can be identified and classified well. An extension of this requirement is that the identified modes are not mixed modes. However, this requirement of non-mixed modes can be waived with a little adjustment in the algorithm. Next requirement or assumption is that the measured modes do not have any modes missing. This means, for example, for the bending mode in x direction, bx_{n-1} exists before bx_n for all the considered n. Similar condition applies for the other types of modes (by_n and t_n). These conditions are generally satisfied for lower modes, which are also usually the modes of interest in model updating.

The algorithm used for the mode matching is explained below:

- 1. Input lists: For the input, the modal participation mass ratio matrix ordered based on the frequencies is required. This is usually obtained directly from FE software. Additionally, the frequencies and modes from the model as well as the measurement is required. The order of the measured mode is also required, i.e. a list that describes the direction of the mode such as [bx, by, t, by, ...]
- 2. From the mass participation matrix, for each mode identify the two distinct directions most strongly excited by the mode.
- 3. From the list of measured modes, read the first mode type in the list. For example, from the list above, this would be bx.
- 4. Determine two candidate modes that match this measured mode as (i) the first mode with the highest contribution in the given direction (candindate 1), and (ii) the first mode whose primary contribution lies in another direction but for which this direction represents the second-highest contribution (candidate 2).
- 5. Select the mode that corresponds to the measured mode. This is done through various checks.
 - (a) The first check is order of candidate 1 and 2. If candidate 1 appers before candidate 2, always select candidate 1.
 - (b) The second check is done when candidate 2 appears before candidate 1. This suggests a possibility of mixed mode. Check the ratio of the modal mass participation for the dominant direction and second dominant direction (required direction). If this ratio is higher than a pre-specified tolerance, then conclude that the candidate 2 is a pure mode, and thus disregard candidate 2 and select candidate 1.
 - (c) If candidate 2 is not a pure mode based on the tolerance test, then a traditional test needs to be carried out to determine which candidate mode to be chosen. For this, an error function defined as the weighted sum of error in frequency and modeshapes (MAC) is used (Eq. C.3) The candidate mode with lower error is chosen.

$$J_{ij} = \alpha \left| \frac{f_{M,i} - f_{E,j}}{f_{E,j}} \right| + \beta MAC(\phi_{M,i}, \phi_{E,j})$$
 (C.3)

- 6. Once a model mode is matched to a measured mode, it is excluded from further matching to avoid duplication.
- 7. The procedure is repeated for all measured modes in the order specified by the measured_order list. For modes that cannot be matched (e.g., no candidate exists in the required direction), a placeholder mode is assigned to indicate a missing match.
- 8. The final output consists of two lists: one containing pairs of matched mode shapes (measured and model), and the other containing pairs of matched frequencies. These outputs preserve the order of the measured modes, allowing direct comparison of modal properties between the measurement and the model.

Figure F.12 and Figures F.10, F.11 depicts the relation between the relative values of MPM ratio in different directions with the pure modes for the results of Case 3.

The proposed algorithm has a few strengths over the traditional mode-matching based on error function. The first advantage of using this is since the method relies on classifying the modes, much like how we would classify it based on how they look, for the cases of all pure modes, the method will always work. This is especially useful when multiple modes appear similar due to sparsity of sensor distribution. The method based on error tend to struggle in such cases, as the error based on MAC could be misleading at times. The method based on error can also give different results based on the weights used, making the choice important. The current method does not have any such requirement for the weights. The value for tolerance is required, but this term is much more intuitive, with choosing a higher value generally working. The other advantage is that this method ensures that a same mode from the model does not match with two modes from the measurements. This one-to-one correspondence reduces possibilities of mismatching the modes.

However, the proposed method also has some limitations. The limitations are usually related to the assumptions, with the biggest limitation being if the modes are missing. When a mode is missing in the measurement side, this would affect the matching of all the modes of that type. Another potential limitation for this method is that it may not be appropriate for local modes. As the method relies on a more global properties, and global direction of mode shapes, the method fails to capture the differences in mode shapes where local behaviour is governing. Finally, while the method does work for mixed modes for the model mode shapes, mixed modes observed in the measurement side will pose issues. This can, however, be circumvented by adjusting the algorithm.



Markov Chain Monte Carlo (MCMC)

Markov Chain Monte Carlo (MCMC) simulation methods are recognized as among the most popular stochastic sampling techniques employed in Bayesian inference [32]. The principal goal of MCMC is to generate samples that are consistent with a complex target distribution, typically the posterior Probability Density Function (PDF) of uncertain model parameters within the Bayesian framework. This simulation approach is essential because, for most practical applications involving multiple parameters, evaluating the posterior distribution requires solving high-dimensional integrals, which cannot generally be calculated analytically [32]. MCMC addresses this challenge by combining Monte Carlo simulation with the concept of Markov chains [21, 32]. The process involves simulating a sequence of states, or samples, that form a Markov chain, whose limiting stationary distribution is designed to be the target PDF [21]. These generated samples can then be used in statistical averaging to estimate various properties and expectations related to the distribution. A foundational and widely used MCMC approach is the Metropolis-Hastings (MH) algorithm, which allows sampling from an arbitrary PDF even when the function defining that PDF is only known up to a scaling constant.

The summary of MCMC how the MCMC process works in given below [21]:

- Step 1: Problem Formulation Before MCMC starts, the hyper-parameters for the MCMC process are defined. This includes number of walkers n_{walker} , prior and likelihood distributions, proposal distribution, $q(\theta_{i+1}|\theta_i)$, and burn-in period, and initial state, θ_0 . The walkers represent independent Markov Chains process that is running at the same time. Each of the walker behaves exactly the same, with the only difference being their initial state. The initial state refers to the first set of "guess" for the parameters that is under investigation. The initial state may be taken as a random realisation of the prior. Doing so ensures that all the walkers start at a different initial state. The proposal distribution refers to the distribution which will be used to generate the potential next point in the Markov chain. Finally, the burn-in period refers to the number of initial samples to be discarded. This is done to remove the region of non-convergence that exists before a chain converges to a stable region.
- Step 2: Initialization As the first step of MCMC, the value of posterior is calculated from the current state, θ_i , which right now is the initial state. This value is calculated from equation 4.1, where the current state, θ_i is substituted for θ . The normalizing constant is not considered.
- Step 3: Checking State Change Then using the proposal distribution, $q(\theta_{i+1}|\theta_i)$, a new state is proposed. In general, the proposal distribution is a normal distribution centred at θ_i , with some variance. This ensures that the new state reasonably close to the current state. Using this new state, the posterior is calculated. Figure D.1 visually illustrates the proposal distribution around

the current state and the probability of selecting the next state, while highlighting how these are related to the posterior distribution.

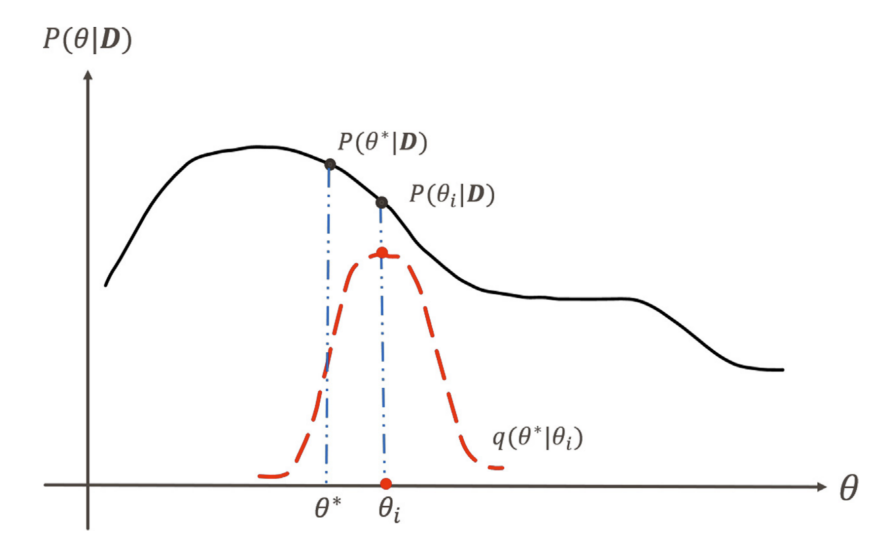


Figure D.1: Proposal Distribution (Red Curve); Posterior Distribution (Black Curve); Current State θ_i ; Proposed State θ^* . (Figure from Lye et al. [21])

• **Step 4: Acceptance Rate** With the posterior from the two states, an acceptance rate can be defined as the ratio of posterior and proposal distribution of the two states as follows:

$$\alpha = \min \left[1, \ \frac{c \cdot p(\mathcal{D} \mid \boldsymbol{\theta}_{i+1}) \cdot p(\boldsymbol{\theta}_{i+1})}{c \cdot p(\mathcal{D} \mid \boldsymbol{\theta}_{i}) \cdot p(\boldsymbol{\theta}_{i})} \cdot \frac{q(\boldsymbol{\theta}_{i} \mid \boldsymbol{\theta}_{i+1})}{q(\boldsymbol{\theta}_{i+1} \mid \boldsymbol{\theta}_{i})} \right]$$
(D.1)

From Eq. D.1, it is seen that the normalizing constant cancels out, justifying the choice of not considering it in the calculation of posterior. Furthermore, with the choice of proposal distribution as normal distribution, which is symmetrical, we get the condition that $q(\theta_{i+1} \mid \theta_i) = q(\theta_i \mid \theta_{i+1})$, which eliminates these terms in the expression. The final expression becomes

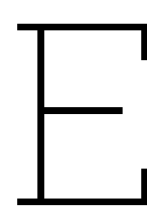
$$\alpha = \min \left[1, \frac{p(\mathcal{D} \mid \boldsymbol{\theta}_{i+1}) \cdot p(\boldsymbol{\theta}_{i+1})}{p(\mathcal{D} \mid \boldsymbol{\theta}_{i}) \cdot p(\boldsymbol{\theta}_{i})} \right]$$
(D.2)

This expression returns a 1 if the new posterior is higher than the current posterior, and the ratio of the two if the new posterior is lower than the current posterior.

- Step 5: Next State Check A random number, r, is then generated from a uniform distribution between 0 and 1. If we satisfy the condition that $\alpha \geq r$, then the new state is accepted, and the current state moves to this new state. This setup ensures that the chain converges towards the region of high posterior, while still allowing for exploration around the high posterior region. If the new state is accepted, the new state is added to the Markov chain. If the new state is not accepted and the chain stays at the current state, a duplicate of the current state is not added to the Markov chain.
- Step 6: Exploration and Convergence Depending on the previous step, the current state θ_i either changes or stays the same. The steps 2 through 5 is repeated numerous times, until stop criterion is satisfied. The stop criterion is usually when maximum number of steps is completed or if the chain has converged based on the autocorrelation values.
- Step 7: Burn-in Period If the Markov chain has converged, this will appear as the chain moving within a set region for multiple steps. The statistics of the chain in this region provides the

statistics of the posterior. To evaluate this, the initial region, called the burn-in period, where the walker was still exploring towards convergence must be removed. This ensures that the posterior statistics is not skewed by samples that have not converged.

The samples that remain after discarding the burn-in period represents the samples that have been directly sampled from the posterior distribution. Thus, plotting the histogram of these samples would provide a visual indication on how the posterior looks, while computing the statistics from these samples will give us the statistics of the posterior.



Fitting Probability Distribution

The current work attempts to gain a posterior distribution of the parameters, based on updating the model with the measured frequencies and mode shapes. As Case 3 saw the best result in generalisation, the results of the case 3 was fitted into a standard probability distribution. Table E.1 gives the shape and scale factors for the log-normal distribution for different parameters. The location parameter is 0 for all the parameters. Log-normal distribution was chosen over normal, as the updated parameters showed a slight tilt towards the lower values. Fig E.1 shows the log-normal distribution being fitted to the posterior samples.

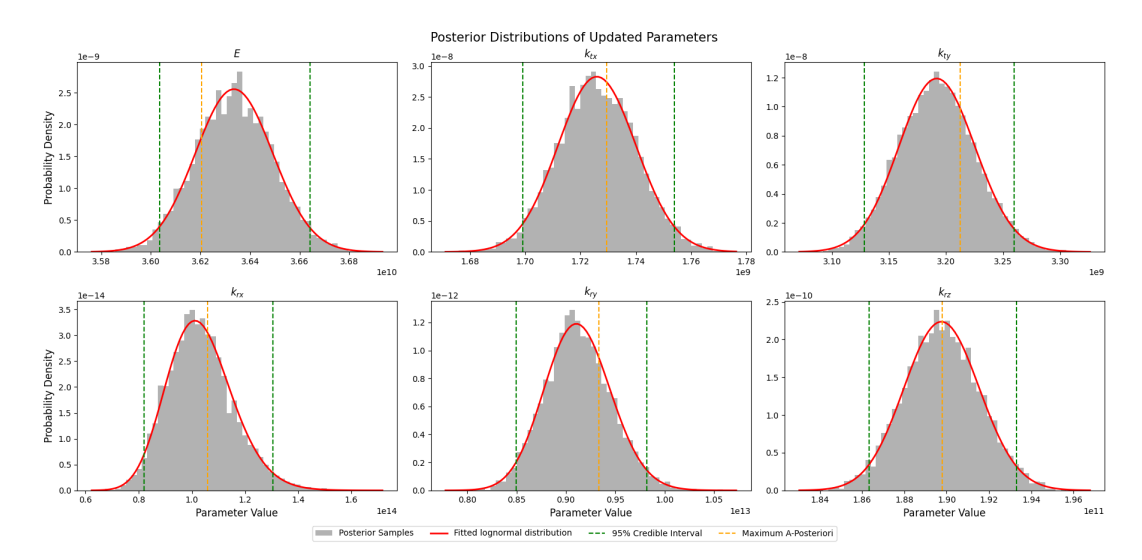


Figure E.1: Marginal posterior distribution of parameters

Table E.1: Parameter Statistics

Parameter	Shape	Scale	MAP	
E_{conc}	4.30×10^{-3}	3.63×10^{10}	3.62×10^{10}	
K_{tx}	8.18×10^{-3}	1.73×10^{9}	1.73×10^{9}	
K_{ty}	1.05×10^{-2}	3.19×10^9	3.21×10^{9}	
K_{rx}	1.19×10^{-1}	1.03×10^{14}	1.06×10^{14}	
K_{ry}	3.68×10^{-2}	9.12×10^{12}	9.34×10^{12}	
K_{rz}	9.40×10^{-3}	1.90×10^{11}	1.90×10^{11}	



Additional Figures and Results

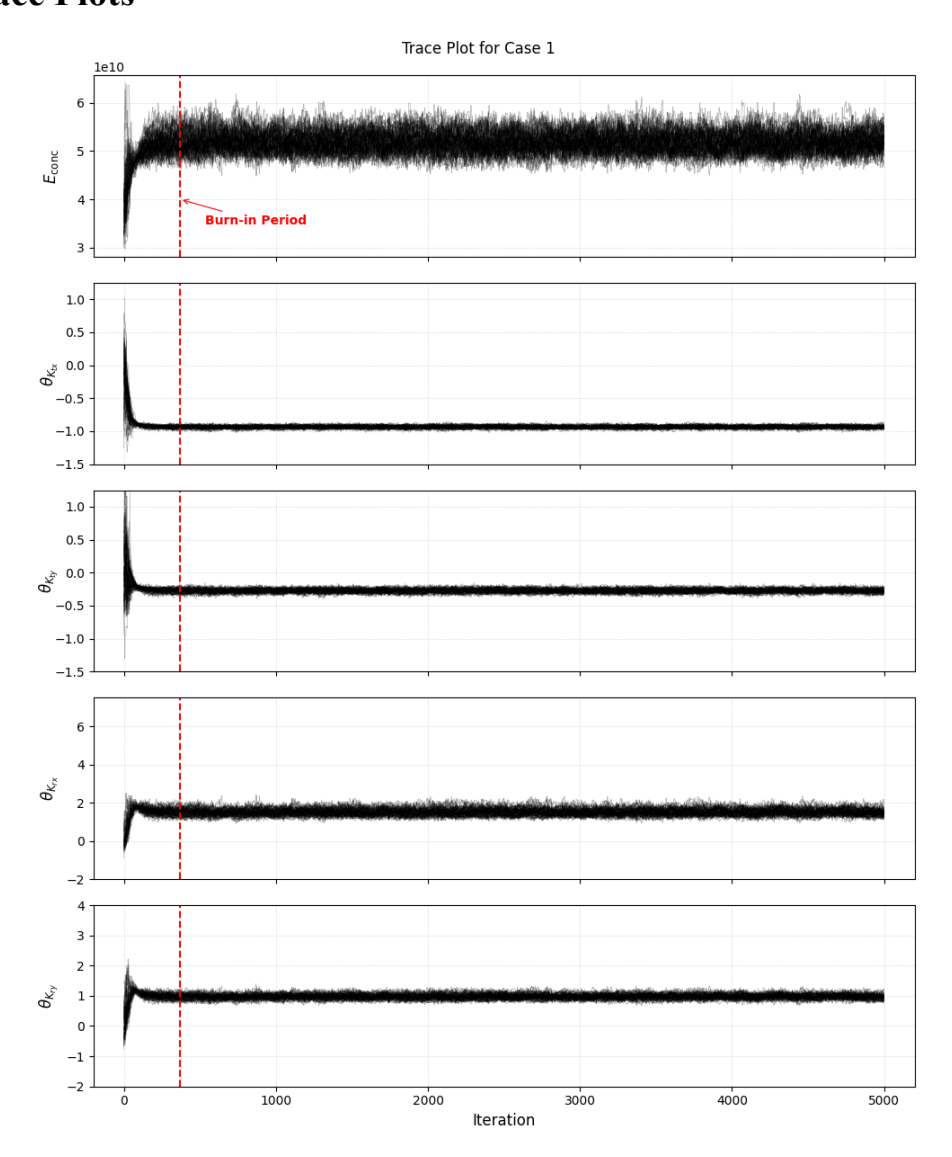


Figure F.1: Trace Plot for Case 1

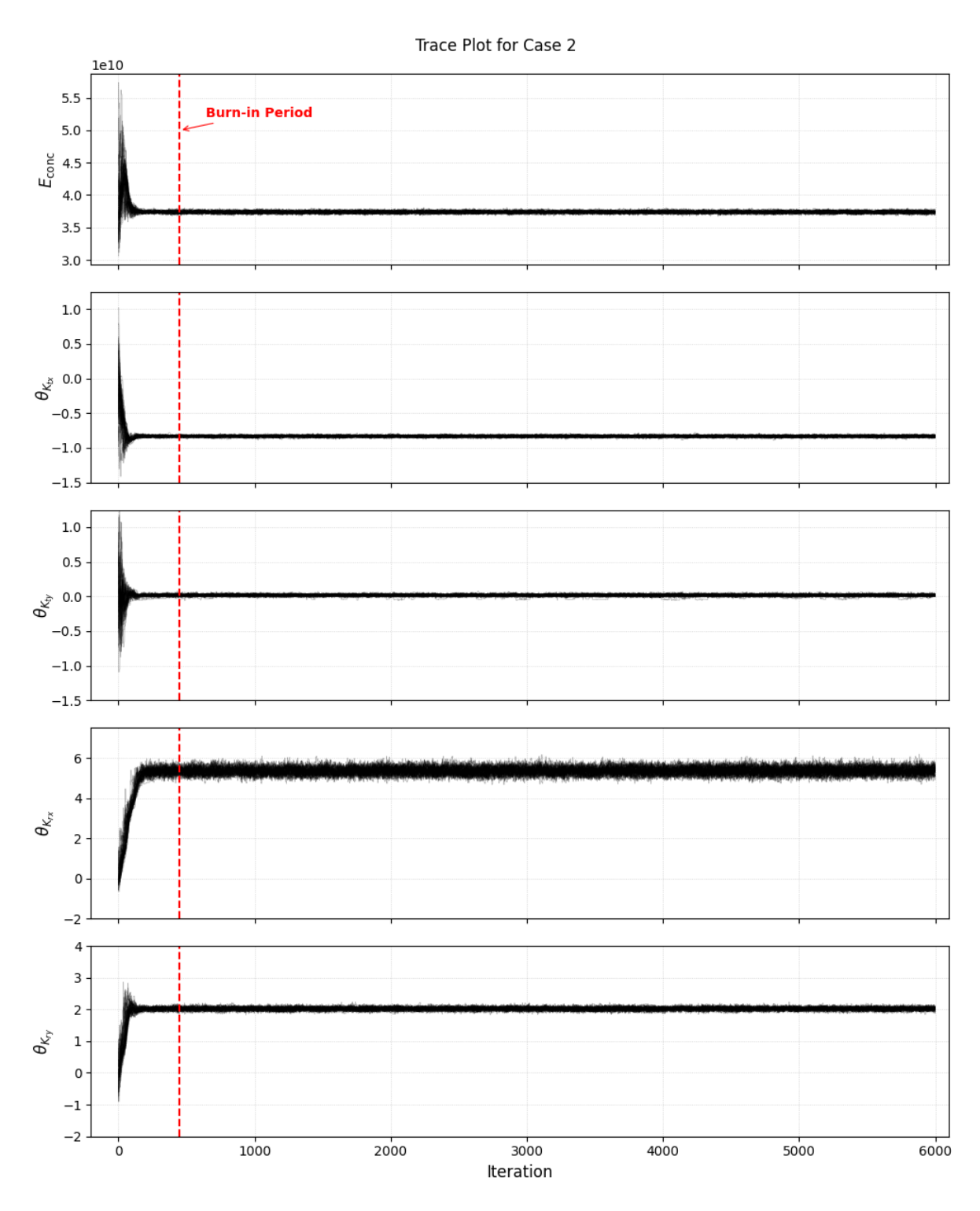


Figure F.2: Trace Plot for Case 2

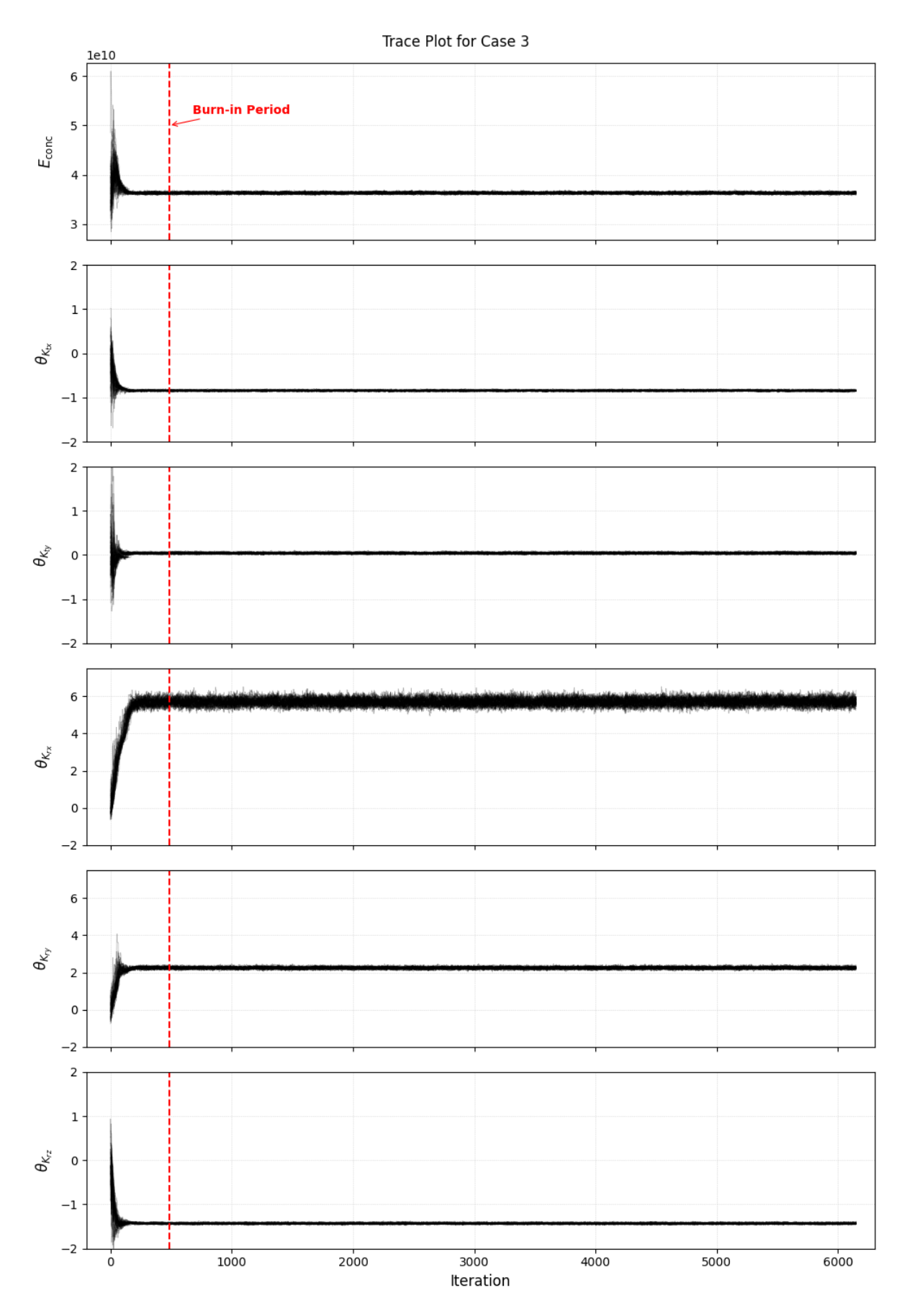


Figure F.3: Trace Plot for Case 3

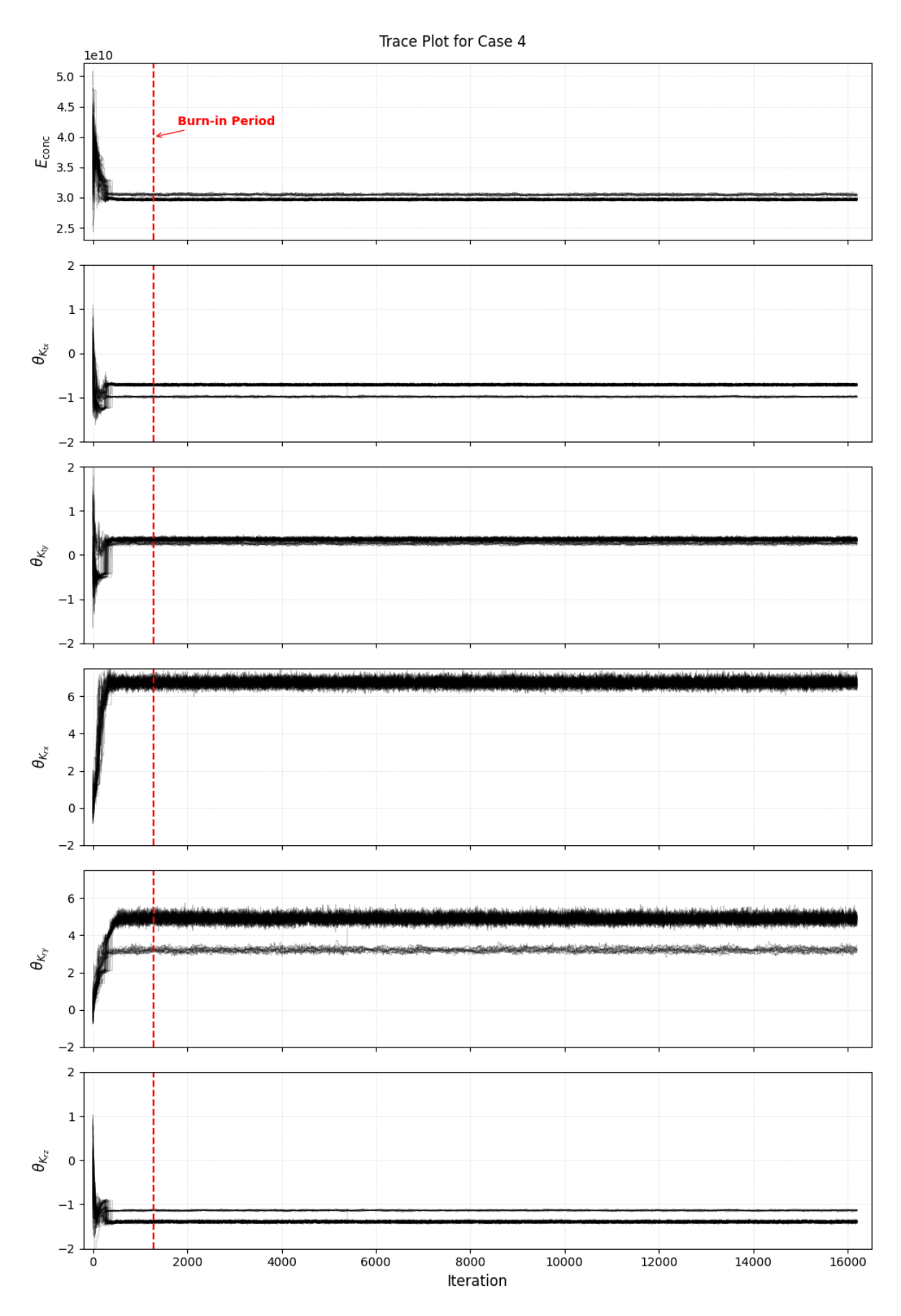


Figure F.4: Trace Plot for Case 4

F.2. Corner Plot for Parameter

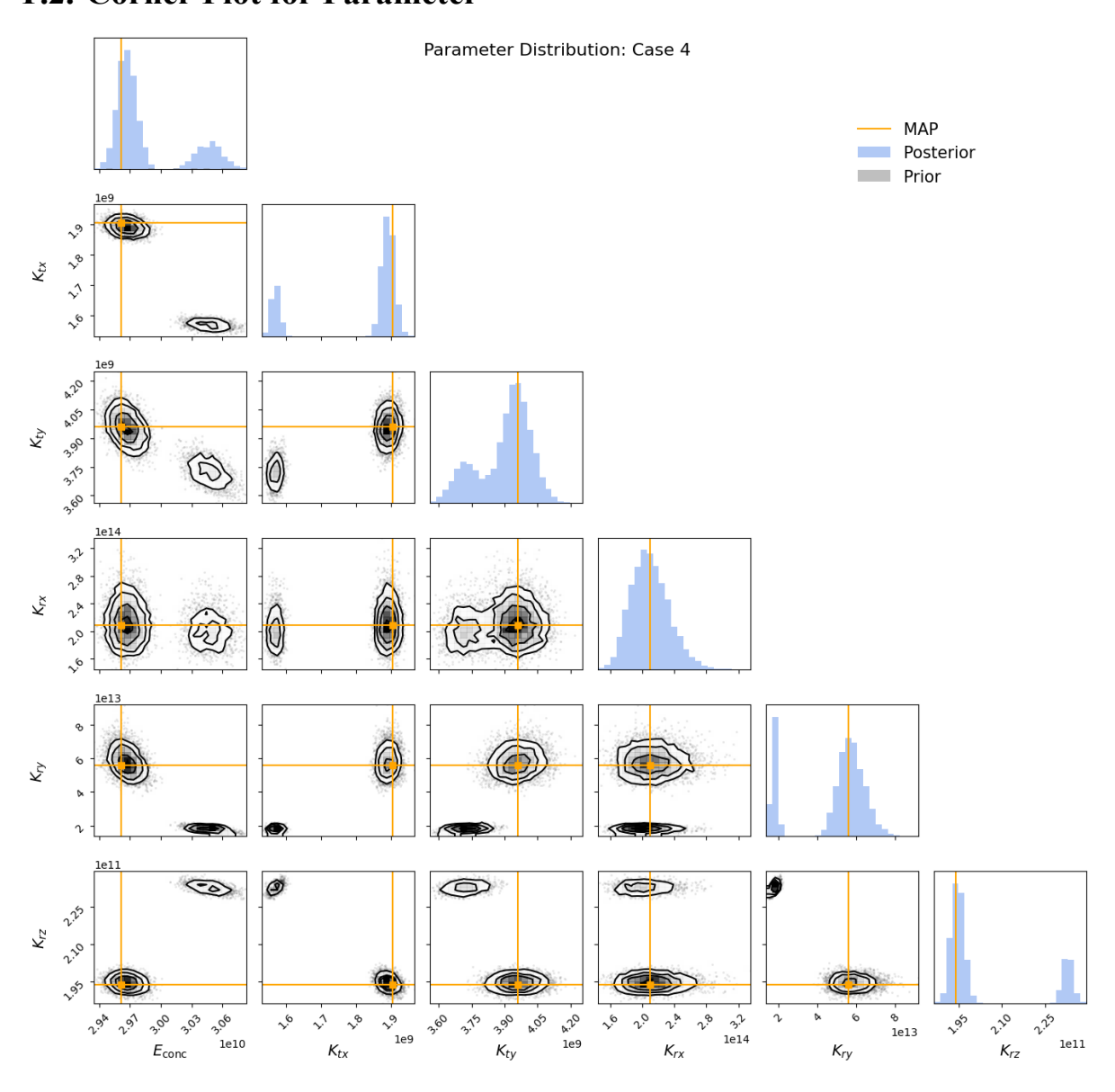


Figure F.5: Corner Plot for Parameters for Case 4

F.3. Corner Plot for Frequencies

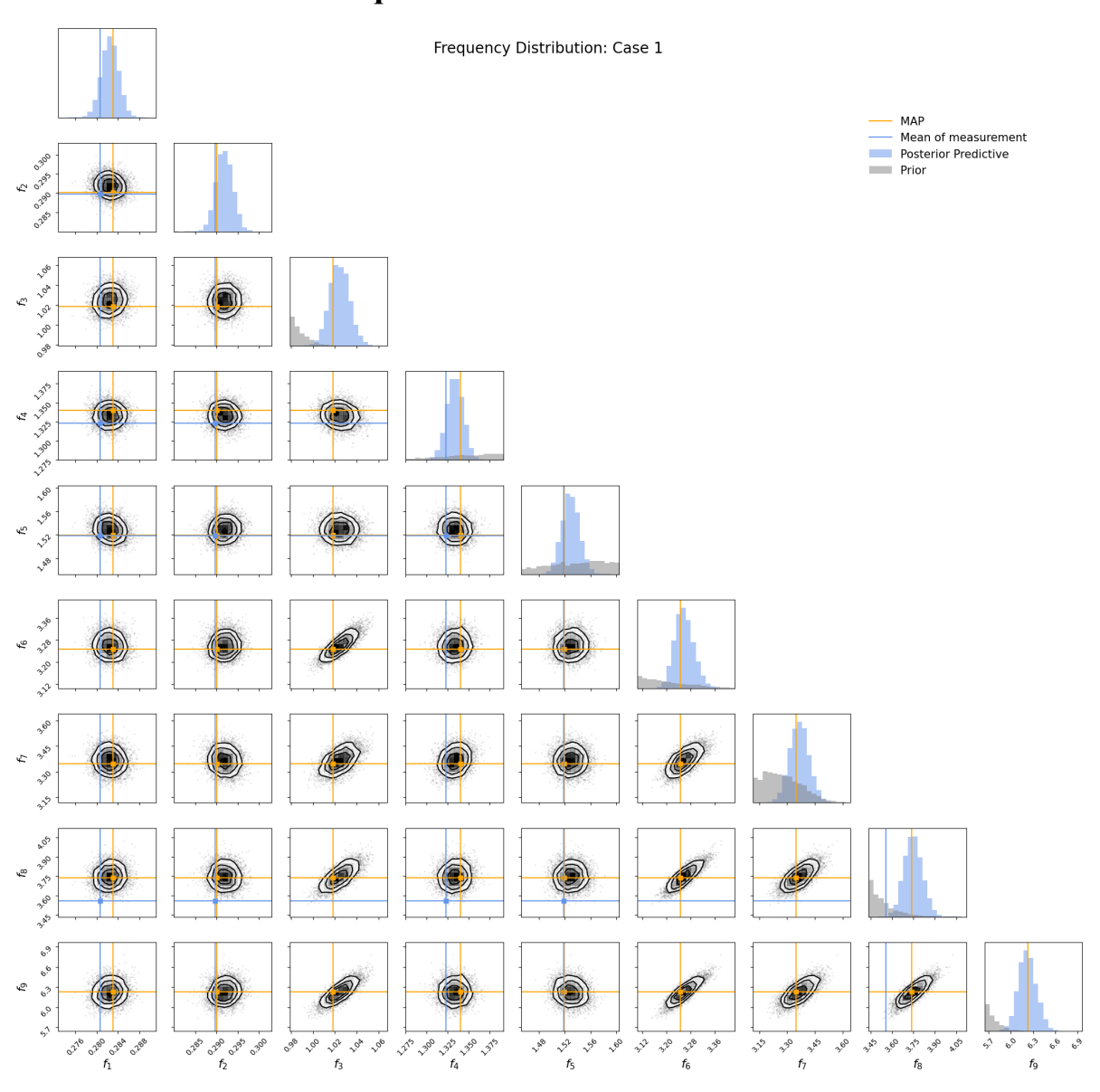


Figure F.6: Corner Plot for Frequencies for Case 1

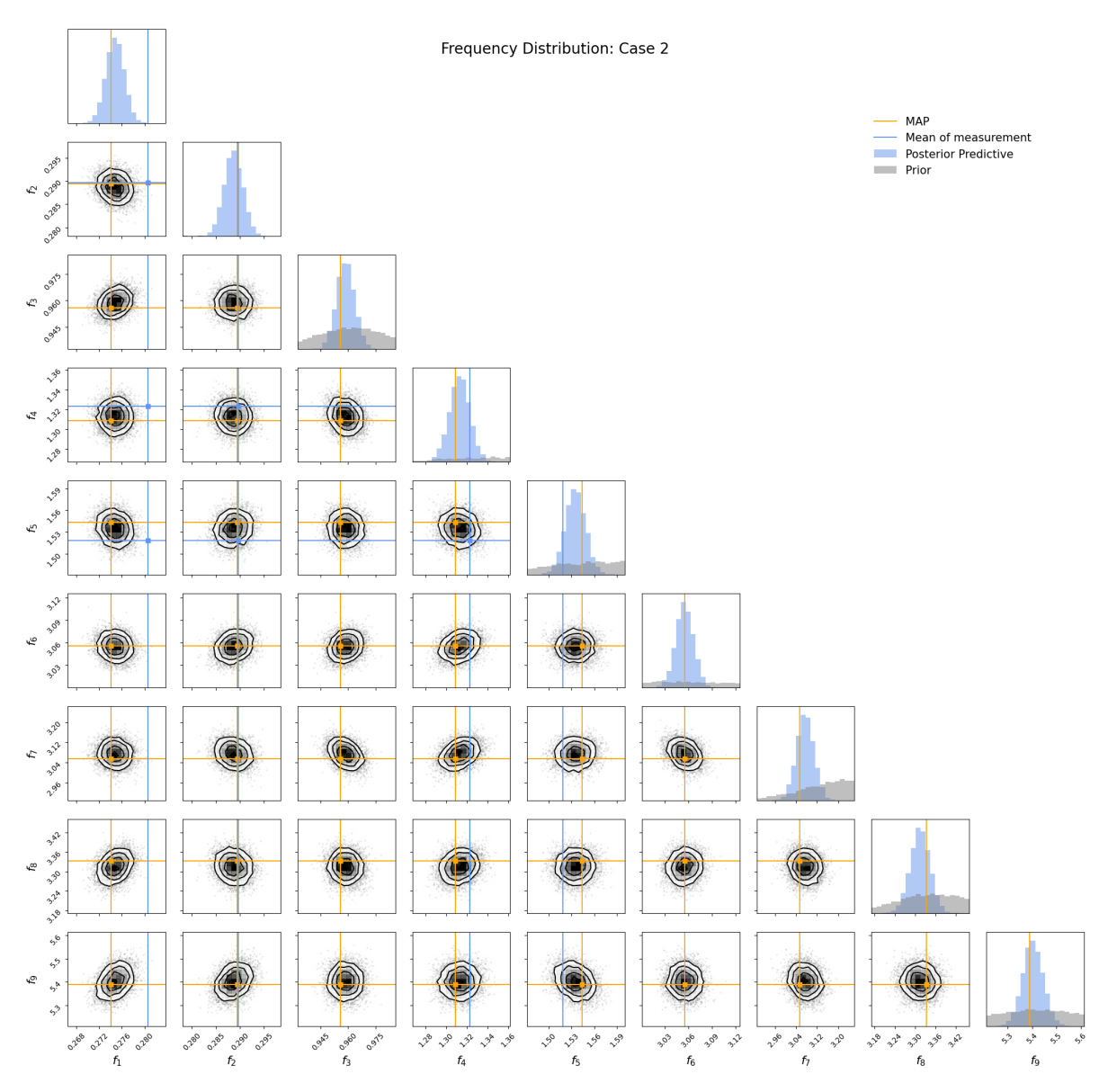


Figure F.7: Corner Plot for Frequencies for Case 2

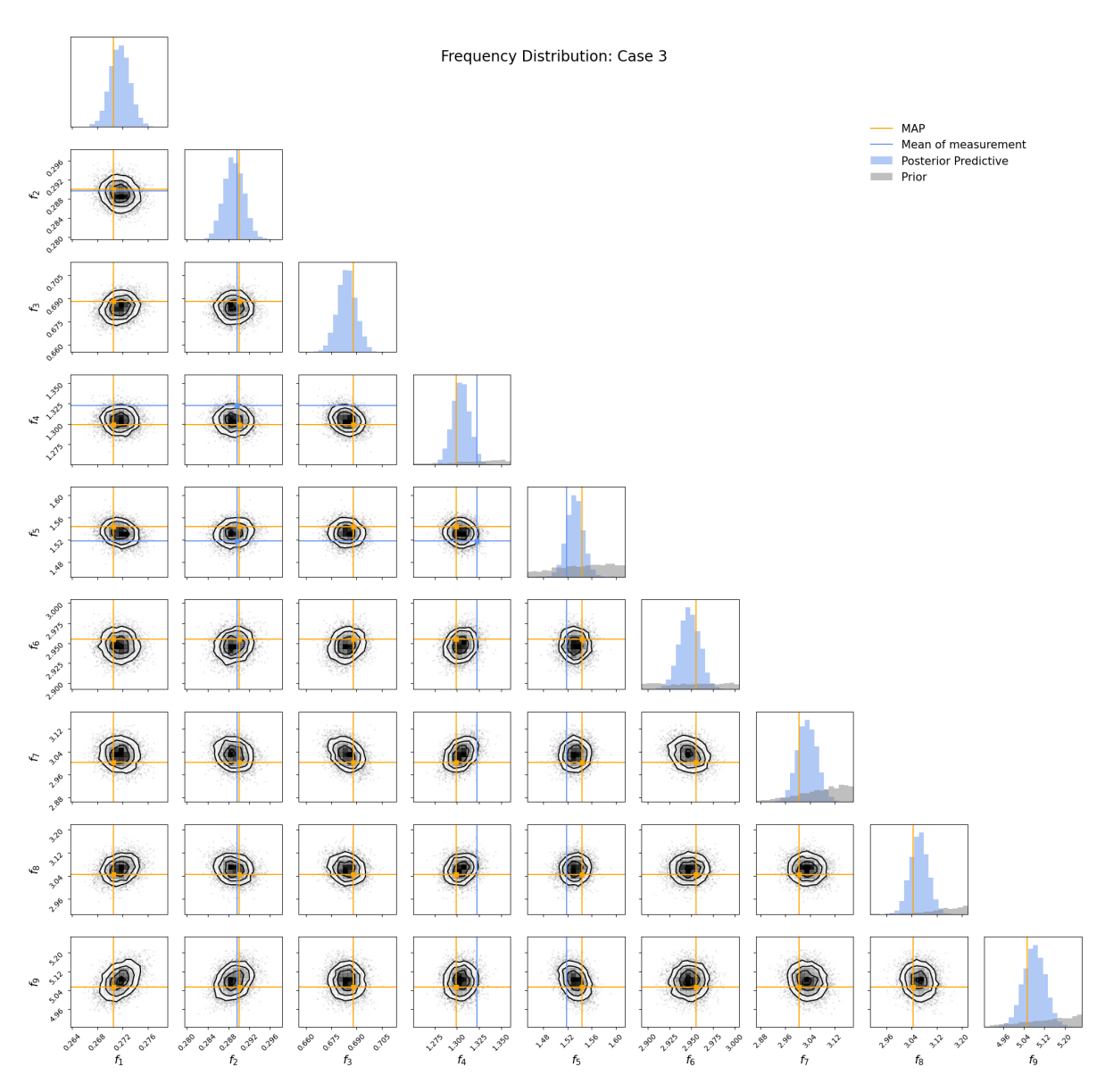


Figure F.8: Corner Plot for Frequencies for Case 3

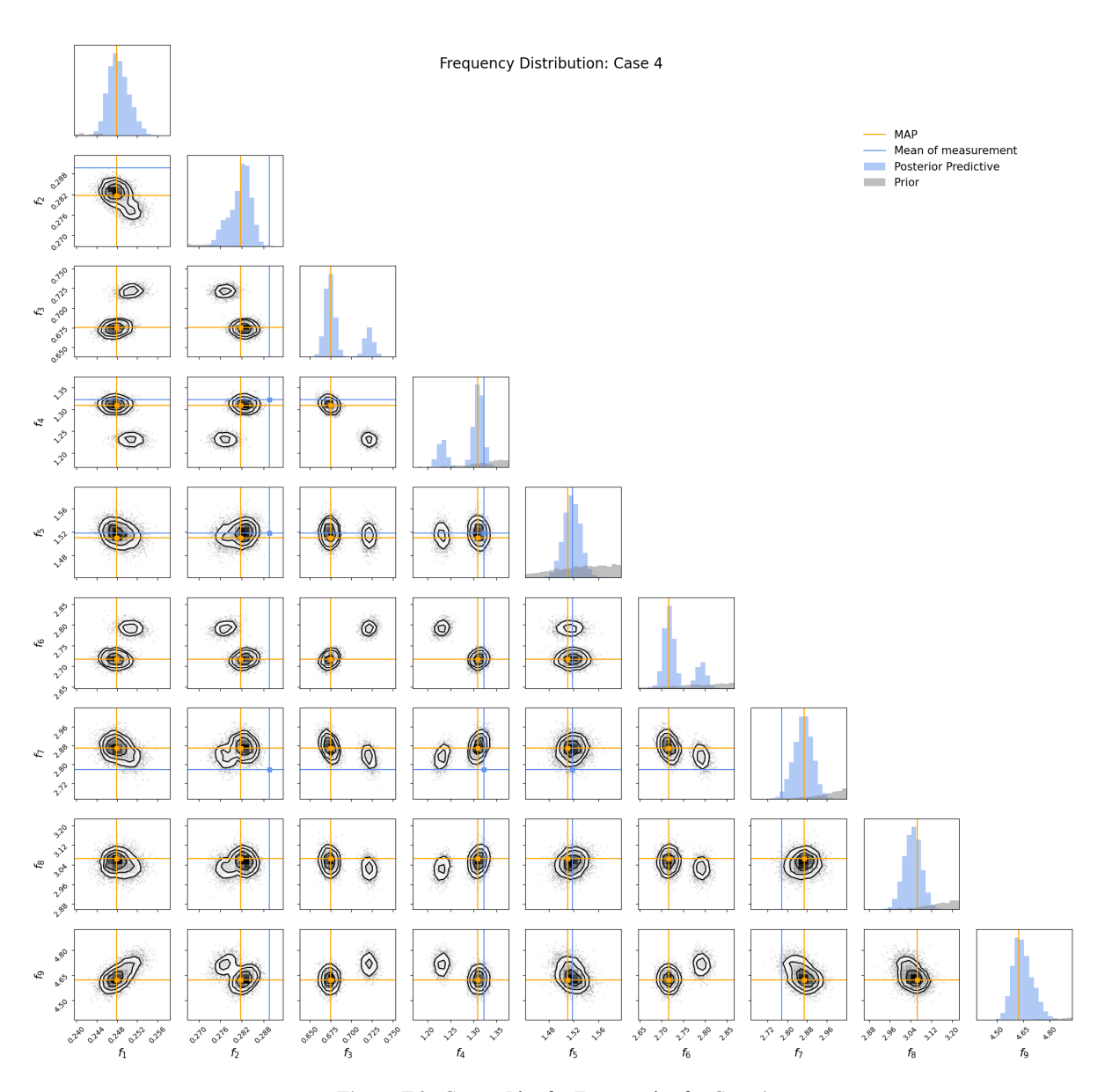


Figure F.9: Corner Plot for Frequencies for Case 4

F.4. Standard Deviation of Parameters

Table F.1: Standard Deviation of parameters across different cases

Param	Unit	Nominal	Case 1	Case 2	Case 3	Case 4
$E_{\rm conc}$	N/m^2	3.76×10^{9}	2.11×10^{9}	1.61×10^{8}	1.56×10^{8}	3.56×10^{8}
K_{tx}	N/m	8.74×10^8	2.41×10^7	1.44×10^7	1.41×10^7	1.39×10^8
K_{ty}	N/m	8.82×10^8	5.39×10^7	2.95×10^7	3.34×10^7	1.19×10^8
K_{rx}	Nm/rad	5.61×10^{11}	7.35×10^{11}	9.89×10^{12}	1.24×10^{13}	2.44×10^{13}
K_{ry}	Nm/rad	5.47×10^{11}	2.29×10^{11}	2.49×10^{11}	3.36×10^{11}	1.80×10^{13}
K_{rz}	Nm/rad	1.46×10^{11}	_	_	1.78×10^9	1.64×10^{10}

F.5. Mode Visualization in 3D

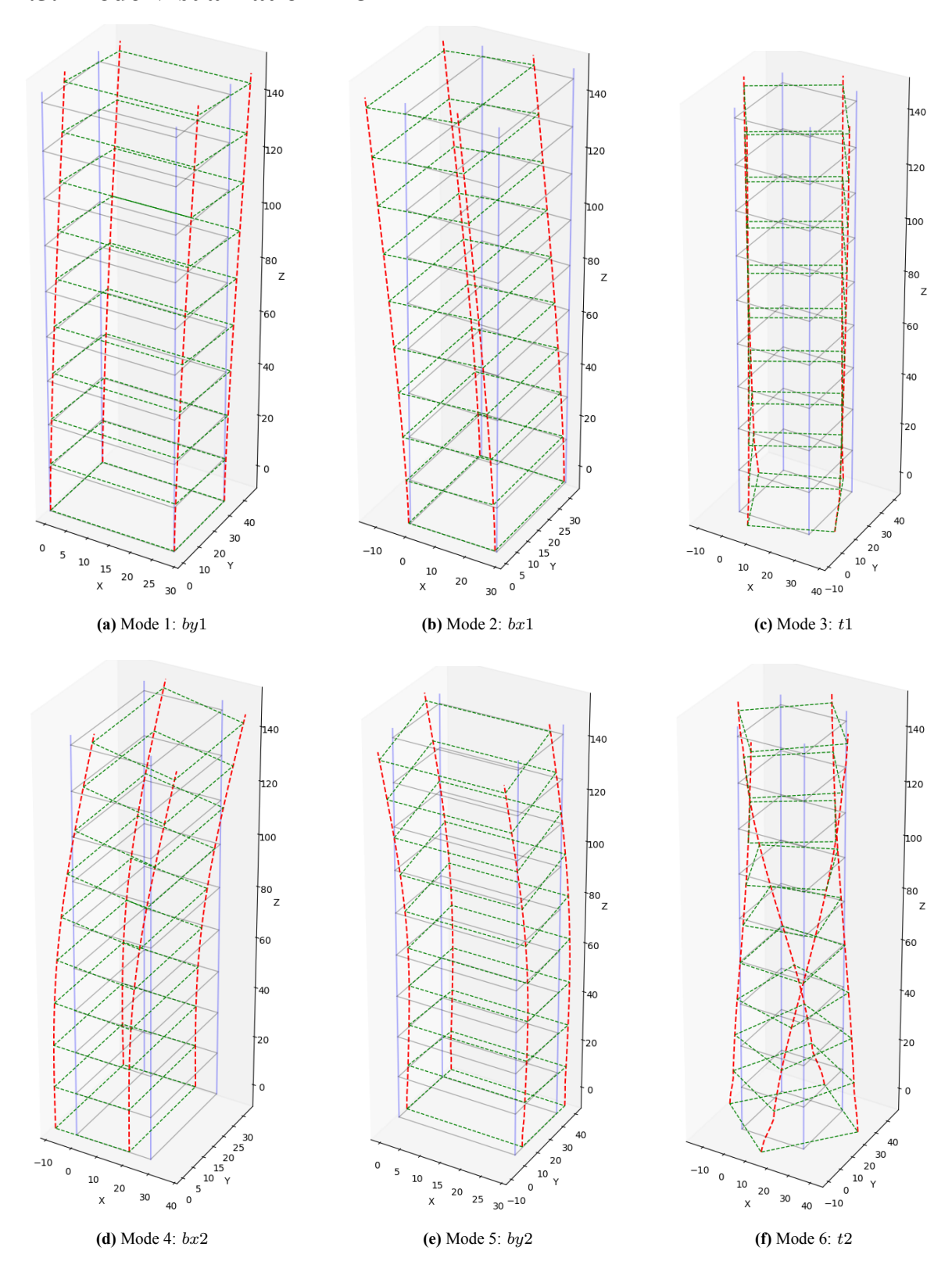


Figure F.10: Mode shapes 1-6 for the converged model of Case 3.

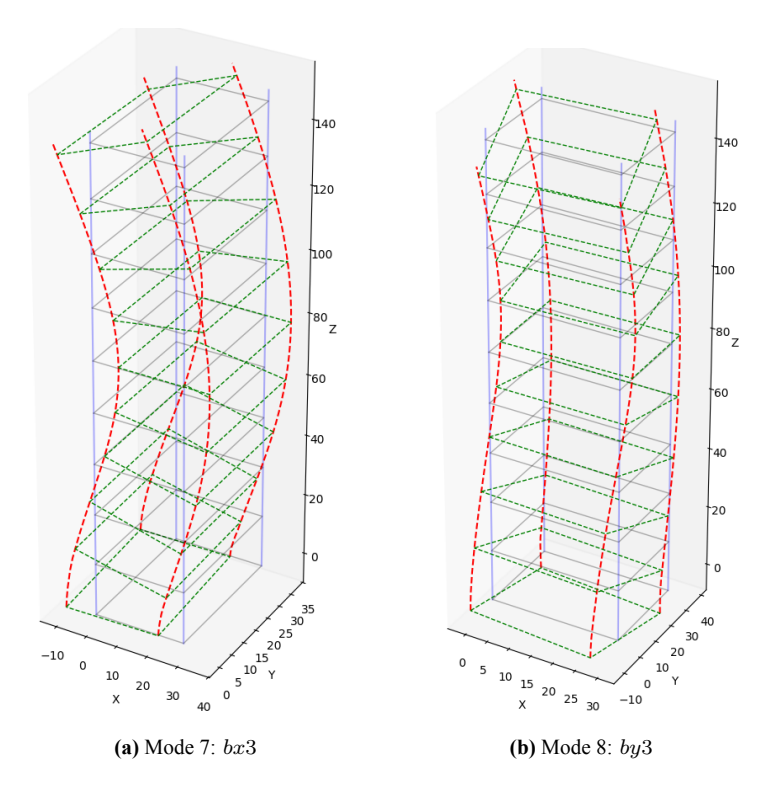


Figure F.11: Mode shapes 7-8 for the converged model of Case 3.

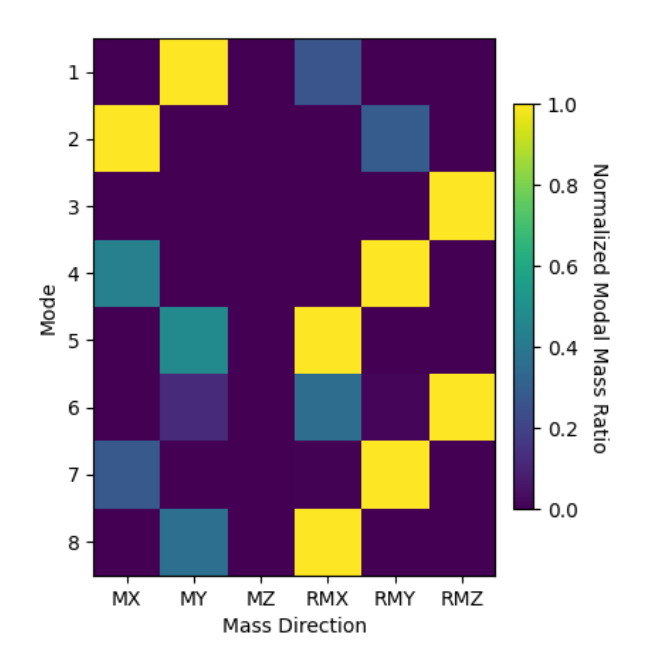


Figure F.12: Normalized Modal Mass Participation Ratio. Here M refers to Mass, RM refers to Rotational Mass and the X, Y, Z refers to direction. For each mode (row), the entries have been normalised with the highest value for that mode (row)